Characteristic Measurement of Discharge Currents from Electrostatic Discharge Generators

静電気試験器による放電電流の特性測定に関する研究

March 2007
平成19年3月

Ikuko Mori
森　育子

Summary

In conjunction with high speed and low voltage operation of ICs, the electromagnetic (EM) immunity of electronic equipment has been degrading. Especially the transient EM fields due to electrostatic discharge (ESD) events have broadband frequency spectra, which cause a serious failure in high-tech information equipment. From this viewpoint, the International Electrotechnical Commission (IEC) has prescribed an ESD-immunity test. For instance, in the IEC 61000-4-2, an ESD-immunity test simulating ESD events from a charged human body is specified and a typical discharge current waveform for contact discharge of an ESD generator (hereafter called an ESD-gun) is given in detail. The contact discharge is an IEC-recommended way in which discharge currents are injected into the equipment under test (EUT) in direct contact with the ESD-gun. On the other hand, air discharge is a way applied when the contact discharge cannot be conducted such as to insulated surfaces of the EUT, in which, by approaching the charged ESD-gun onto the EUT with pressing the switch of the gun, discharge currents are injected into the EUT through a spark gap. In contact discharge of an ESD-gun, injected discharge currents increase in proportion to charge voltages and have good reproducibility. There, however, remains a question if contact discharge not accompanied by a spark is appropriate for a test method simulating real ESD phenomena. While air discharge with the spark is said to be a severer immunity test than the contact discharge, its discharge currents do not always increase with charge voltages, and can be affected by approaching speed of the gun. This leads the current waveform to have poor reproducibility. Thus the IEC does not show the details of discharge currents for air discharge. For ESD events, on the other hand, it has been widely known as a strange phenomenon in the related industries that in comparison of high voltage ESD in several kilovolts, low voltage ESD in several hundred volts generates EM fields having more broadband frequency spectra. The ESD of this kind causes more serious failure to electronic devices, while the mechanism has not yet been elucidated.

In this study, from this perspective, firstly we proposed a method for calculating the resultant magnetic near-field due to discharge currents for contact discharge, and showed that the proposed method is effective in predicting the dependence on charge voltages of peak levels of the magnetic near-fields. Secondly, to grasp the characteristics of discharge currents for air discharge in view of approaching speed of the ESD-gun, we measured discharge currents with respect to the approaching speed, and revealed that between peaks and rise time of the discharge current waveforms a specific relationship exists regardless of the approaching speed. For low voltage ESDs in particular, to grasp the characteristics of contact and air discharges of an ESD-gun with charge voltages lower than 2 kV, though the IEC prescribes the charge voltages above 2 kV for immunity testing, we conducted both discharges onto a 50-Ω SMA connector, and investigated the dependence of current peaks and rise time on charge voltages. Moreover, by comparing the characteristics of observed current waveforms of both discharges, we examined the test condition at low charge voltages. This thesis gathers

the above-mentioned studies together, which consists of the following five Chapters.

Chapter-1 deals with the introduction, the background and purpose of this study, and the contents and organization of this thesis.

Chapter-2 describes calculation of magnetic near-fields generated by contact discharge of an ESD-gun. With an equivalent circuit model to explain discharge currents for contact discharge, we proposed a method to calculate voltage waveforms induced in a magnetic-field probe. After confirming the feasibility of the circuit model by contact discharge of an ESD-gun on a 50-Ω SMA connector, we showed both by calculation and wideband measurement using a 6-GHz digital oscilloscope the dependence on charge voltages of the magnetic near-fields generated by contact discharge of an ESD-gun.

Chapter-3 describes characteristic measurement of transient currents injected by air discharge of an ESD-gun onto an IEC-recommended current transducer (hereafter a target) and a ground assumed a chassis. Firstly, onto the target, intentionally changing approaching speed of the ESD-gun, we conducted a wideband measurement of discharge currents with a 6-GHz digital oscilloscope. As a result, we showed that, despite the dependence of peaks and rise time of the discharge current waveforms on the approaching speed of the gun, there exists a specific relationship between them regardless of the approaching speed. Secondly, we conducted characteristic measurement of transient currents for air discharge onto the ground. In discharges onto a ground, discharge currents cannot be directly observed, and in air discharge, there may be a discrepancy of the tip electrode from the discharge target point, which would make the current estimation via a magnetic-field probe difficult. From this reason, we proposed a method that can estimate discharge currents from magnetic fields simultaneously measured with two magnetic-field probes regardless of the distance between the discharge target point and the probes. After verifying the proposed method for contact discharge of an ESD-gun on a 50-Ω SMA connector, we showed that the above-mentioned specific relationship between peak and rise time of discharge currents holds also for air discharge of an ESD-gun onto a ground.

Chapter-4 describes characteristic comparison of discharge currents for contact and air discharges of an ESD-gun from the viewpoint of ESD-immunity tests. Through wideband measurement of discharge current waveforms for contact discharge of an ESD-gun with low charge voltages on a 50-Ω SMA connector, we investigated the dependence of peaks and rise time on charge voltages. The results revealed that for charge voltages below 2 kV the approaching speed of the ESD-gun does not almost affect the current waveform and that air discharge at charge voltages below 1 kV can provide a severer immunity test than contact discharge.

Chapter-5 describes the conclusion of this study and the future subjects.

Contents

List of Figures

List of Tables

Chapter 1

Introduction

1.1 Background and Purpose of this study

In conjunction with high speed and low voltage operation of ICs, the electromagnetic (EM) immunity of electronic equipment has been degrading. Especially the transient EM fields due to electrostatic discharge (ESD) events have broadband frequency spectra, which cause a serious failure in high-tech information equipment [1−2]. From this viewpoint, the International Electrotechnical Commission (IEC) has prescribed an ESD-immunity test. For instance, in the IEC 61000-4-2, an ESD-immunity test simulating ESD events from a charged human body is specified and a typical discharge current waveform for contact discharge of an ESD generator (hereafter called an ESD-gun) is given in detail [3].

The contact discharge is an IEC-recommended way in which discharge currents are injected into the equipment under test (EUT) in direct contact with the discharge electrode of the ESD-gun. On the other hand, air discharge is a way applied when the contact discharge cannot be conducted such as to insulated surfaces of the EUT, in which, by approaching the charged ESD-gun onto the EUT with pressing the switch of the gun, discharge currents are injected into the EUT through a spark gap. In contact discharge, injected discharge currents increase in proportion to charge voltages and their waveforms have good reproducibility. There, however, remains a question whether or not the contact discharge not accompanied by a spark is appropriate for a test method simulating real ESD phenomena. While air discharge with the spark is said to be a severer immunity test than the contact discharge, its discharge currents

do not always increase with charge voltages, and can be affected by approaching speed of the gun [4]. This leads the current waveforms to have poor reproducibility. Thus, for air discharge, the IEC does not show the details of discharge current waveforms. For ESD events, on the other hand, it has been widely known as a strange phenomenon in the related industries that in comparison of high voltage ESD in several kilovolts, low voltage ESD in several hundred volts generates EM fields having more broadband frequency spectra. The ESD of this kind causes more serious failure to electronic devices, while the mechanism has not yet been elucidated [2].

In this study, from this perspective, firstly we proposed a method for calculating the resultant magnetic near-field due to discharge currents for contact discharge, and showed that the proposed method is effective in predicting the dependence on charge voltages of peak levels of the magnetic near-fields. Secondly, to grasp the characteristics of discharge currents for air discharge in view of the approaching speed of the ESD-gun, we measured discharge currents with respect to the approaching speed, and revealed that between peaks and rise time of the discharge current waveforms a specific relationship exists regardless of the approaching speed. For low voltage ESD events in particular, to grasp the characteristics of contact and air discharges of an ESD-gun with charge voltages lower than 2 kV, though the IEC prescribes the charge voltages above 2 kV for immunity testing, we conducted both discharges onto a 50-Ω SMA connector, and investigated dependence of the current peaks and rise time on charge voltages. Moreover, by comparing the characteristics of observed current waveforms of both discharges, we examined the best condition at low-charge voltages. This thesis gathers the above-mentioned studies together.

In this chapter, an immunity test against electrostatic discharges and organization of this thesis are described.

1.2 Immunity test against Electrostatic discharge

As described in the preceding section, an ESD-immunity test simulating ESD events from a charged human body is being prescribed as "IEC 61000: Electromagnetic compatibility (EMC), Part 4-2: Tsting and measurement techniques, Electrostatic discharge test"(**IEC 61000-4-2**) by International Electrotechnical Commission (IEC) [3]. This standard is being adopted in Japan by Japanese Industrial Standards as "JIS C 61000-4-2". The is one of the immunity tests aimed at electrical and electronic equipment subjected to electromagnetic (EM) noise, such as "Radiated, radio-frequency, electromagnetic field immunity test" (IEC 61000-4-3), "Electrical fast transient/burst immunity test" (610004-4), and "Surge immunity test" (61000-4-5)[5].

In the IEC 61000-4-2, by injecting discharge currents into the EUT from the ESD-gun, malfunctions and destructions of electronic devises are tested. The IEC 61000-4-2 defines in detail,

- Typical waveform of the discharge current
- Range of test levels
- Test set-up
- Test procedure.

The object of this standard is to establish a common and reproducible basis for evaluating the performance of electrical and electronic equipment when subjected to electrostatic discharges. In addition, it includes electrostatic discharges that may occur from personnel to objects near vital equipment.

1.2.1 ESD-gun

Figure 1.1 shows the appearance of a commercially available ESD-gun and an equipped high voltage generator. In this study, a Noise-Ken products ESD-gun (TC-815P) and

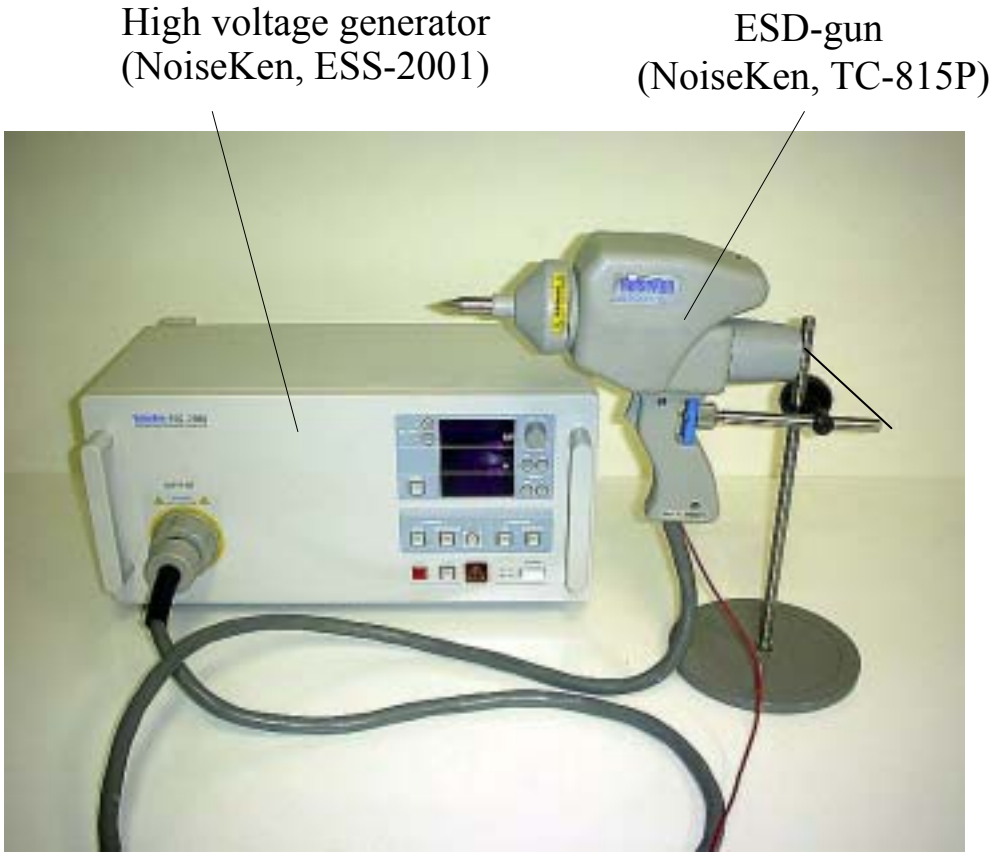

Figure 1.1: Appearance of a commercially available ESD-gun and its equipped high voltage generator.

its equipped high voltage generator (ESS-2001) are used. The ESD-guns specified by the IEC consists of the following parts:

- Discharge resistaor R
- Energy-storage capacitor C
- Charging resistor R_d
- Exchangeable tip electrodes
- Discharge return cable
- Porwer supply unit

Although details of the inner structure are not given, the discharge return cable is prescribed to have a length of approximately 2 m. The ESD-gun is also required to be sufficiently insulated to prevent the discharge current from flowing through some part of the output terminal to a human body or conductive surfaces of the EUT. The discharge resistance R and the energy storage capacitor C correspond to a human skin resistance of 330 Ω and a human-body capacitance of 150 pF, respectively. Figures 1.2 (a) and (b) show the inner structure of an ESD-gun and its simplified equivalent circuit, respectively. As the circuit shown in Figure 1.2 (b), the charge accumulated by the DC power supply is discharged from the tip electrode through the resistor R. The tip electrode is made of stainless steel, and is exchanged according to current injection methods for the one with different shapes and dimensions, which are shown in Figures 1.3 (a) and (b) for contact and air discharges, respectively.

1.2.2 Calibration method

To obtain the similar results by using different ESD-guns, in the IEC 61000-4-2, discharge current waveform is specified in detail: in advance of the discharge against the EUT, the IEC requires calibration of current waveform for contact discharge on an IEC-recommended current transducer (Pelligrini target, hereafter called a target). A typical current waveform for the contact discharge is shown in Figure 1.4.

Figures 1.5 (a) and (b) show the appearance and inner structure of a commercially available target, respectively. Also shown in Figure 1.5 (c) is an equivalent circuit at low frequencies of the target. The target consists of a flat electrode for current injection, 25 resistors of 51 Ω (combined resistance: R_1=2 Ω), 5 resistors of 48 Ω (combined

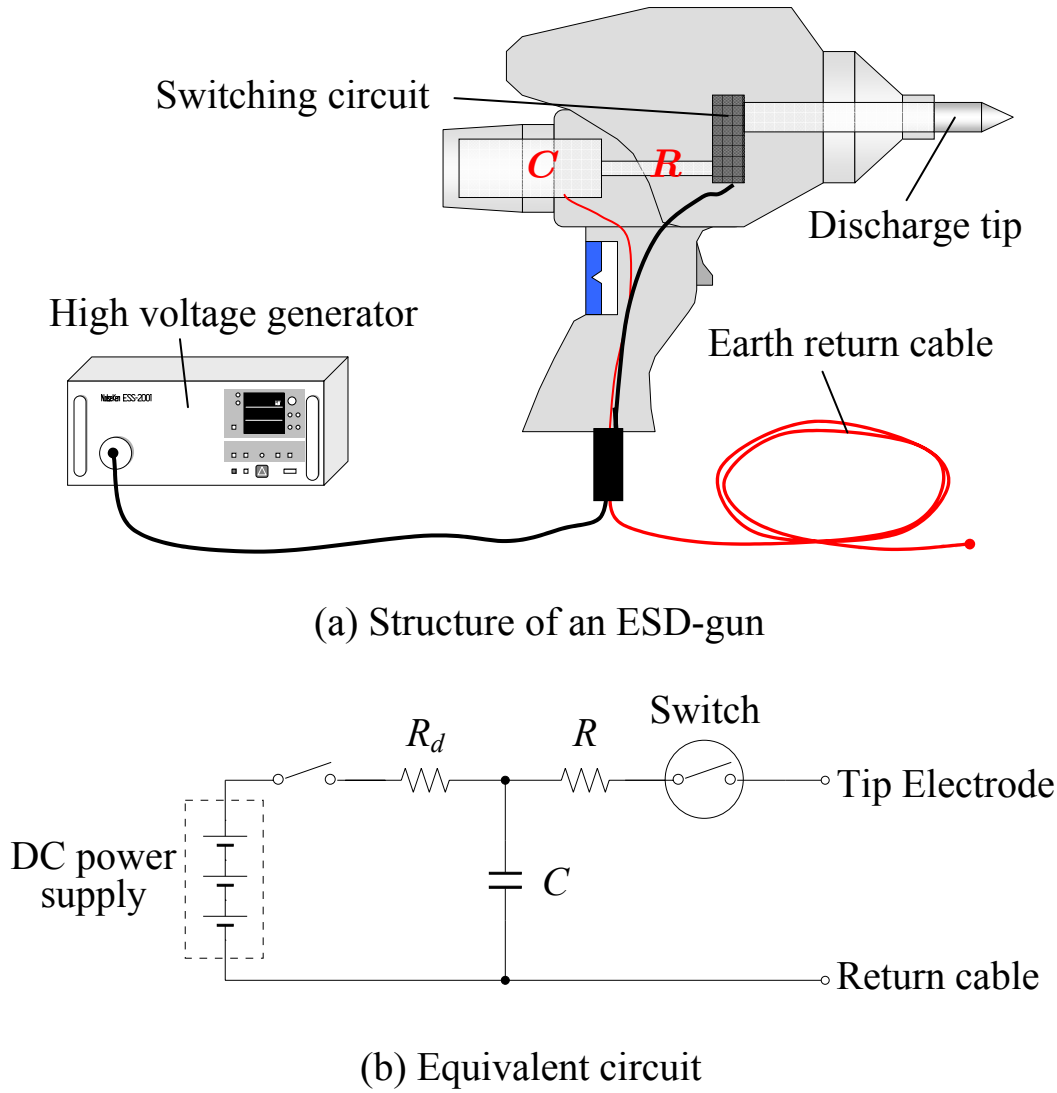

Figure 1.2: Inner structure of an ESD-gun (a) and its simplified equivalent circuit (b).

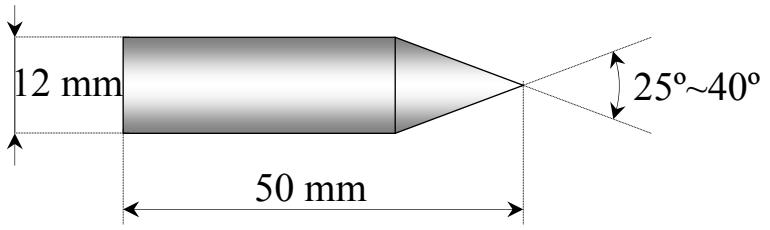

(a) For contact discharge

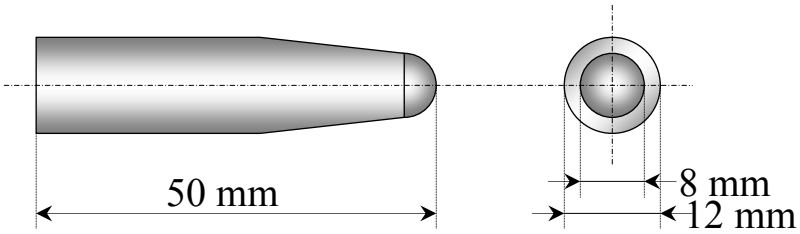

(b) For air discharge

Figure 1.3: Dimensions of tip electrodes; (a) for contact discharge and (b) for air discharge.

resistance: R_2=48 Ω), and a 50-Ω N-type connector (characteristic impedance: Z_0=50 Ω). Since stray capacitance and parasitic inductance of the shunt resistors can be negligible at low frequencies, let $i(t)$ be the injected current on the upper electrode, then the voltage $v(t)$ appearing across a termination load of Z_0=50 Ω is given as,

$$\begin{aligned} v(t) &= Z_0 \times \frac{R_1}{R_1 + R_2 + Z_0} \times i(t) \\ &= 50 \times \frac{2}{2 + 48 + 50} \times i(t) \\ &= i(t) \end{aligned} \tag{1.1}$$

In this way, the current injected on the electrode can be observed as a voltage waveform appearing across the termination load. In addition, this voltage waveform is required to be observed by using measurement instruments with a bandwidth of 1 GHz and above. Concerning the frequency characteristics of this target[6], however, the transfer impedance is known to have a resonance around 3 GHz [7].

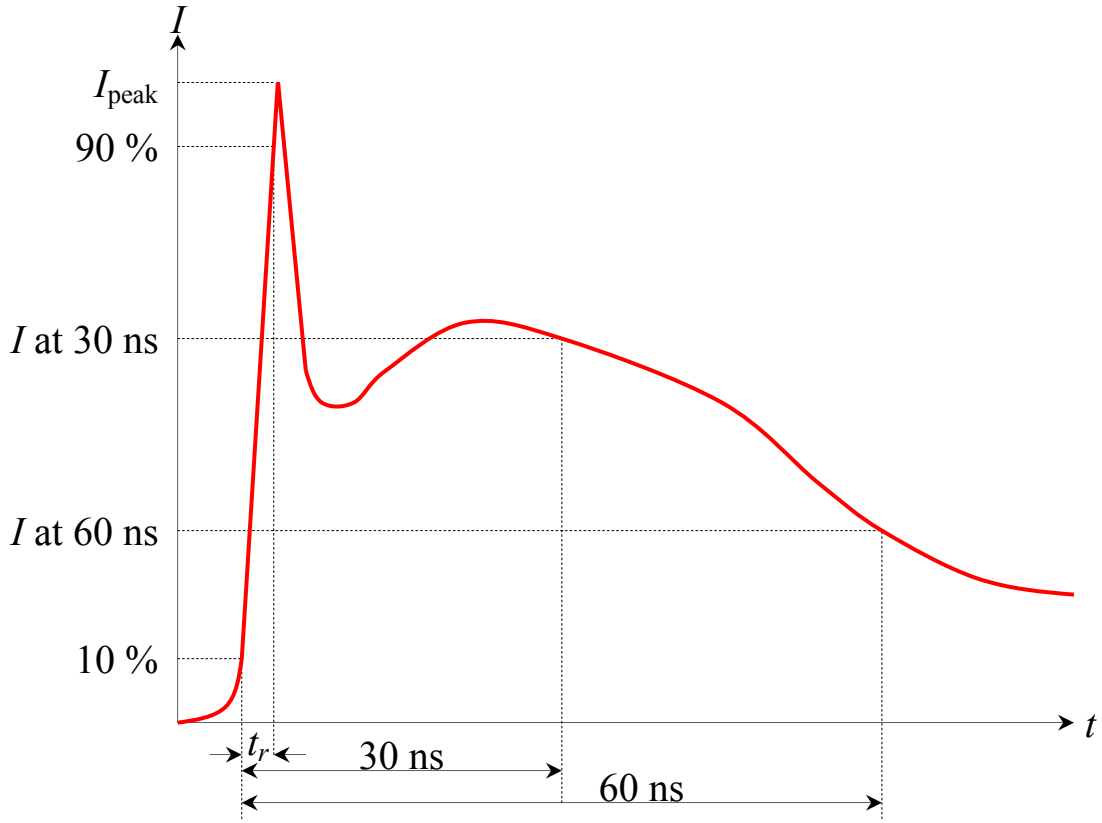

Level	Charge voltage	I_{peak}	t_r	I at 30 ns	I at 60 ns
1	2 kV	7.5 A	0.7∼1.0 ns	4 A	2 A
2	4 kV	15 A	0.7∼1.0 ns	8 A	4 A
3	6 kV	22.5 A	0.7∼1.0 ns	12 A	6 A
4	8 kV	30 A	0.7∼1.0 ns	16 A	8 A

Figure 1.4: Typical current waveform of contact discharge for calibration of ESD-guns by the IEC-recommended current transducer (Pellegrini target) .

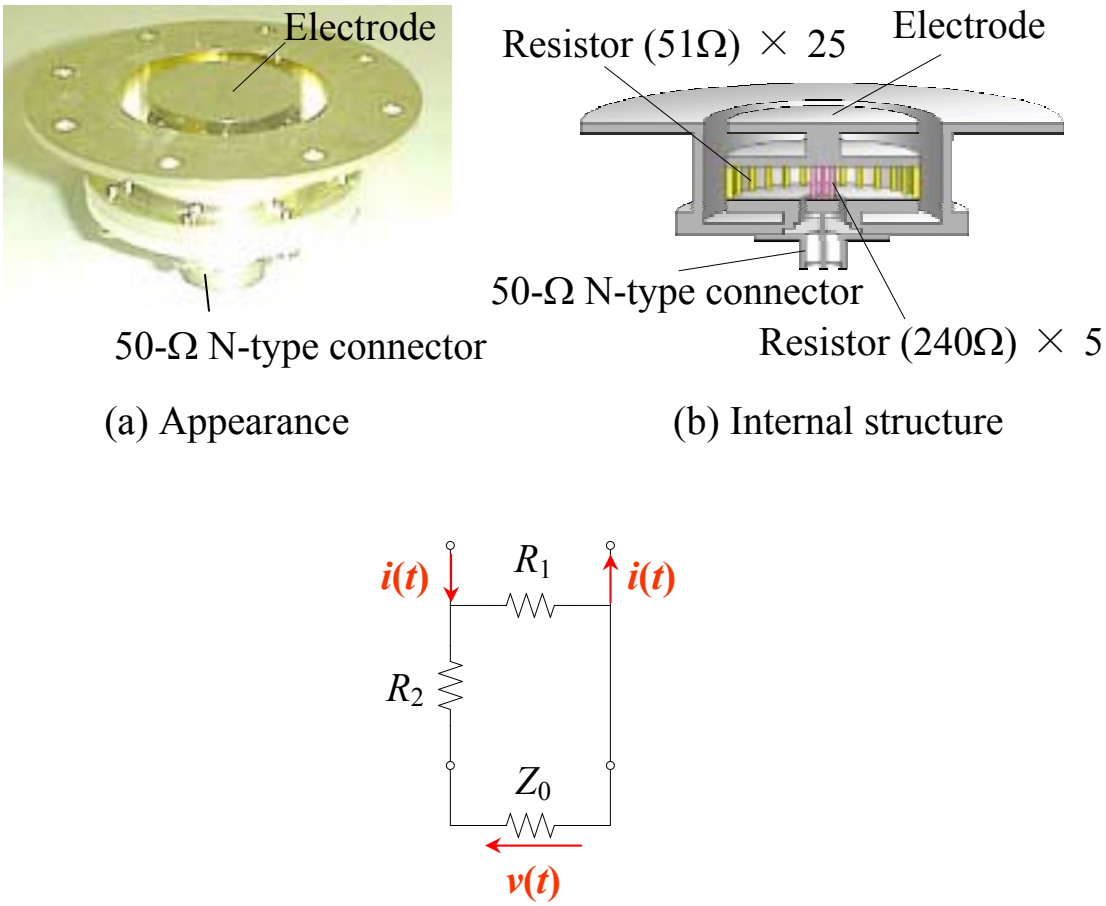

Figure 1.5: Appearance of the IEC-recommended current transducer (Pellegrini target) (a), its internal structure (b), and equivalent circuit at low frequencies (c).

1.2.3 Test method

Based on the methods injecting the discharge current into equipment under test (EUT), the IEC prescribes two discharge modes along with test voltages (charge voltages) [3]. One is "contact discharge" and the other is "air discharge". They are as follows:

- Contact discharge: the ESD-gun discharges after direct contact of the tip electrode with a conductive surface of the EUT
- Air discharge: the charged gun is quickly approached until discharges occur across a gap between the tip electrode of the gun and the surface of the EUT

From the standpoint of reproducibility, the IEC recommends the contact discharge. The air discharge is applied to the EUT when contact discharge is not applicable such as to the insulated surfaces of the EUT. Though the approaching speeds of the tip electrode (ESD-gun) affect the current waveforms [4], the air discharge is faithful to the real ESD phenomenon owing to the existence of a spark.
Table 1.1 shows the test levels of contact and air discharges. The level "X" is an open level to be negotiated between the manufacturer and the purchaser or to be defined by the product committee. Note that the test levels for the air discharge are not always related to severity levels for the EUT immunity.
The reason why two types of discharge method are used for ESD immunity tests can be traced back to the establishment of ESD standards. In 1984, the IEC 61000-4-2 was first published as the IEC 801-2 (Ed.1) by the IEC TC65/SC65A/WG3. Here, TC is the abbreviation of technical committee, SC is that of subcommittee, and WG is that of working group. TC65/SC65A/WG3 deals with industrial-process measurement and control. Based on the idea of being faithful to real ESD phenomena, air discharge was adopted as a current injection method. Owing to the poor reproducibility of the discharge current waveforms for the air discharge, however, in 1989 the revised edition (the IEC 801-2 (Ed.2)) was adopted and contact discharge has become the IEC-recommended way. For the purpose of applying the standard to all the electronic equipment dealt by TC77/SC77B, in 1995 it was republished as the IEC 1000-4-2. In

Table 1.1: Test level

Contact discharge		Air discharge	
Level	Test voltage [kV]	Level	Test voltage [kV]
1	2	1	2
2	4	2	4
3	6	3	8
4	8	4	15
X	Special	X	Special

1997, it has been renamed as the IEC 61000-4-2 due to the adoption of a new numbering system [3],[8]. In addition, the revision is scheduled in 2009.

A test method in which the discharge current of the ESD-gun is injected directly into the EUT is called "direct application", and a test method in which the discharge current is injected into a horizontal coupling metal plane or a vertical coupling metal plane is called "Indirect application". The direct application assumes a direct discharge from a charged human-body to electronic equipment, and the indirect application assumes a discharge to the object (such as a door knob) near the electronic equipment from a charged human-body.

1.2.4 Test results

Test results should be classified in terms of the loss of function or degradation of performance of the equipment under test. The recommended classification is as follows.

- normal performance within limits specified by the manufacturer, requestor or purchaser
- temporary loss of function or degradation of performance which ceases after the disturbance ceases, from which the equipment under test recovers its normal performance, without operator intervention
- temporary loss of function or degradation of performance, the correction of which requires operator intervention

- loss of function or degradation of performance which is not recoverable, owing to damage to hardware or software, or loss of data

As a result of applying test specified in this standard, the EUT should not be in critical or unstable conditions. In case malfunction does not occur and after application of the test the basic function in the specification is maintained, the test results are judged good.

1.3 Organization of this thesis

This thesis consists of the following five Chapters.

Chapter-1 deals with the introduction. The background, the purposes and contents of this study, and the organization of this thesis were described.

Chapter-2 describes calculation of magnetic near-fields generated by contact discharge of an ESD-gun. With an equivalent circuit model to explain discharge currents for contact discharge [9], we proposed a method to calculate voltage waveforms induced in a magnetic-field probe. After confirming the feasibility of the circuit model by contact discharge of an ESD-gun on a 50-Ω SMA connector, we showed both by calculation and wideband measurement with a 6-GHz digital oscilloscope the dependence on charge voltages of the magnetic near-fields generated by contact discharge of an ESD-gun.

Chapter-3 describes characteristic measurement of transient currents injected by air discharge of an ESD-gun onto a target and a ground. Firstly, intentionally changing approaching speed of the ESD-gun onto the target, we conducted a wideband measurement of discharge currents with a 6-GHz digital oscilloscope. As a result, we showed that, despite the dependence of peak and rise time of the discharge current waveforms on the approaching speed of the gun, there exists a specific relationship between them regardless of the approaching speed. Secondly, characteristic estimation of discharge currents injected by air discharge of an ESD-gun was conducted. In discharges onto a ground, discharge currents cannot be directly observed, and in air discharge, there may be a discrepancy of the tip electrode from the discharge target point, which would make the current estimation via a magnetic-field probe difficult. From this reason, we proposed a method that can estimate discharge currents from magnetic fields simultaneously measured with two magnetic-field probes regardless of the distance between the discharge target point and the probes. After verifying the proposed method for contact discharge of an ESD-gun on a 50-Ω SMA connector, we showed that the above-mentioned specific relationship between peaks and rise time of discharge currents holds also for air discharge of an ESD-gun onto a ground.

Chapter-4 describes characteristic comparison of discharge currents for contact and air discharges of an ESD-gun. Through a wideband measurement of discharge current waveforms for contact discharge of an ESD-gun with low charge voltages on a 50-Ω SMA connector, we investigated the dependence of peaks and rise time on charge voltages. The results revealed that at charge voltages below 1 kV the approaching speed of the ESD-gun does not almost affect the current waveform and also that air discharge can provide a severer immunity test than contact discharge.

Chapter-5 describes the conclusion of this study and the future subjects.

References

[1] For example, T.Takagi, "Research and development on EMC/EMI measurements and technologies in Japan", J.IEICE, **J79-B-II**, No. 11, pp. 718–726, Nov.,1996 (in Japanese).

[2] M.Honda, "EMI aspects of the meato-metal ESD to the electronic equipment", J.IEICE,Vol.**78**, No. 9, pp. 849-850, Sep.,1995.

[3] Japanese Industrial Standards Committee, "Electromagnetic Compatibility (EMC)–Part 4:Testing and measurement techniques–Section 2. Electrostatic discharge immunity test", JIS C 1000–4–2: 1999 (IEC 61000-4-2:1995/Amd.1), 1999 (in Japanese).

[4] For example, M.Masuigi, "Analysis of transient responses of electric fields accompanied by a movement of a discharge electrode", Trans. IEICE, Vol.J76-B-II, No.11, pp. 916—917, Nov., 1993 (in Japanese).

[5] Y. Akao, "Kankyoudenjikougaku no kiso (Basis of Electromagnetic engineering)", pp. 45–52, 1991 (in Japanese).

[6] J. Sroca, "Target Influence on the Calibration Uncertainty of ESD Simulators", Proc. of IEEE International Symposium on EMC, Zurich, 37G4, 2001.

[7] T.Gotoh,O.Fujiwara,S.Isigami,Y.Yamanaka, "Characteristic measurement of transfer impedence of Pellegrini target in contact discharge with ESD-gun", IEICE Technical reaport, EMCJ2003-68, MW2003-165, pp. 9-14, Oct., 2003.

[8] For example, N.Murota, "Characteristics of the discharge current by the human charge model ESD simulator", IEICE Trans. Commun.Vol. J79-B-II, pp. 789-796, 1996 (in Japanese).

[9] O.Fujiwara,T.Tanaka,Y.Yamanaka,"An equivalent circuit modeling of discharge current injected in contact with an ESD-gun", IEEJ Trans.FM., VOl.123, No. 8, pp. 784–789, Aug.,2003.

Chapter 2

Calculation of magnetic near-fields generated by contact discharge

2.1 Introduction

With the high speed and low voltage operation of ICs, the electromagnetic (EM) immunity of electronic devices has been degrading. Especially the transient EM fields due to electrostatic discharge (ESD) events have broadband frequency spectra, which cause serious failure to high-tech information equipment [1−2].

From this perspective, the International Electro-technical Commission (IEC) has specified an immunity test of such electronic equipment against ESD events. For instance, in the IEC 61000-4-2 [3], a test method simulating ESD events from a charged human body is prescribed, in which a typical current waveform for contact discharge of ESD-guns is given. Two methods for injecting discharge currents to equipment under test (EUT) are given along with test voltages (charge voltages):"contact discharge" in which the ESD-gun discharges after direct contact with the EUT, and "air discharge" in which discharge occurs across a gap between the tip electrode of the gun and surfaces of the EUT. The latter is applicable for EUT whose surface is insulated when the former cannot be conducted. The contact discharge is a way that the IEC recommended.

Before the ESD-immunity tests are performed on actual EUT, by injecting the discharge current directly onto a target, the current waveform of the contact discharge of the gun is required to be calibrated. Since discharge process of the gun remains unclear and the transfer impedance of the target has frequency dependence, even if the discharge current waveform satisfies the IEC-prescribed one, there is no guarantee

that the current can be injected into the actual EUT [4–8]. In order to elucidate these problems, the discharge mechanism of contact discharges of an ESD-gun must be clarified. From this point of view, an equivalent circuit model was proposed for contact discharge of an ESD-gun based on its geometrical structure [9], and the decisive factors for the discharge current were clarified.

In this chapter, using the equivalent circuit model to explain discharge currents for contact discharge, we propose a method to calculate voltage waveforms induced in a magnetic-field probe. After confirming the feasibility of the circuit model by contact discharge of an ESD-gun on a 50-Ω SMA connector, we show both by calculation and wideband measurement with a 6-GHz digital oscilloscope the dependence on charge voltages of the magnetic near-fields generated by contact discharge of an ESD-gun.
Note that the magnetic near-field generated by the contact discharge of the ESD-gun should couple with the EUT. Thus grasping both the magnetic field level and its dependency on a charge voltage are useful to improve the immunity of electronic devices.

2.2 Measurement method of magnetic near-fields

Because the target has a frequency dependent transfer impedance, we first measured simultaneously discharge currents of the contact discharge on a 50-Ω SMA connector and the resulting magnetic near-field. Secondly, contact discharges onto the ground and its resultant magnetic near-field were measured.

Figure 2.1 (a) shows a measurement set-up for contact discharge on a 50-Ω SMA connector. As a ground, an aluminum square plate with a size of 1 m was placed horizontally and the ESD-gun was fixed perpendicularly in contact with its center. The gun was connected to the ground through an earth return cable with a radius of 0.55 mm, which had a length of 50 cm for convenience, although the cable length specified in the IEC standard is 2 m.

Figure 2.1 (b) shows configuration of the tip electrode and a magnetic field probe. The probe shown in Figure 2.2 was positioned so that the center of the loop is at a distance of d=13.5 mm from the axis of the tip electrode, and is 8.0 mm in height from the ground. Its output was connected to a digital oscilloscope with a frequency band of 6-GHz and a sampling speed of 20 GHz through a 50-Ω coaxial cable. Figure 2.2 indicates the external appearance of the shielded probe and the internal structure of the loop. The probe consists of a loop (external size: 10 mm, loop diameter: a=4.5 mm, self-inductance: L_c=13.8 nH) made of a semi-rigid cable with a characteristic impedance Z_0 of 50 Ω, which is built in an acrylic cuboid for protection. In order to reduce the effects of electric field coupling, a 1.0 mm gap is created at the center of the outer conductor, and the inner and the outer conductors for half of the loop are connected[10].

Ten discharges at a charge voltage of V_C=0.3 kV on the inner conductor of the SMA connector were performed. The currents injected into the inner conductor of the SMA connector and the resultant magnetic near-field were simultaneously observed as voltage waveforms with the oscilloscope described above.

Next, the ESD-gun was set in contact with the ground (1m×1m) perpendicularly and the resultant magnetic near-fields for contact discharges of the ESD-gun were observed.

Figure 2.3 shows the configuration of the tip electrode and the magnetic field probe for contact discharge on the ground. The magnetic field probe is placed in the same way as was done for the contact discharge on the SMA connector. Discharges were performed ten times each at charge voltages from V_C=1.0 kV to 8.0 kV in 0.5 kV increments, and the resulting near-fields were observed as voltage waveforms induced at the probe.

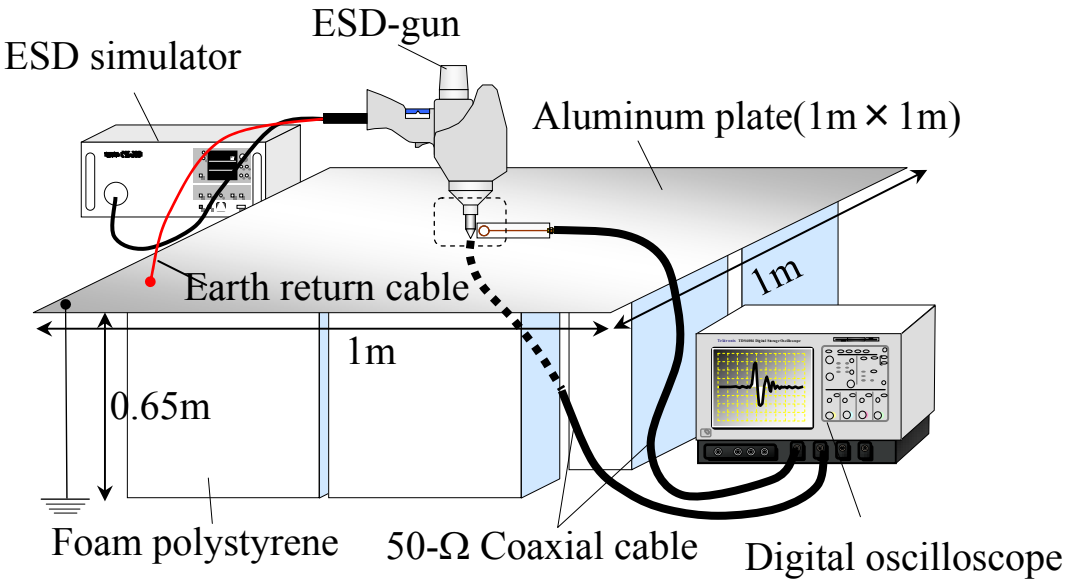

(a) Measurement set-up

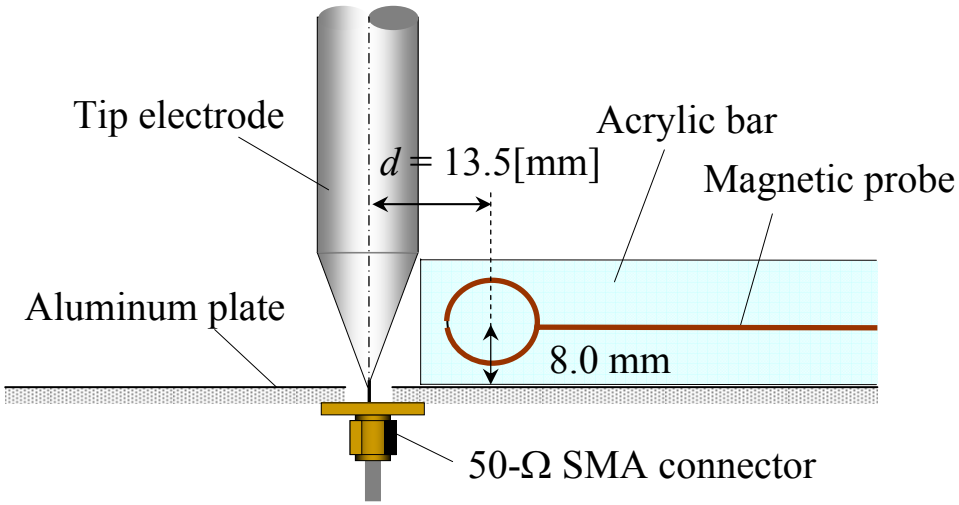

(b) Configuration of magnetic probe

Figure 2.1: Measurement set-up for contact discharge on a 50-Ω SMA connector (a) and configuration of a tip electrode and a magnetic probe (b).

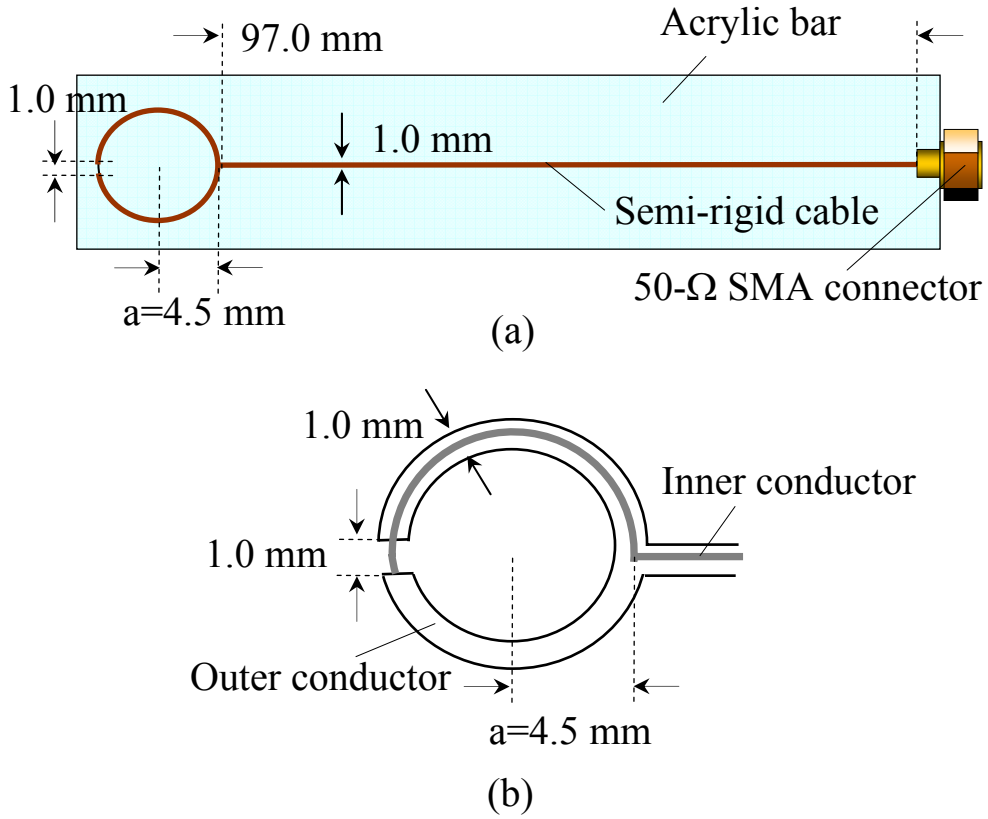

Figure 2.2: Appearance of a shielded magnetic field probe (a) and structure of its loop.

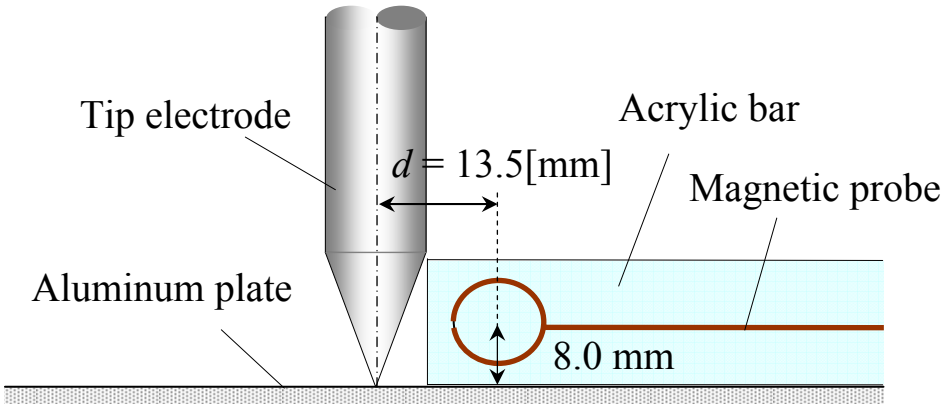

Figure 2.3: Configuration of the tip electrode and the magnetic probe for contact discharge on a ground.

2.3 Calculation method of magnetic near-fields

2.3.1 Equivalent circuit model for an ESD-gun

The equivalent circuit model consists of two circuits: an equivalent circuit that provides the first peak in the discharge current (referred to as Mode A), and the other that provides the second peak (Mode B). Figure 2.4 shows equivalent circuits in the Laplace domain for contact discharge of the ESD-gun with a charge voltage of V_C, to the inner conductor of the 50-Ω SMA connector. C and R in the figure represent capacitance and skin resistance of a human body, respectively. L represents the inductance built in the switching circuit, which used to control rise time of the discharge current waveforms, L_t represents the parasitic inductance of the tip electrode, and L_R represents the self-inductance of the earth return cable. In addition, C_{t1} and C_{t2} represent stray capacitance of the tip electrode, and C_R represents that above the ground.

The circuit parameters in the figure, except the capacitance C, the resistance R, and the inductance L, were determined based on the dimensions of the ESD-gun. However, because the internal structure of the switching circuit remains unknown, the inductance L was determined so that rising slope and peak of the calculated waveforms for the discharge current could match those of the measured waveforms. The circuit parameters obtained in this way are summarized in Table 2.1[9]. Note that when Z_0 in Figure 2.4 is 0 Ω, the figure gives an equivalent circuit for contact discharge of the ESD-gun onto a ground.

Based on the equivalent circuits described above, the current $I(s)=I_A(s)+I_B(s)$ flowing through the tip electrode in the Laplace domain can be calculated, and the current $i(t)$ in the time domain can be obtained by applying numerical inverse Laplace transform to the $I(s)$.

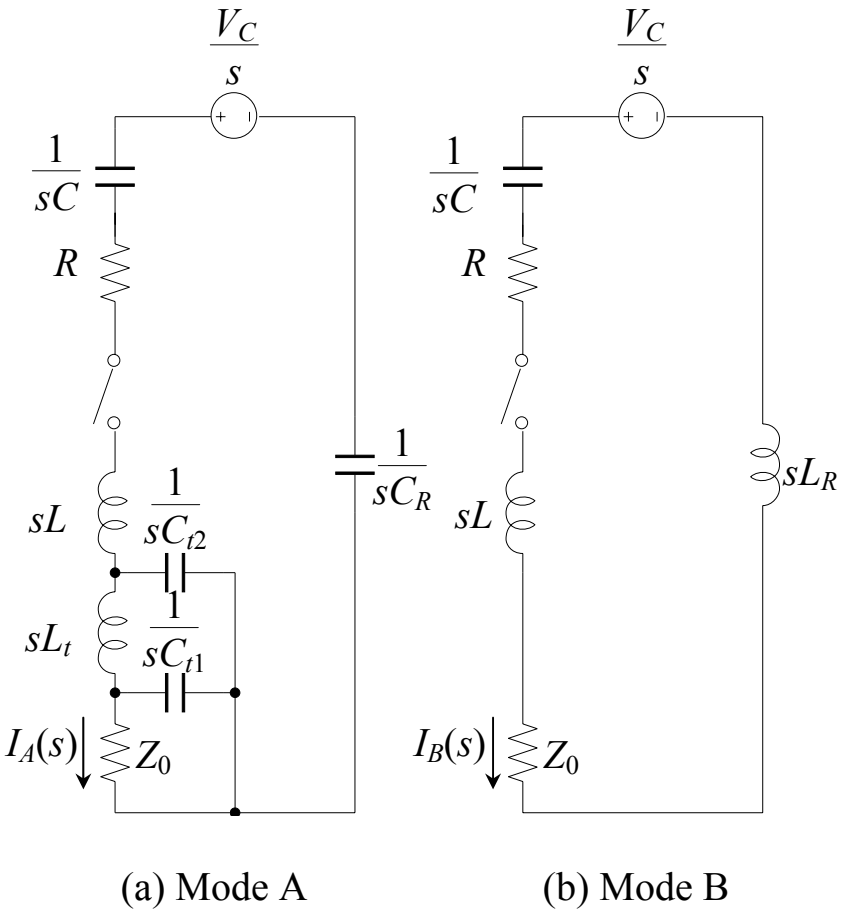

Figure 2.4: Equivalent circuits in the Laplace domain to calculate discharge currents for contact discharge of the ESD-gun.

Table 2.1: Numerical values of the circuit parameters [9].

ESD-gun	C	150 pF
	R	330 Ω
	L	420 nH
	L_t	54.8 nH
	C_{t1}	0.54 pF
	C_{t2}	2.24 pF
	C_R	3.13 pF
Earth return cable	L_R	638 nH
SMA connector	Z_0	50 Ω

2.3.2 Calculation method for curent and magnetic near-field

Under the assumption that the current waveform $i(t)$ calculated in the previous section flows only through the axis of the tip electrode, the flux interlinking the probe can be obtained in a closed form, and the output voltage waveform $v(t)$ for the magnetic probe is calculated from

$$v(t) = -2\pi f_L \mu_0 \left(d - \sqrt{d^2 - a^2}\right) \times \int_0^t \frac{\partial i(t')}{\partial t'} \exp\left\{-2\pi f_L (t - t')\right\} dt' \tag{2.1}$$

where f_C=$Z_C/2\pi L$. Here, Z_C(=50Ω) and L_C(=13.8 nH) represent the characteristic impedance and the self-inductance of the semi-rigid cable of the magnetic field probe, respectively. d represents the distance from the axis of the tip electrode to the center of the loop, and a(=4.5 mm) represents the loop radius of the probe.

2.4 Results and discussion

2.4.1 Contact discharge to the SMA connector

Figures 2.5(a) and (b) show examples of the observed waveforms of discharge currents and those of the resultant magnetic near-fields, respectively, for contact discharge of an ESD-gun on the SMA connector at a charge voltage of V_C=300 V. Note that the discharge current waveform in Figure 2.5(a) is the voltage waveform appearing at a 50-Ω load of the SMA connector and the magnetic near-field in Figure 2.5 (b) represents output voltage waveform at the probe, which were observed as voltage waveform with the 6-GHz digital oscilloscope. The lower figures represent enlarged waveforms from the beginning of the discharge to 5 ns of the waveforms in the upper figures. The thick solid line and the solid circles in the figures indicate measured values, and the thin solid line indicates values calculated from the equivalent circuits in Figure 2.4.

From Figures 2.5 (a) and 2.5 (b), it is found that calculated waveforms for discharge current and magnetic near-field of contact discharge on the SMA connector approximately agreed with the observed waveforms in rising slopes. The reason why the calculated waveforms after the first peak do not match the observed ones is because the earth-return cable in Mode B of the equivalent circuit shown in Figure 2.4 (b) was replaced with a lumped inductance. On the enlargement of the initial rising slope (0–0.5ns) of the current waveforms shown in Figure 2.5 (a), the calculated one shows a gentle increase, while the measured one has a swell. Moreover, as a differential of the current waveform, the swell is emphasized on the measured magnetic near-field waveform shown in Figure 2.5 (b). This can be explained as follows. In case of the contact discharge, the capacitor of the ESD-gun is charged, and then the accumulated charge is discharged through the tip electrode. As a result, a discharge should occur in the switching circuit just before the ESD-gun is actuated, which could be observed as a swell in the waveform. Because the observed waveform in the magnetic near-field includes a factor of time differential for the discharge current, as can be seen in Eq. (2.1), changes in the rising slope of the discharge current at the initial stage of the magnetic near-field waveform are emphasized as seen in Figure 2.5 (b).

2.4.2 Contact discharge to the ground

Figure 2.6 (a) shows the calculated waveforms for discharge current generated by contact discharge of an ESD-gun onto the ground, and Figures 2.6 (b) and (c) show the calculated and observed waveforms of the magnetic near-field. Figure 2.6 (c) is an enlargement of the period from the beginning of the rising slope to 5ns for the waveform in Figure 2.6 (b), as was done in Figure 2.5. The thick solid lines in Figures 2.6 (b) and (c) indicate measured waveforms, and the thin solid lines indicate calculated ones obtained by substituting the discharge current waveform in Figure 2.6(a) into Eq. (2.1). Note that the discharge current waveforms in Figure 2.6 (a) was obtained from Z_0=0 Ω in Figures 2.4 (a) and (b). In the figure, the calculated waveform from Eq. (2.1) of the magnetic near-field fairly matches the observed one up to the first peak. After that period, however, the calculated waveforms do not match the measured ones because of the oscillation of the calculated waveforms. The reason for the latter may be because the contact resistance between the tip electrode and the ground and the skin resistance of the electrode in Mode A in Figure 2.4 are ignored, and the earth return cable in Mode B in Figure 2.4 is replaced with a lumped inductance. In addition, compared with the calculated discharge current waveform for the contact discharge on the SMA connector shown in Figure 2.5 (b), the waveform for the contact discharge on the ground significantly oscillates as shown in Figure 2.6 (b). The reason is that, in calculation for the ground, the characteristic impedance of Z_0=50 Ω for the SMA connector was taken as 0 Ω and the damping time constant became shorter for the discharge on the ground than on the SMA connector.

2.4.3 Dependence on charge voltages of peak levels of magnetic near field

Figure 2.7 shows the dependence on charge voltages of peak levels of the magnetic near-field observed through the magnetic field probe in contact discharges of the ESD-gun onto the ground. The horizontal axis indicates charge voltage V_C in kV and the vertical axis indicates the peak values in V for the observed and calculated peak voltages. Both are in logarithmic scales. The results of 10 times measurements at each of the charge

voltages are given as "means value ± standard deviation". The calculated results from the equivalent circuits in Figure 2.4 are also shown. Note that the characteristic impedance of Z_0 is taken as 0Ω. This figure shows that, in the contact discharge of the ESD-gun, the peak levels of the observed magnetic near-field are almost proportional to the charge voltage, and this trend agrees with the calculated ones.

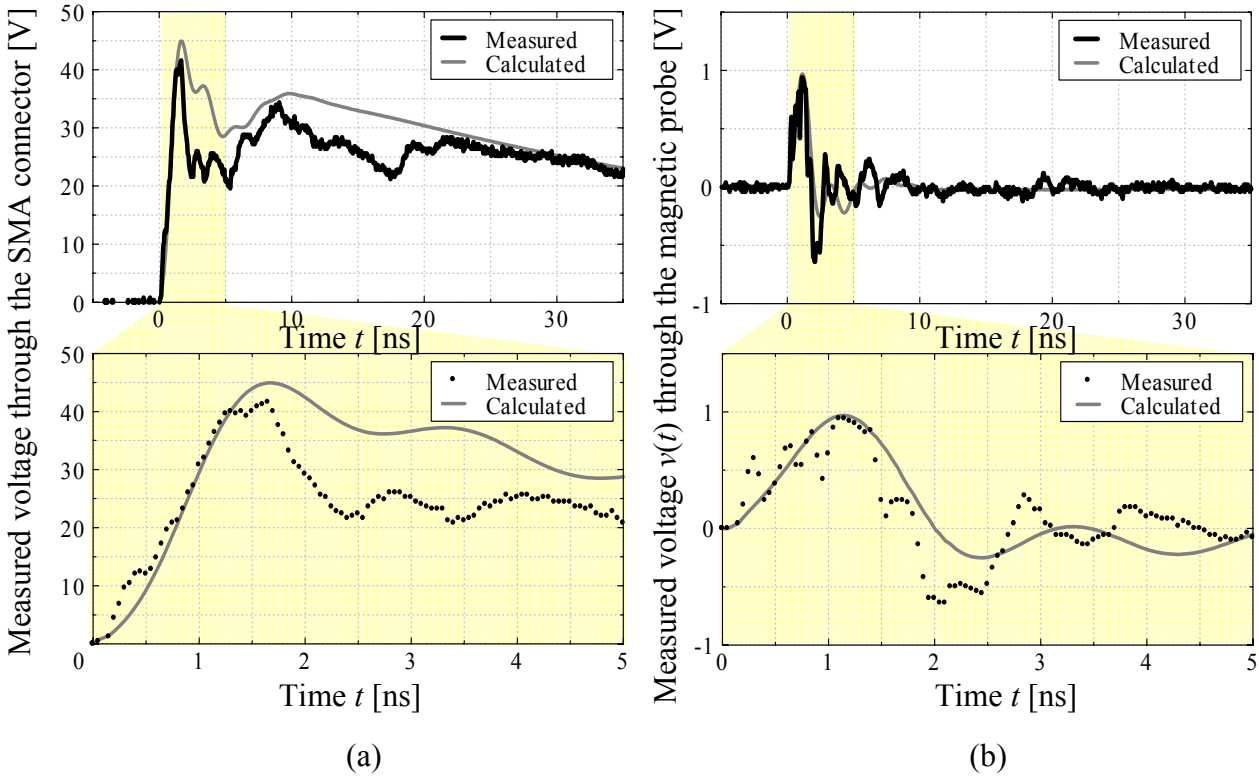

Figure 2.5: Measured and calculated waveforms of (a) a discharge current and (b) a magnetic near-field for contact discharge on the 50-Ω SMA connector (V_C=0.3 kV).

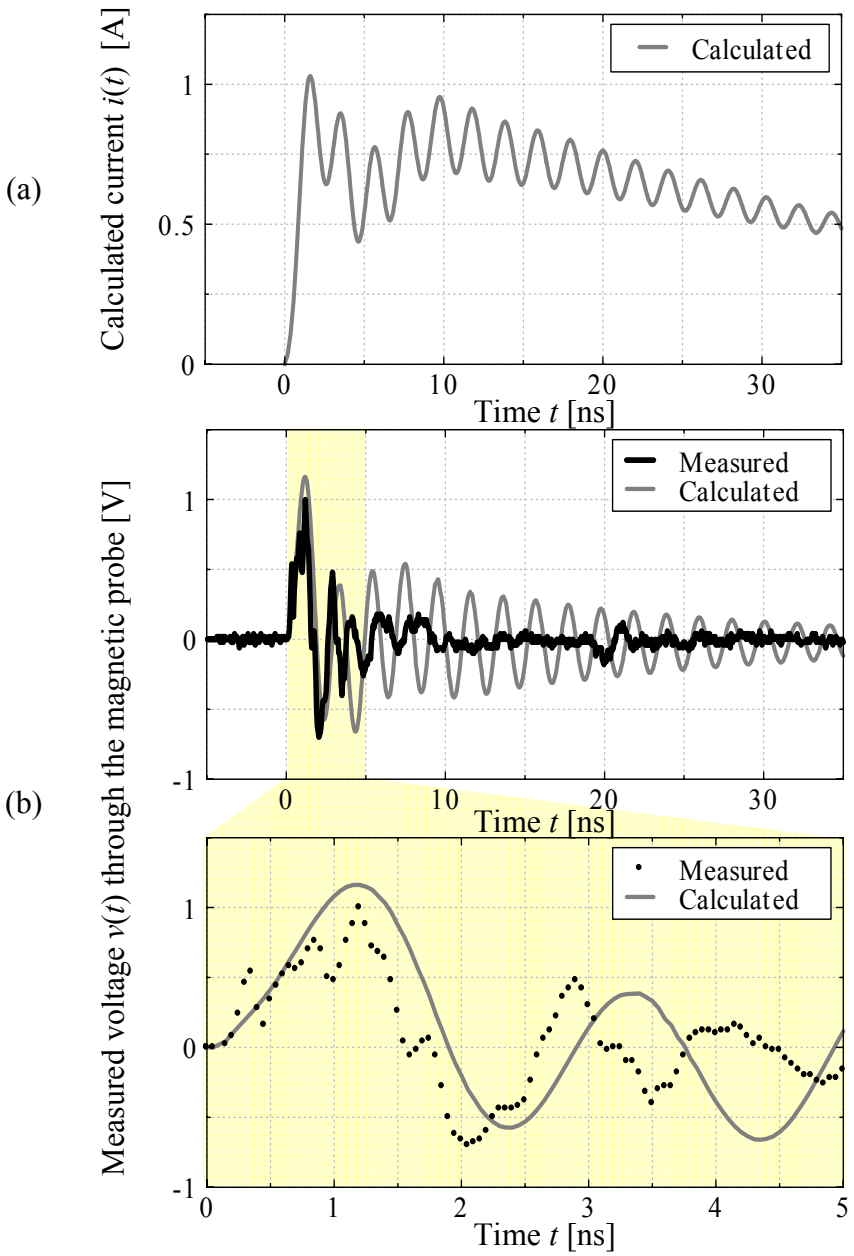

Figure 2.6: Calculated waveform of a discharge current and (b) measured and calculated magnetic near-field waveforms for contact discharge on the ground (V_C=0.3 kV).

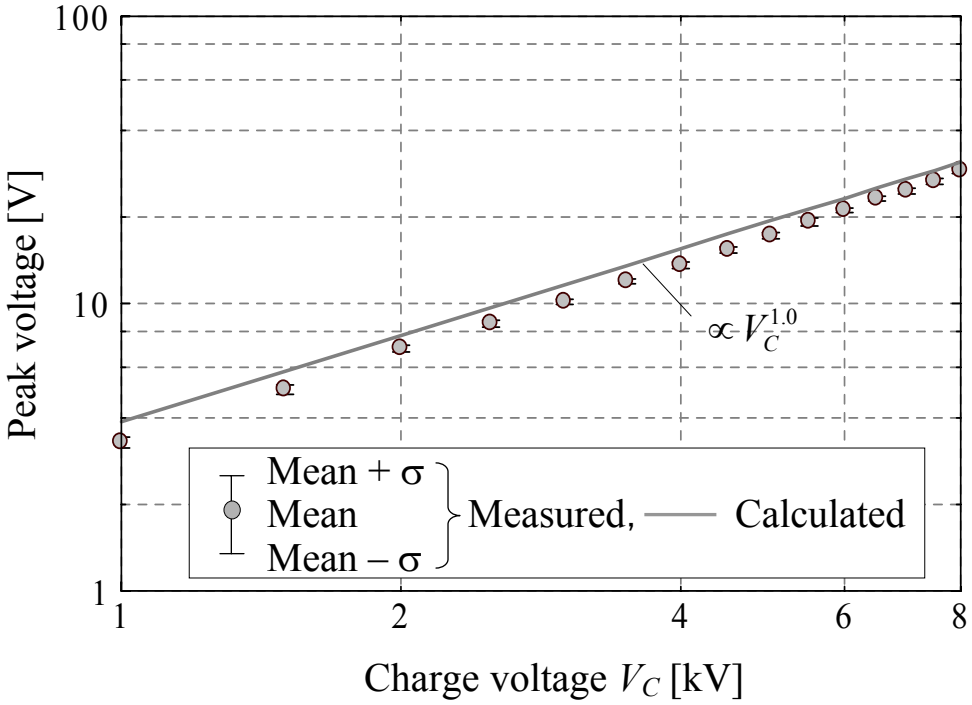

Figure 2.7: Dependence on charge voltages of peak levels of the waveforms measured with the magnetic probe.

2.5 Conclusion

Immunity testing for electronic equipment against ESD is described in the IEC standard, but even in the contact discharge, there is no guarantee that the IEC prescribed waveform is surely injected into actual EUT. In this chapter, firstly, in order to confirm the feasibility of an equivalent circuit model in Ref. [9], we measured with a 6-GHz wideband digital oscilloscope the discharge currents through a 50-Ω SMA connector and the resultant magnetic near-field for contact discharge. Secondly, we measured the magnetic near-field for contact discharge onto a ground, and examined the dependence on charge voltages of peak levels of the magnetic near-field. The result showed that in contact discharge, peaks of the magnetic near-field are almost proportional to the charge voltage, and this trend approximately agrees with the calculated results.
Future tasks are predicting the discharge current waveforms of the air discharge and elucidating the dependence on the charge voltage of the magnetic near-field in this case.

References

[1] For example, T. Takagi, "Research and Development on EMC/EMI Measurements and Technologies in Japan", The Trans. of IEICE, Vol. J79-B-II, No.11, pp. 718–726, Nov.,1996.

[2] M. Honda, "EMI Aspects of the Metal-Metal ESD to the Electronic Equipment", J.IEICE, Vol.78, No.9, pp. 849–850, Sep., 1995.

[3] Japanese Industrial Standards Committee: "Electromagnetic Compatibility (EMC) -Part 4 : Testing and measurement techniques -Section2. Electrostatic discharge immunity test", JIS C 1000-4-2: 1999 (IEC 61000-4-2: 1995/Amd. 1),1999.

[4] J. Sroca, "Target Influence on the Calibration Uncertainty of ESD Simulators", Proc. of IEEE International Symposium on EMC, Zurich, 37G4, 2001.

[5] T. Gotoh, O. Fujiwara, S. Ishigami, Y. Yamanaka, "Characteristic measurement of transfer impedance of Pellegrini target in contact discharge with ESD-gun", IEICE Technical Report, EMCJ2003-68, pp. 9–13,Oct., 2003 (in Japanese).

[6] For example, R. Jobava, D. Pommerenke, D. Karkashadze, P. Shubitidze, R. Zaridze, S. Frei and M. Aidam, "Computer Simulation of ESD from Voluminouos Objects Compared to Transient Fields of Humans," IEEE Trans. EMC, Vol. 42, No. 1, pp. 54–65, Feb., 2000.

[7] N. Murota, "Characteristics of the Discharge Current by the Human Charge Model ESD Simulator", The Trans. of IEICE, Vol. J79-B-II, No.11, pp. 789–796, Nov., 1996.

[8] G. Cerri, R. De Leo and V. Mariani Primiani, "Theoretical and Experimental Evaluation of Electromagnetic Fields Radiated by ESD," Proc. 2001 IEEE EMC International Symposium, Montreal, Canada, pp. 1269–1272, 2001.

[9] O. Fujiwara, H. Tanaka, Y. Yamanaka, " An Equivalent Circuit Modeling of Discharge Current Injected in Contact with an ESD-gun", IEEJ Trans. FM, Vol. 123, No. 8, pp. 784–789, 2003.

[10] S.Nitta, Y.Kami, Y.Sato, A.Sugiura, S.Seto and O.Fujiwara: EMC Handbook, Asakura Bookstore, pp. 479–480, 1999.

Chapter 3

Characteristic measurement of transient currents injected by air discharge

3.1 Discharges onto the target

3.1.1 Introduction

The transient EM fields due to electrostatic discharge (ESD) events, which have broad-band frequency spectra, cause serious failure to high-tech information equipment [1−2]. From this perspective, an ESD-immunity test is being specified in the IEC 61000-4-2[3], which consists of contact and air discharges of an ESD-gun simulating the ESD events from a charged human body. The ESD-gun is required to calibrate with a specified current waveform injected by contact discharge on a specially designed target [3]. The current waveform for air discharge, however, is not being specified due to bad reproducibility, whose mechanism has not yet been elucidated. In addition, the waveform for air discharge is known to be affected by approaching speed of the gun [4]. Since actual ESD events occur with sparks, air discharge should be more faithful to them. Thus grasping the behavior of the current injected by air discharge would be helpful to establish the better ESD immunity testing.

In this chapter, to grasp the characteristics of discharge currents for air discharge in view of approaching speed of the gun, we measure the discharge currents for air discharge onto the target with respect to its approaching speed. The effects of the approaching speed on the discharge current behavior are also examined.

3.1.2 Measurement method of discharge current waveforms

Figure 3.1 shows a measurement set-up for air discharge of an ESD-gun onto the target. As a ground, an aluminum square plate with a size of 1m was placed horizontally at a height of 0.65m from the floor. The target was fixed at the center of the aluminum plate and was connected to a 6-GHz wide-band digital oscilloscope through a 50-Ω coaxial cable. As mentioned before, this target is a current transducer, which enables us to observe currents injected onto the input electrode as voltages appearing across a 50-Ω termination load. The ESD-gun was first fixed above the target vertically, and was connected to the aluminum plate through an earth return cable with a radius of 0.55 mm, which had a length of 50 cm for convenience, although the cable length specified in the IEC standard is 2 m.

An enlarged photo around the tip electrode and the target is shown in Figure 3.2. As shown in the figure, an ESD-gun was hung with a spring from wooden frame, and was approached to the target at a constant possible speed until a spark between the tip electrode and the target occurred. In this case, two intentionally speeds of approach were set: fast approach and slow approach. The former is the way that makes the ESD-gun approach rapidly to the target, and the latter is that making it approach as slow as possible. Current waveforms injected onto the target were observed as voltage waveforms appearing across a termination load of the 50-Ω coaxial cable with a digital oscilloscope (input resistance: 50Ω; bandwidth: 6 GHz, sampling rate: 20 GHz, resolution: 8 bit). 30 times measurements were made for the air discharge at each of the two approaching speeds.

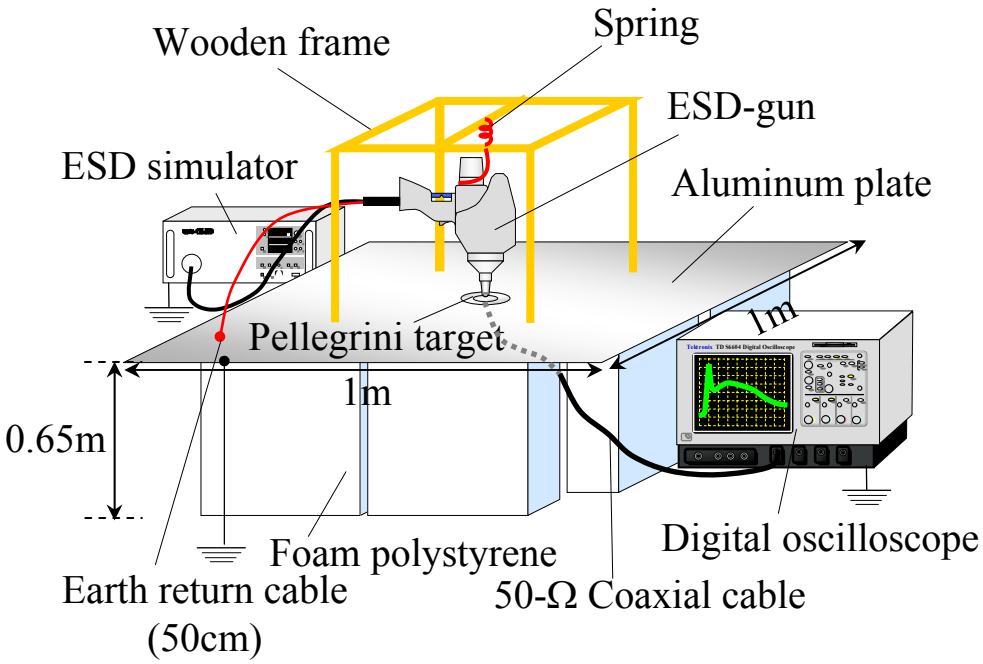

Figure 3.1: Measurement set-up for air discharge onto Pellegrini target.

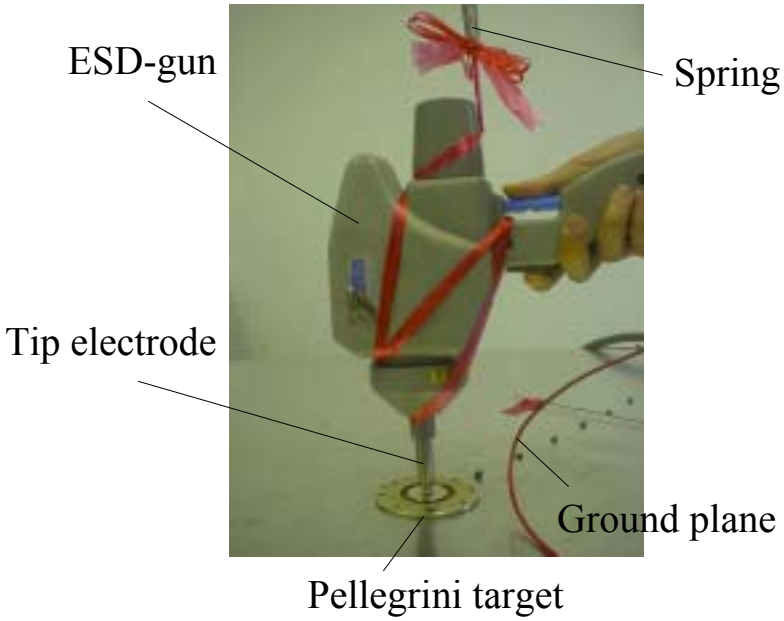

Figure 3.2: Photo around the tip electrode and Pellegrini target.

3.1.3 Results and discussion

Figures 3.3 and 3.4 show the current waveforms observed for the fast and slow approach of the ESD-gun with charge voltages of 3 kV and 8 kV, respectively. The abscissa and ordinate indicate time t in ns and current $i(t)$ in A, respectively. The lower figures show enlargements of the waveforms in the upper figures during a period of 0-5 ns. Thick black and thin red lines in the figures show typical waveforms of the discharge currents having the maximum and minimum first peaks, respectively, among the 30-times observed waveforms. Dotted lines show the current waveform specified in the IEC standard for contact discharge.

From these figures, it is found that the approaching speed greatly affects the discharge current waveforms: fast approach produces the shorter rise time and the higher current peaks compared to those for the slow approach. It is also found that in comparison with the case for the contact discharge, the fast approach gives a sharp current with a steeper rise-time and a higher peak, while the slow approach gives a gentle current with the shorter rise-time but the lower peak. The current waveforms after 20 ns almost overlap for all the cases.

Figure 3.5 shows the frequency spectra of the current waveforms observed for the ESD-gun with a charge voltage of 8 kV, together with those of the waveforms for contact discharge, which were obtained in the following way. Denote by $F(f)$ the frequency spectrum. Then it was calculated simply from

$$F(f) = E\left[\left|\int_{-\infty}^{\infty} i(t)\exp(-j2\pi ft)dt\right|\right] \tag{3.1}$$

where $i(t)$ is the discharge current. $E[\cdot]$ means "taking an expectation", which was obtained here as a value averaged over 30-times measurements for the air discharges and over 10 times for the contact discharge. As can be seen in the figure, the frequency spectrum for fast approach has the higher frequency components above 400 MHz, while the spectra below 80 MHz seem to be almost the same for all the cases.

In order to examine the properties of the discharge current behavior with respect to the approaching speeds of the ESD-gun, we obtained from the measured current waveforms

a relationship between their rise-time and current peak, which is shown in Figure 3.6. Also shown in the same figure is the IEC specified relationship between rise-time and current peaks for the contact discharge. The abscissa and ordinate indicate the rise-time t_r and first-peak current i_p normalized to the charge voltage V_C of the observed current waveforms, respectively. Notice that both rise-time and current peaks are given in logarithmic scales. Small circles indicate all the results obtained for the fast and slow approaches, respectively. The details of legends are shown in the figure. Large circles with bars represent "mean $\pm$ standard deviation" for the fast and slow approaches, respectively. Yellow zone shows the range of the rise time specified in the IEC standard for contact discharge.

Likewise in Figures 3.3 and 3.4, Figure 3.6 demonstrates that the fast approach gives the shorter rise-time and higher current peaks compared to those for the slow approach, which gives the shorter rise-time but lower current peak than the case for the contact discharge. The figure also indicates that there is a specific relationship between rise-time t_r and current peak i_p normalized to the charge voltage V_C regardless of the approaching speeds. An approximated equation for representing the above relation can be expressed as

$$\frac{i_p}{V_C} \propto t_r^{-0.75} \tag{3.2}$$

which is shown in Figure 3.6 with a solid line. This expression should include the frequency characteristics of the target and digital oscilloscope. Since the oscilloscope has a 6-GHz bandwidth, accurate measurement can be done for the waveform with a rise-time of over 100 ps. The target, however, is known to have a resonance at around 3 GHz for its transfer impedance [5], while the transfer impedance was also shown in Ref. [6] to have a flat frequency response below 1 GHz . This finding shows that the observed waveform with a rise-time of over 0.35 ns should be identical to the injected current from the ESD-gun via the target, which ensures that Eq. (3.2) holds for the slow approach.

For the fast approach, however, all the obtained rise-times are shorter than 0.35 ns, which needs to modify Eq. (3.2) according to the frequency response of the target.

Nevertheless, the specific relation expressed as Eq. (3.2) must be helpful to understand the current behavior and available to predict the worst-case ESD immunity testing for the air discharge even though it has poor reproducibility for the injected currents.

Note that we confirmed the specific relationship by the similar measurement using another commercially available ESD-gun (the Schaffner product), which is given by $\frac{i_p}{V_C} \propto t_r^{-0.50}$ [7]. In addition, the above equation has also been proven by Ref. [8] in the following way. The reference used a charged spheroid to simulate the ESD event from a hand-held metal piece, and experimentally showed the dependence on the arc length of the rise time and current peak for air discharge of a charged metal spheroid with a charge voltage of 5 kV. Using those results, we newly derived an approximated equation that can explain the relationship between the rise time and current peak for air discharge of such a metal spheroid, which is given by

$$\frac{i_p}{V_C} \propto t_r^{-0.61}. \tag{3.3}$$

These findings support that Eq. (3.2) holds between the rise time and current peak due to air discharge injection despite the poor reproducibility of the current waveforms.

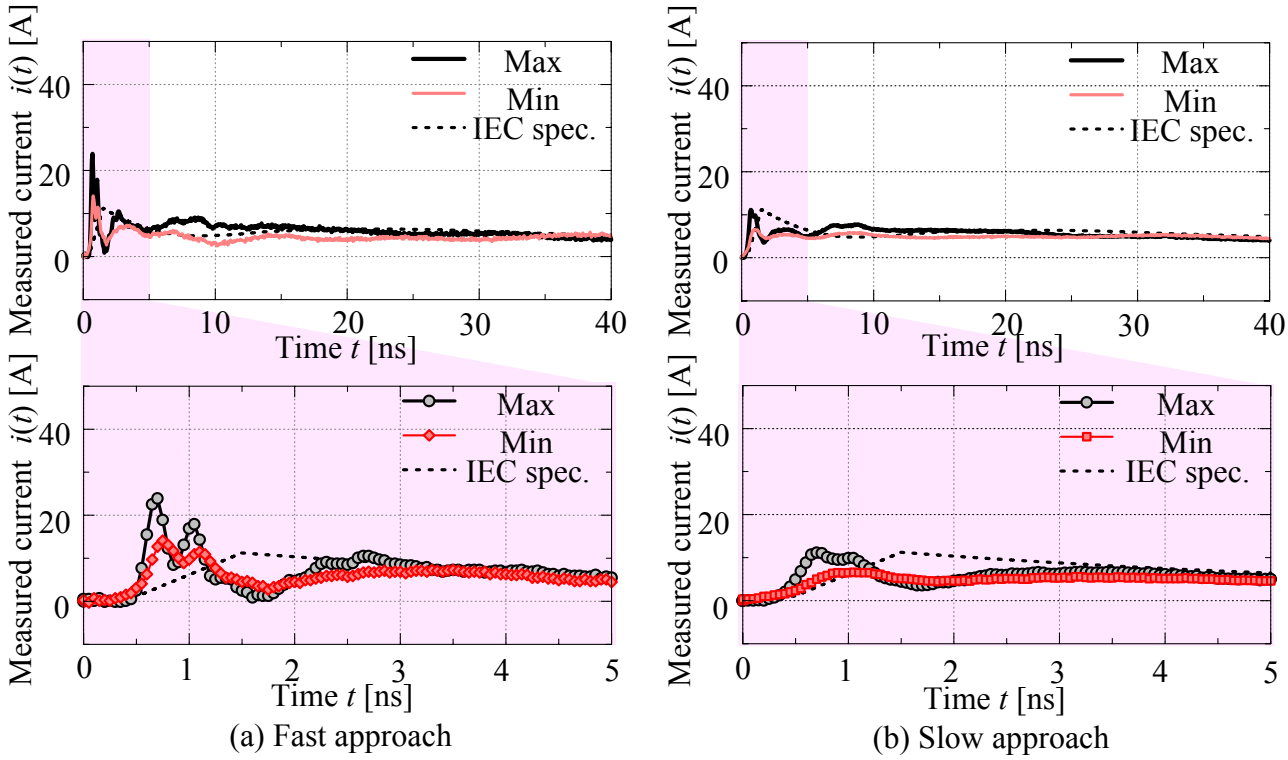

Figure 3.3: Measured waveforms for (a) fast approach and (b) slow approach of the ESD-gun with a charge voltage (V_C=3 kV).

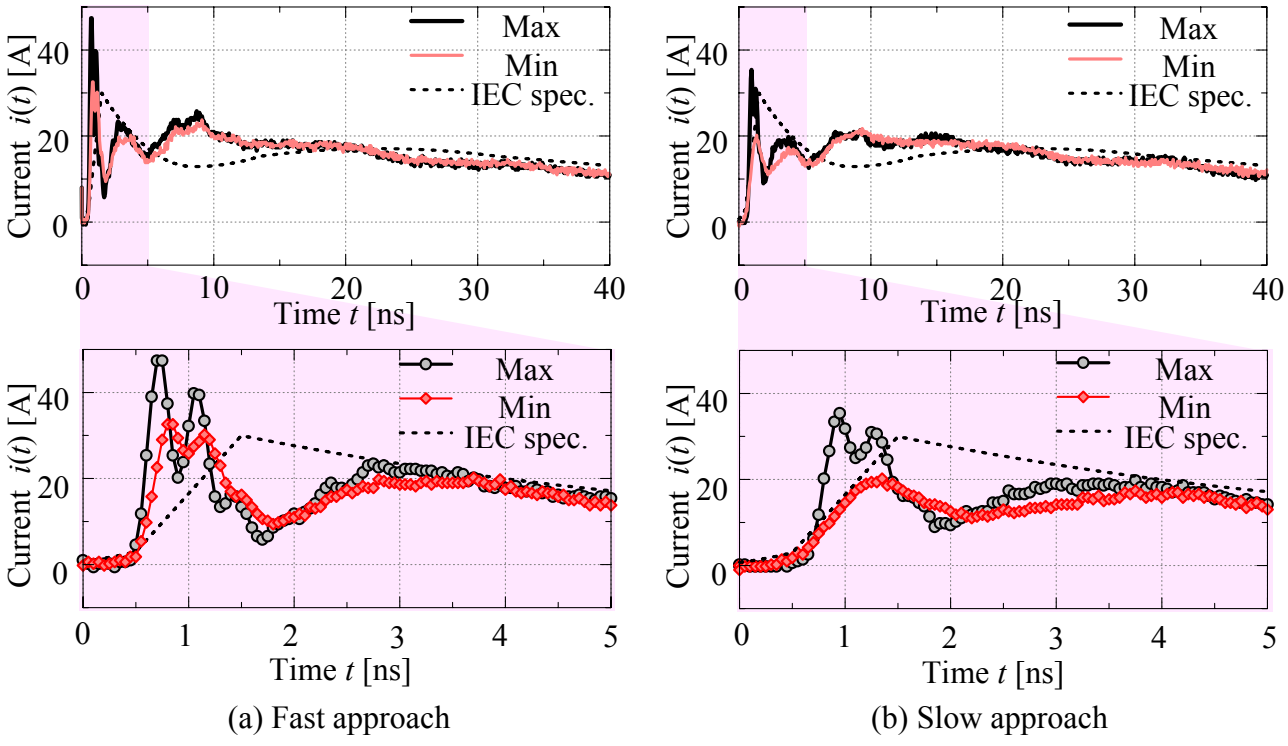

Figure 3.4: Measured waveforms for (a) fast approach and (b) slow approachof the ESD-gun with a charge voltage (V_C=8 kV).

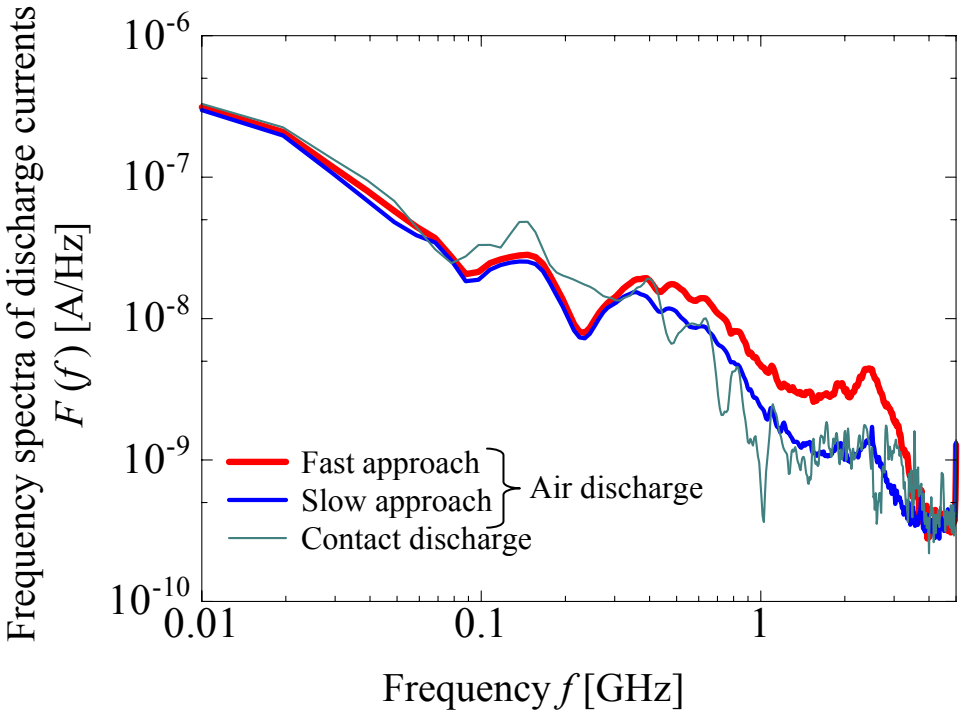

Figure 3.5: Power spectra of discharge currents (V_C=8 kV).

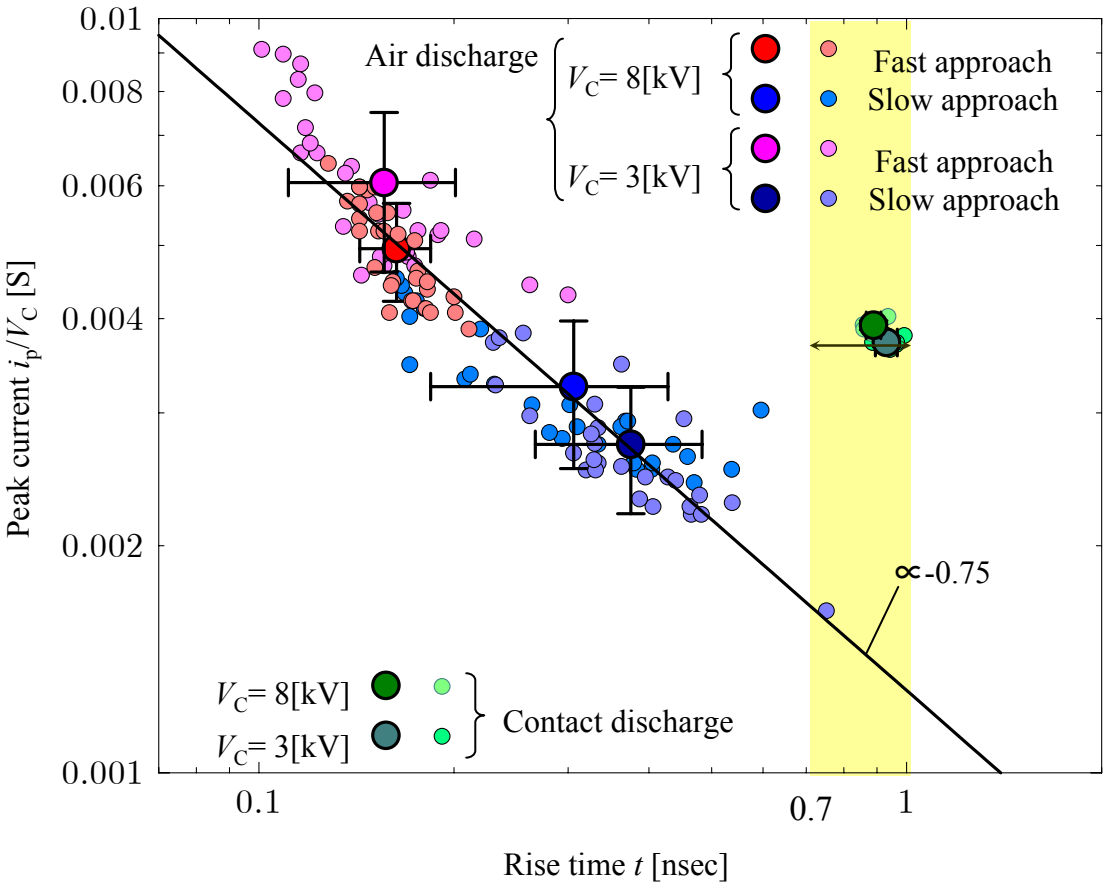

Figure 3.6: Relationship between the current peak divided by the charge voltage.

3.1.4 Conclusion

In conjunction with the approaching speed to the target and charge voltages, wide-band measurement of the discharge currents injected onto the target for air discharge of an ESD-gun has been done. As a result, it was found that the approaching speed greatly affects the waveforms of the discharge current with respect to the rise-time and current peaks. In comparison with the contact discharge, the fast approach produces the shorter rise time and the higher current peak, while the slow approach gives the shorter rise time but the lower peak, which was also confirmed from the frequency spectra of the discharge currents. Moreover, a specific relationship between the rise time and current peak was observed for air discharge of the ESD-gun regardless of its approaching speed, as follows:

$$\frac{I_p \cdot t_r^{\xi}}{V_C} = \text{constant}\,(\xi < 1)\,. \tag{3.4}$$

In view of the frequency response of the target, further measurement of the rise-time versus current peak with respect to the approaching speed for the air discharge should be done. From this perspective, in the next section, air discharge onto a ground is conducted in order to confirm whether or not the specific relationship described here holds.

3.2 Discharges onto a ground

3.2.1 Introduction

In the preceding section, to grasp the characteristics of discharge currents for the air discharge in view of the approaching speed of the ESD-gun, intentionally changing approaching speed of the gun, we conducted a wideband measurement of discharge currents with a 6-GHz digital oscilloscope.

As a result, we have shown that, for air discharge onto the target, despite the dependence of peaks and rise time of the discharge current waveforms on the approaching speed, there exists a specific relationship of

$$\frac{I_p \cdot t_r^{\xi}}{V_C} = \text{constant}\,(\xi = 0.75 < 1) \tag{3.5}$$

between them regardless of approaching speed of the gun [9]. However, transfer impedance of the target is frequency dependent [5–6], and the specific relationship above can be affected by the frequency characteristics of the target.

In this section, we investigated experimentally whether or not the relationship in Eq. (3.5) can be obtained for air discharge onto a ground. In case of discharges onto a ground assumed a chassis, discharge currents cannot be directly observed, and in case of air discharge, there may be a discrepancy of the tip electrode from the discharge target point, which would make the current estimation via a magnetic-field probe difficult. From this reason, in this section, we proposed a method that can estimate discharge currents from magnetic fields simultaneously measured with two magnetic-field probes regardless of the distance between the discharge target point and the probes.

3.2.2 Estimation method of discharge currents

Measurement method for magnetic near-field

Figure 3.7 shows a measurement set-up for air discharge onto the ground of an ESD-gun. Figure 3.7 (a) shows the overall measurement set-up, and Figure 3.7 (b) shows an enlargement around the tip electrode and magnetic field probe. As can be seen in Figure 3.7 (a), a 1-meter square aluminum plate is placed as a ground, and the ESD-gun is positioned above the center of the ground. The gun is hung via a spring from a wooden frame so that the approaching speed is kept relatively constant. The same shielded magnetic field probe shown in Figure 2.2 was used [10] .

In the set-up in Figure 3.7 (b), we assume that generated discharge current flows uniformly and concentrated along the axis of the tip electrode of the gun. Let $v(t)$ be the voltage induced in the magnetic field probe set at a distance d from the axis of the tip electrode, then the discharge current $i(t)$ is given by

$$i(t) = \frac{L}{\mu_0 a}\left(\frac{d}{a} + \sqrt{\left(\frac{d}{a}\right)^2 - 1}\right)\left\{\frac{v(t)}{Z_0} + \int_0^t v(t') \cdot \frac{dt'}{L}\right\}. \tag{3.6}$$

Here, μ_0 is magnetic permeability in vacuum, L is self-inductance of the magnetic field probe, and Z_0 is the characteristic impedance.

Eq. (3.6) indicates that the discharge current can be calculated from the induced voltage waveform in the magnetic field probe. However, this value is dependent upon the distance d between the tip electrode and the probe, which means that a deviation of the discharge point from the discharge target point can cause an error in the estimated current.

Figure 3.8 shows an image which represents this deviation of the tip electrode from the discharge target point in case of discharges onto the ground. In the air discharge, when the charged gun approaches, let δ be a deviation that appears in the distance d between the discharge point and center of the magnetic field probe. Then the estimated discharge current has the relative error ε due to the deviation δ, which is represented

by

$$\varepsilon = \frac{\frac{\delta}{a} + \sqrt{\left(\frac{d+\delta}{a}\right)^2 - 1} - \sqrt{\left(\frac{d}{a}\right)^2 - 1}}{\frac{d}{a} + \sqrt{\left(\frac{d}{a}\right)^2 - 1}}. \tag{3.7}$$

where d indicates the distance between the center axis of the tip electrode and the center of the magnetic field probe. The minimum distance, apperaing when the probe is pushed against the tip electrode, is d=12 mm.

Figure 3.9 shows the relative errors of estimated currents due to the deviation of the tip electrode from the discharge target point, which are calculated from Eq. (3.7). In the figure, the horizontal axis indicates the rate δ/a of the deviation δ with respect to the probe radius a(= 4.5 mm), and the vertical axis indicates the relative error ε for the discharge current. This figure indicates that a deviation comparable to the loop radius causes the estimated error exceeding 35 %.

Estimation method for discahrge current

In this section, we propose a method for estimating discharge currents for air discharge of an ESD-gun, which is independent of the distance between the discharge point and the magnetic field probe. Figure 3.10 shows the measurement configuration for estimating the discharge currents from the induced voltages in two magnetic field probes. As shown in the figure, the two magnetic field probes (called probe A and probe B) are arranged so that they are equidistant ($2d$ = 28 mm) from the center axis of the tip electrode. In a real air discharge, however, the tip electrode is not necessarily in the center of the two probes and some deviation toward one of the probes can be expected (in the figure a deviation toward probe B is shown). If this deviation δ occurs along the center line on a surface parallel to the loop surface of the two probes, then the distance between the center of each probe and the axis of the tip electrode is d + δ or d - δ as shown in Figure 3.10. Letting $v_A(t)$ and $v_B(t)$ be the voltages induced in probes A and B, respectively, one has the discharge current $i(t)$ given by

$$i(t) = \frac{L}{\mu_0 a}\left(\frac{d+\delta}{a} + \sqrt{\left(\frac{d+\delta}{a}\right)^2 - 1}\right)\left\{\frac{v_A(t)}{Z_0} + \int_0^t v_A(t') \cdot \frac{dt'}{L}\right\}$$

$$= \frac{L}{\mu_0 a}\left(\frac{d-\delta}{a}+\sqrt{\left(\frac{d-\delta}{a}\right)^2-1}\right)\left\{\frac{v_B(t)}{Z_0}+\int_0^t v_B(t')\cdot\frac{dt'}{L}\right\}. \tag{3.8}$$

In Eq. (3.8), using

$$I_A=\frac{v_A(t)}{Z_0}+\int_0^t v_A(t')\cdot\frac{dt'}{L},\ I_B=\frac{v_B(t)}{Z_0}+\int_0^t v_B(t')\cdot\frac{dt'}{L} \tag{3.9}$$

one has δ given by

$$\delta = a\cdot\sqrt{\left(\frac{I_A-I_B}{I_A+I_B}\right)^2\left(\frac{d}{a}\right)^2-\frac{1}{4}\cdot\frac{(I_A-I_B)^2}{I_AI_B}}. \tag{3.10}$$

Substitution of Eq. (3.10) into Eq. (3.8) yields,

$$i(t)=\frac{L}{\mu_0 a}\left[\frac{d}{a}+\sqrt{\left(\frac{I_A-I_B}{I_A+I_B}\right)^2\left(\frac{d}{a}\right)^2-\frac{1}{4}\cdot\frac{(I_A-I_B)^2}{I_AI_B}}\right.$$
$$\left.+\sqrt{\left\{\frac{d}{a}+\sqrt{\left(\frac{I_A-I_B}{I_A+I_B}\right)^2\left(\frac{d}{a}\right)^2-\frac{1}{4}\cdot\frac{(I_A-I_B)^2}{I_AI_B}}\right\}^2-1}\right]\times I_A(t), \tag{3.11}$$

which shows that the discharge current can be calculated only from the voltages induced in probe A and B.

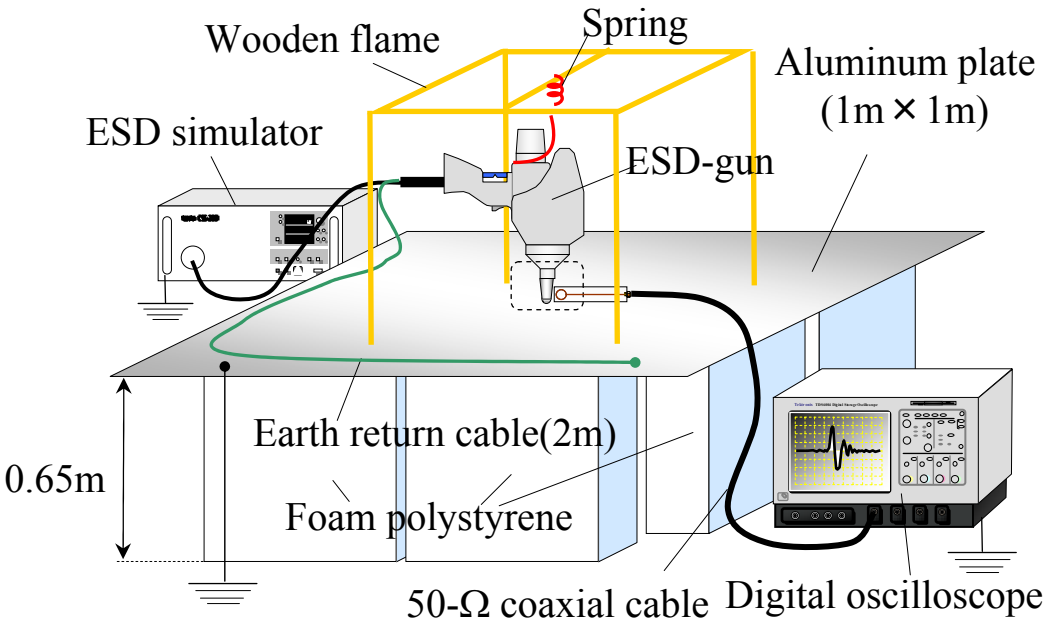

(a) Measurement set-up

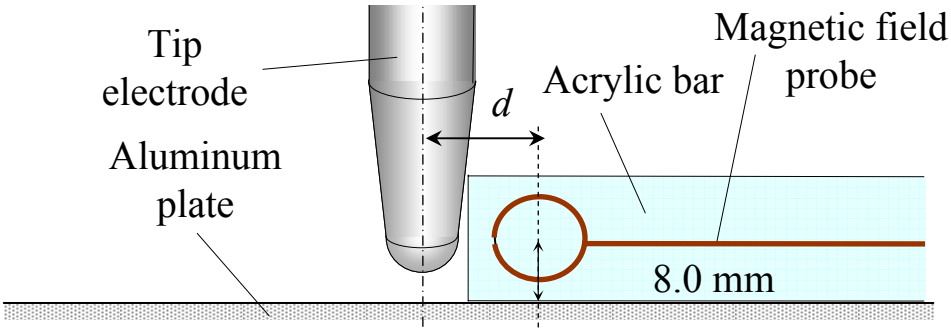

(b) Configuration of magnetic probe

Figure 3.7: Measurement set-up for air discharge onto a ground (a) and configuration of the tip electrode and the magnetic field probe(b)

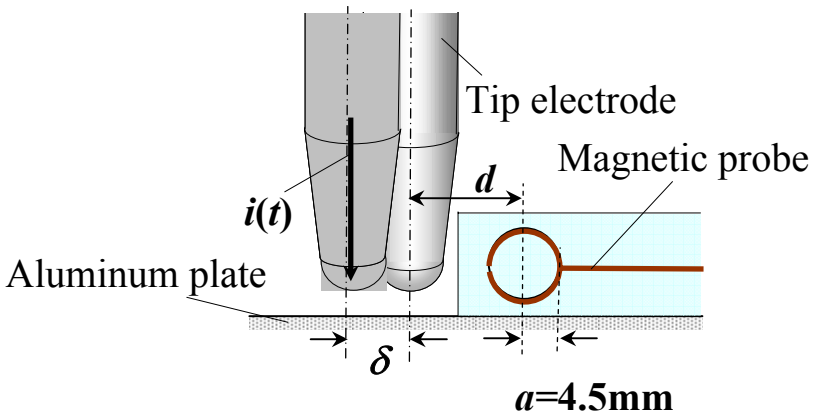

Figure 3.8: An image of deviation from the discharge point for air discharge onto a ground.

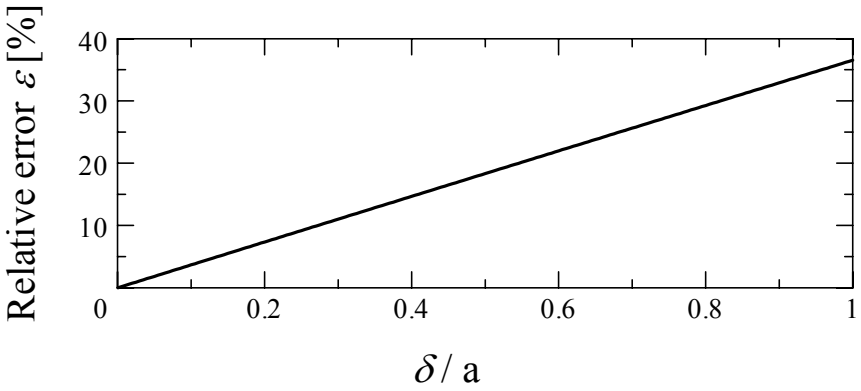

Figure 3.9: Relative errors of estimated currents due to deviation of the tip electrode from the discharge point.

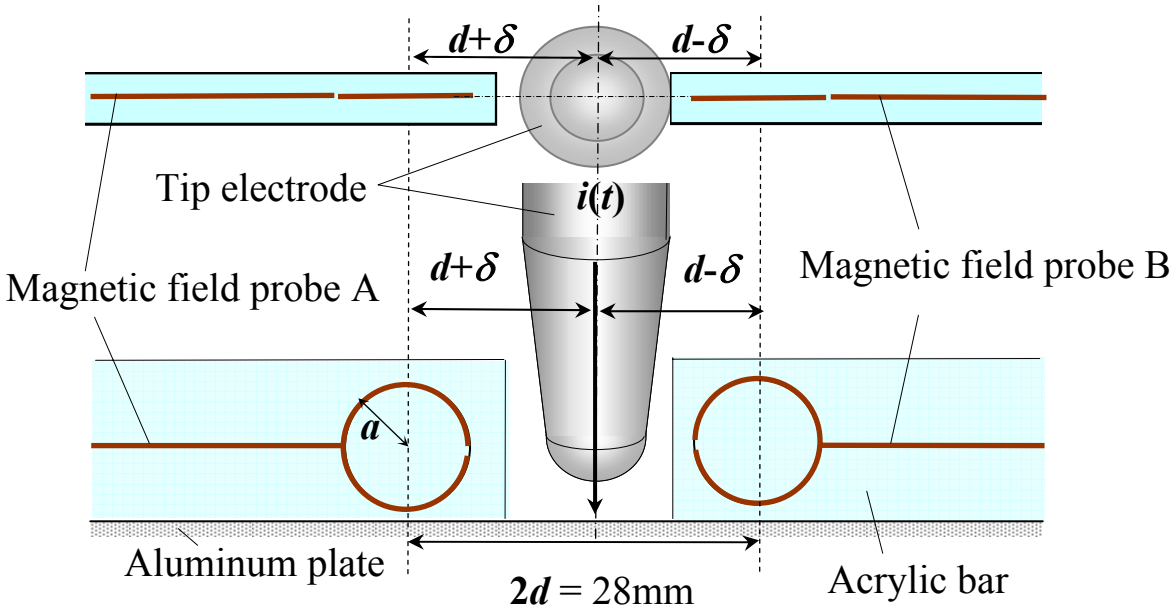

Figure 3.10: Measurement configuration for calculating discharge currents from induced voltages through two magnetic field probes.

3.2.3 Results and discussion

In this section, firstly, by simultaneous measurement of discharge current and magnetic near-fields for contact discharge on a 50-Ω SMA connector, we validate the method proposed in the previous section.
Secondly, we estimate the discharge current for air discharge onto the ground based on the measured waveforms for magnetic near-fields with respect to the relationship between charge voltage and approaching speed of the gun.

Contact discharge on an SMA conncetor

We conducted contact discharge on a 50-Ω SMA connector, whose frequency characteristics are flat up to 12 GHz, and then estimated the discharge current using the proposed method. Figure 3.11 shows the configuration of the magnetic field probes. The magnetic field probes are fixed on the ground surface in opposition to each other ($2d$=28 mm), and their outputs are connected via coaxial cables to a digital oscilloscope (input resistance: 50 Ω; bandwidth: 6 GHz; sampling frequency: 20 GHz; quantization bits rate: 8 bits). The output for the SMA connector was connected to another digital oscilloscope (input resistance: 50 Ω; bandwidth: 1.5 GHz; sampling frequency: 8 GHz, quantization bit rate: 8 bits).
Figure 3.12 shows voltage waveforms induced in the two magnetic field probes placed equi distantly from the tip electrode (a) and measured and calculated current waveforms for contact discharge on a 50-Ω SMA connector (b). From the figure, it is found that because the frequency characteristics of both probes are not the same and thus the measured waveforms do not match perfectly even though the two magnetic field probes are equidistant. On the other hand, the discharge current waveforms estimated from them closely match the measured waveforms.
Figure 3.13 represents voltage waveforms induced in the two magnetic field probes placed intentionally at a different distance from the tip electrode (a) and measured and calculated current waveforms (b) for contact discharge of on a 50-Ω SMA connector. In this case, the deviation δ is set 2 mm, and thus the distance between center of the probe A and axis of the tip electrode is 16 mm, while the distance between that

of the probe B and the axis is 12 mm. The figure shows that the measured induced voltage is higher in the magnetic field probe B than in probe A. On the other hand, the discharge current estimated from the induced voltages of the two probes is found to be between the estimated waveforms for either probe, and to closely match the measured waveforms.

Air discharge onto a ground

In the set-up in Figure 3.11, by approaching the charged ESD-gun with pressing the switch toward the ground until a discharge happens, we simultaneously observed the voltages induced in the two magnetic field probes. Note that by using a stainless-steel pole as a guide when approaching the gun toward the ground, and by approaching the gun closer to the ground with pushed the side opposite to the gun handle against the pole, the tip electrode of the gun was moved without any deviations perpendicular of the loop of the two probes. Charge voltages V_C were from 1 kV to 5 kV in 1 kV increments, and twelve trials were performed for each of two methods for the each charge voltage: a method in which discharge was performed by moving the gun toward the ground rapidly (approaching speed: about 20 - 25 cm/s; referred to as the fast approach), and a method in which the discharge was performed by moving the gun as slowly as possible (approaching speed: about 1.5 - 2 cm/s; slow approach). Measurements were performed in a room at 28 °C and a relative humidity of 30 %.

The results are shown in Figures 3.14 and 3.15. Figures 3.14 (a) and 3.15 (a) represent the induced voltage waveforms for probe A. Figures 3.14 (b) and 3.15 (b) represent an example of the discharge current waveforms estimated from the induced voltage waveforms in the probes A and B. These figures demonstrate that the peak currents increase with the increase of charge voltages, and the rise time tends to be gentle, and the tendency is more noticeable for the slow approach than for the fast approach at high charge voltages.

Figure 3.16 shows the relationship (mean value $\pm$ standard deviation) between rise time and current peak of the discharge current waveforms. Note that the vertical axis

indicates the current peak divided by the charge voltage. The open circles in the figure indicate the results for the fast approach, and the gray circles represent those for the slow approach. From the figure, it is found that among the discharge current waveforms for air discharges onto the ground, there exists a particular relationship between rise time and normalized current peak regardless of the charge voltages and approaching speed of the gun. It is also found that as charge voltages decrease the normalized peaks increase and rise time decreases and that these trends are not always independent of the approaching speed. The thick solid line in the figure represents a regression line for all of the data, and is given by

$$\frac{I_p \cdot t_r^{\xi}}{V_C} = \text{constant} \ \ (\xi = 0.57)\,, \tag{3.12}$$

which shows a relationship of the same type seen in Eq. (3.5).

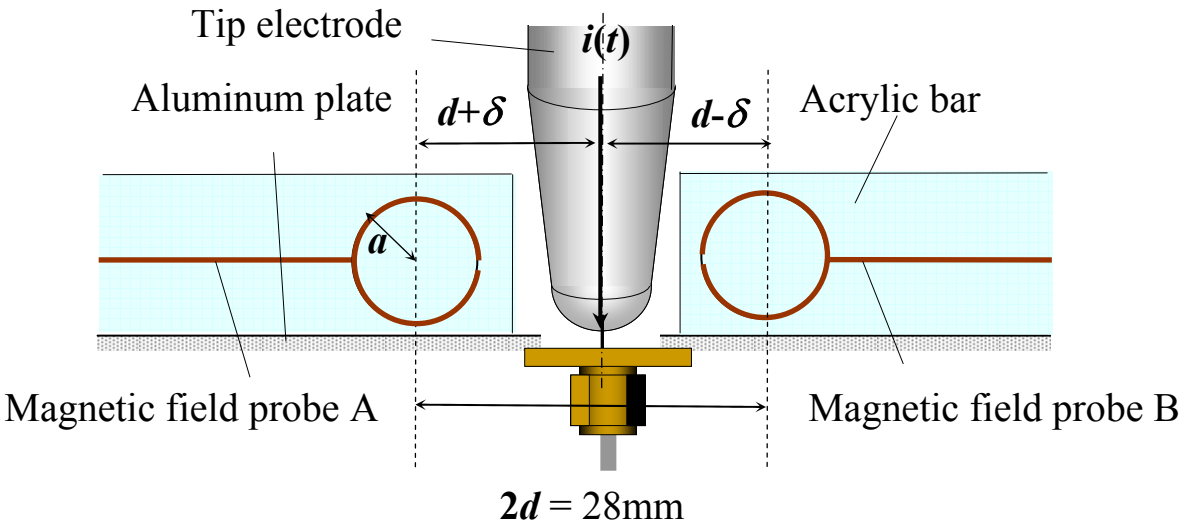

Figure 3.11: Validation of discharge currents estimated through two magnetic field probes for contact discharge to a 50-Ω SMA connector.

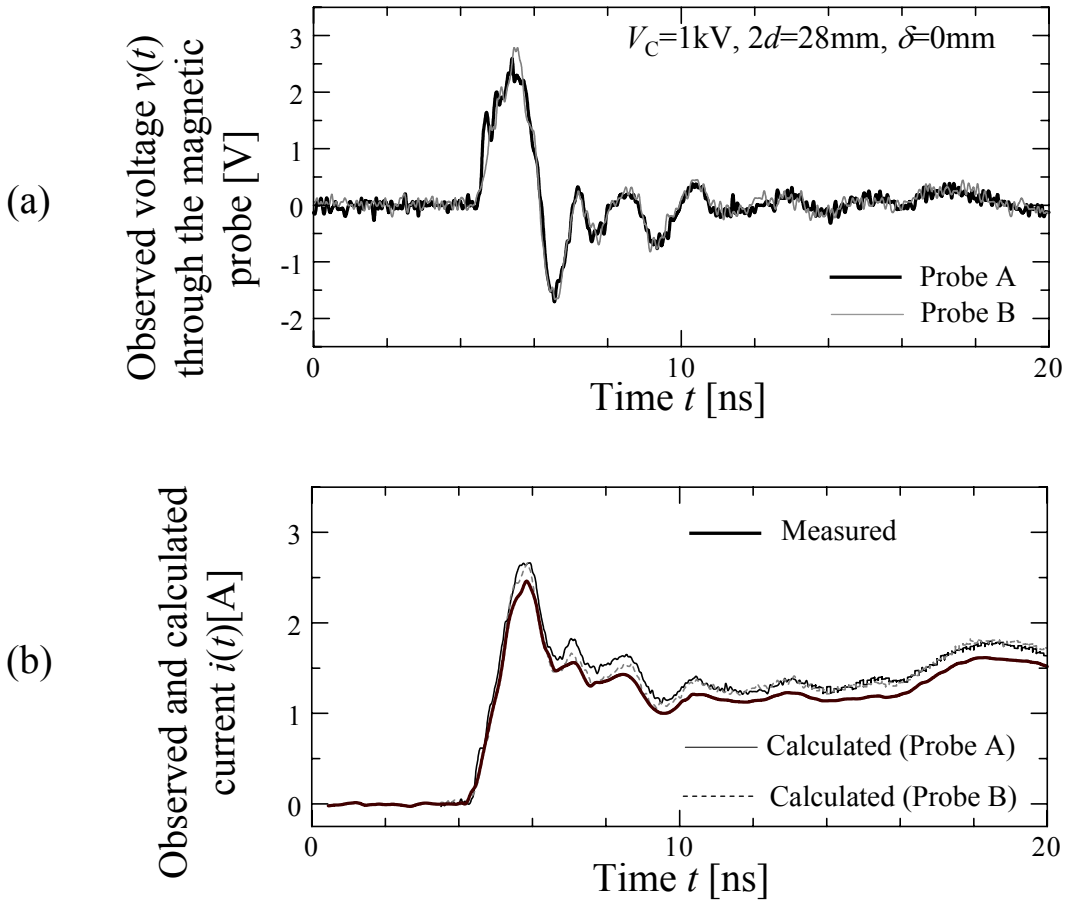

Figure 3.12: Voltage waveforms (a) induced in the two magnetic field probes placed at the equi-distance from the tip electrode and measured and calculated current waveforms (b) for contact discharge on a 50-Ω SMA connector.

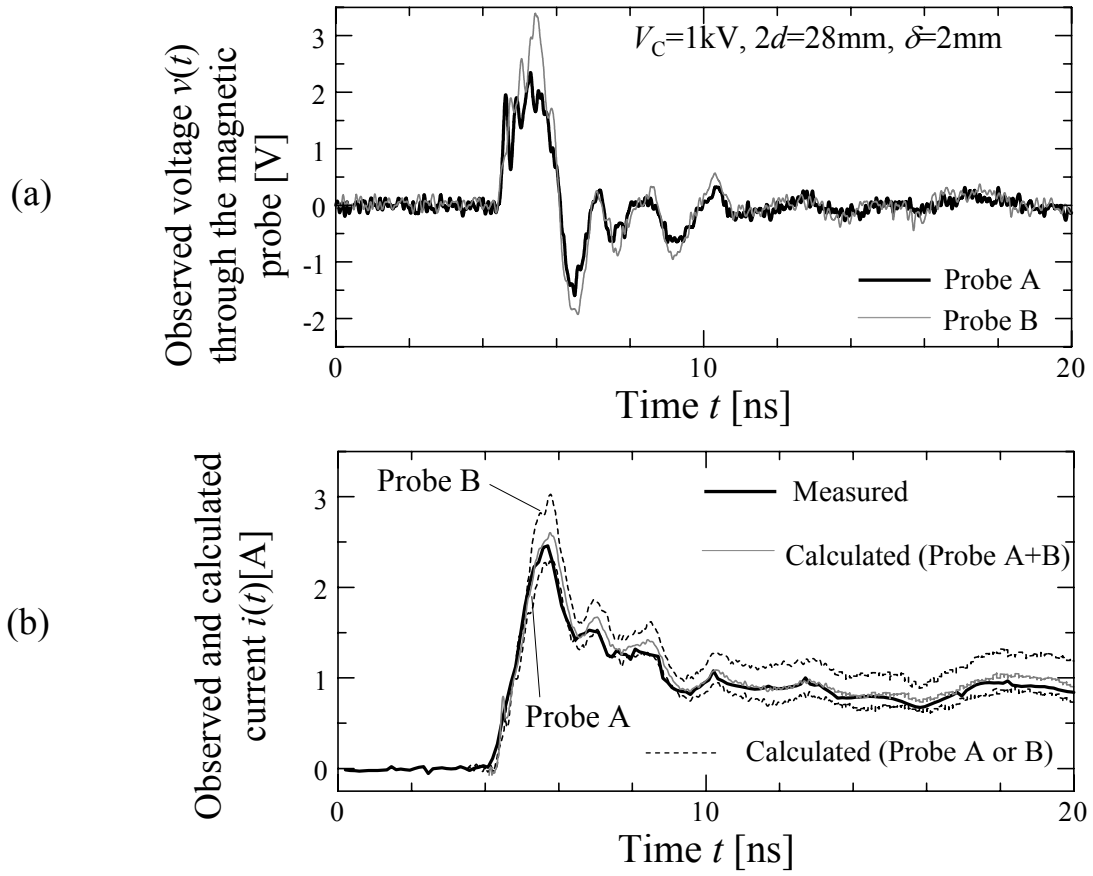

Figure 3.13: Voltage waveforms (a) induced in the two magnetic field probes placed intentionally at different distance from the tip electrode and measured and calculated current waveforms (b) for contact discharge on a 50-Ω SMA connector.

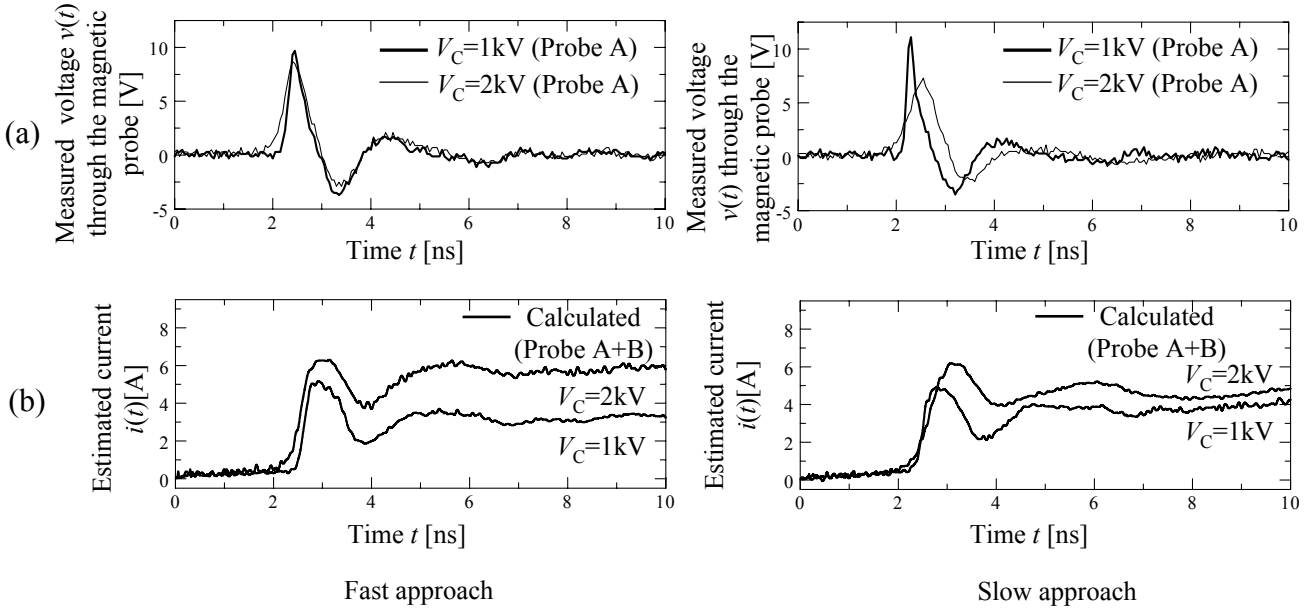

Figure 3.14: Measured voltage waveforms (a) induced in the two magnetic field probes and discharge waveforms (b) estimated for air discharge onto a ground ( ).

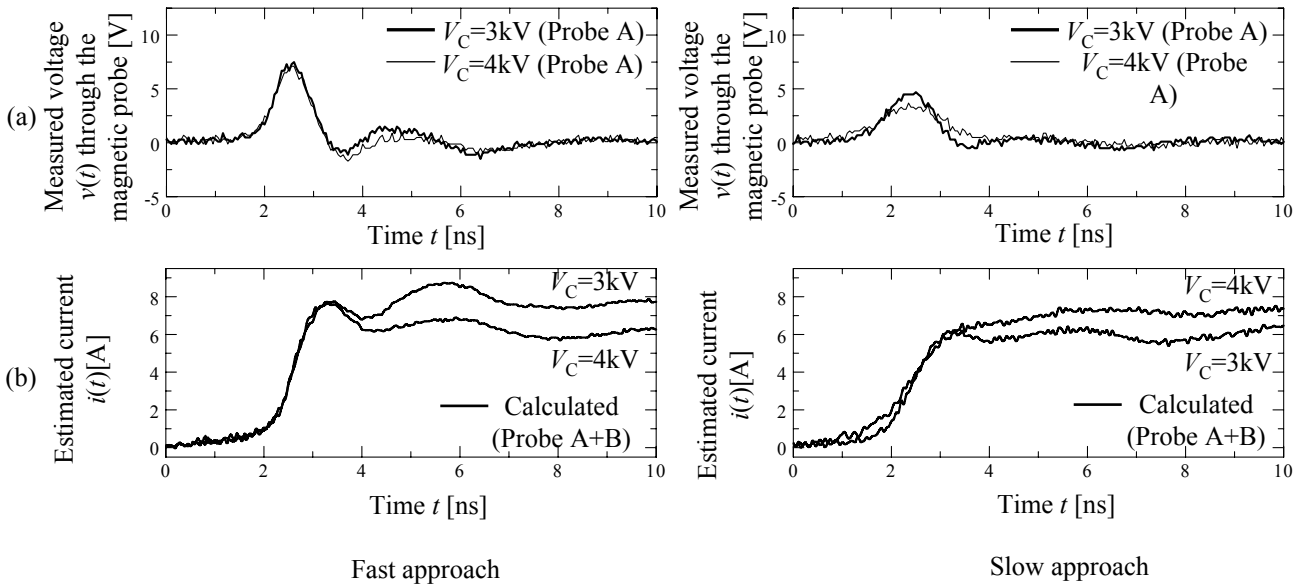

Figure 3.15: Measured voltage waveforms (a) induced in the two magnetic field probes and discharge waveforms (b) estimated for air discharge onto a ground( ).

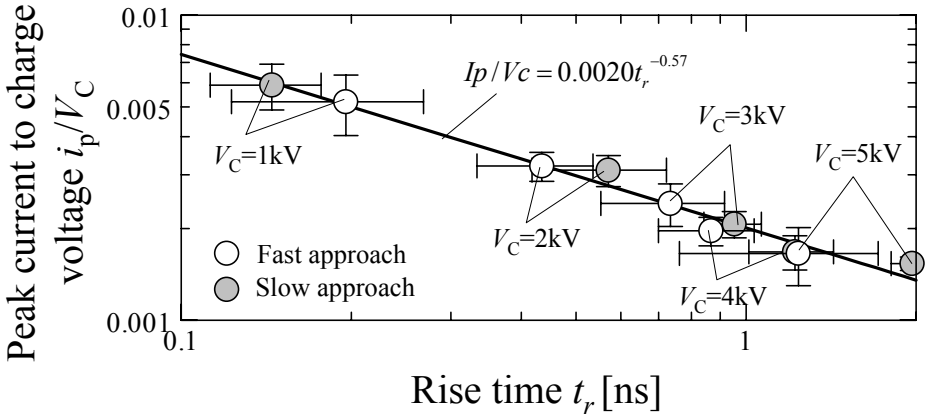

Figure 3.16: Relationship between rise time t_r and current peak i_p of discharge currents for air discharge onto a ground.

3.2.4 Conclusion

To improve the EM immunity of electronic equipment, grasping the characteristics of discharge currents for air discharge of an ESD-gun is useful. Thus we previously measured the discharge currents for air discharge onto an IEC-recommended target, and found that there exists a specific relationship given by Eq.(3.5) (ξ=0.75). In this section, we evaluated whether or not the same relationship holds in an air discharge to the ground.

Firstly, we proposed a method that can estimate discharge currents from magnetic fields simultaneously measured with two magnetic-field probes regardless of the distance between the discharge target point and the probes. After verifying the proposed method for contact discharge on a 50-Ω SMA connector, we showed that the above-mentioned specific relationship between peaks and rise time of discharge currents holds also for air discharge onto a ground. Regardless of the charge voltage or the approaching speed, the specific relationship described above holds in $\xi = 0.57$.

Future tasks include elucidating the mechanism of the specific relationship which holds between peaks and rise time of the current waveforms for the air discharge.

References

[1] For example, T. Takagi, "Research and development on EMC/EMI measurement and Technologies in Japan", The Trans. of IEICE, Vol.J79-B-II, No.11, pp. 718–726, Nov., 1996 (in Japanese).

[2] M. Honda,"EMI aspects of the metal-metal ESD to the electronic equipment", J.IEICE, Vol.78, No.9, pp. 849–850, Sept.,1995 (in Japanese).

[3] IEC 61000-4-2 Second edition, Electromagnetic compatibility (EMC) Part4-2: "Testing and measurement techniques, Electrostatic discharge immunity test",2001.

[4] For example, M.Masuigi, "Analysis of transient responses of electric fields accompanied by a movement of a discharge electrode", Trans. IEICE, Vol.J76-B-II, No.11, pp. 916—917, Nov., 1993 (in Japanese).

[5] J. Sroca," Target influence on the calibration uncertainty of ESD simulators", Proc. Int. Symp. on Electromagn. Compat., Zurich, 37G4,2001.

[6] T. Gotoh, O. Fujiwara, S. Ishigami, Y. Yamanaka, "Characteristic measurement of transfer impedance of Pellegrini target in contact discharge with ESD-gun", IEICE Technical Report, EMCJ2003-68, pp. 9–13,Oct., 2003 (in Japanese).

[7] I. Mori, O.Fujiwara, S. Ishigami, Y. Yamanaka, " A study on rise-timje and peak of the transient current injected through air discharge of an ESD-gun", IEEJ Trans. FM, Vol. 125, No.7,pp. 598–599, 2005.

[8] D. Pommerenke, "ESD:transient fields, arc simulation and rise time limit", Journal of Electrostatics, Vol.36, pp. 31–54, 2005.

[9] I. Mori, O. Fujiwara, S. Ishigami, and Y. Yamanaka, "Characteristic measurement of transient current injected by air discharge of an ESD gun," Proc. 2005 2004 International Symposium on EMC, Sendai, 2D1-1, pp. 417 - 420 June, 2004.

[10] O. Fujiwara, I. Mori, S. Ishigami, and Y. Yamanaka,"Calculation of magnetic near-field generated by the contact discharge of an ESD gun," IEEJ Trans. FM., Vol. 124, No. 9, pp. 763 – 768 Sep., 2004 (in Japanese).

Chapter 4

Characteristic comparison of discharge currents for contact and air discharges

4.1 6-GHz measurement

4.1.1 Introduction

In conjunction with high speed and low voltage operation of ICs, electromagnetic (EM) immunity of electronic devices has been degrading. Especially the transient EM fields due to electrostatic discharge (ESD) events have broadband frequency spectra, which cause a serious failure in high-tech information equipment [1−2]. From this perspective, an ESD-immunity test is being prescribed in the IEC 61000-4-2 [3], which gives two types of discharge methods, that is to say, contact and air discharges of an ESD-gun. The test levels are set from 2 kV to 8 kV for contact discharge, and from 2 kV to 15 kV for air discharge. As a strange phenomenon of ESD, low voltage ESD events (for example, below 3kV) are known to cause more serious damage in electronic devices than high voltage ESD does [2]. This mechanism still remains unknown.

In this section, in order to grasp the behavior of current waveforms injected by the ESD-gun with lower charge voltages below the IEC prescription, we measured with a 6-GHz digital oscilloscope discharge currents for contact and air discharges and show the dependence of rise time and current peak on the charge voltages. Because the

current waveforms for air discharge are affected by approaching speed of the gun with charge voltages in kilo volt [4], we tried two speeds of approach. In addition, to avoid the influence of transfer impedance of IEC-recommended targets, we used as a current injection target a 50-Ω SMA connector which has flat frequency characteristics up to 12 GHz.

4.1.2 Measurement method of discharge currents

Figure 4.1 shows a measurement set-up for air discharge of an ESD-gun (a) and an enlargement around the tip electrode and the inner conductor of a 50-Ω SMA connector. As a ground an aluminum square plate of 1 m each was placed and at the center of it a 50-Ω SMA connector is fixed. The connector is connected via a 50-Ω coaxial cable to a digital oscilloscope with a frequency band of 6 GHz and a sampling frequency of 20 GHz. The ESD-gun was hung vertically above the SMA connector through a spring from a wooden flame, and was connected to the ground through a 2m-long earth return cable. As shown in Figure 4.1 (b), for the purpose of easy contact, a metal plate with a diameter of 6 mm is attached to the inner conductor of the SMA connector.

While pressing the switch for charging, the gun was approached from a distance of about 6 cm the inner conductor of the SMA connector until a spark occurs. The discharge currents injected into the inner conductor were observed as voltage waveforms appearing across a termination load of 50 Ω, and by dividing them with 50Ω the current waveforms are obtained. The charge voltages were set 500 V, 700 V, and from 1 kV to 2.5 kV every 0.5 kV. The gun was approached with two intentionally different speeds: fast approach (approaching speed: approximately 20 cm/s) and slow approach (approaching speed: approximately 2 cm/s). Ten times measurements were conducted every charge voltage and approaching speed.

For contact discharge, the ESD-gun was fixed perpendicularly on the inner conductor of the SMA connector, and observed the discharge current waveform by the same way. Five times measurements every charge voltage were done.

The measurements were performed in a room at 26 °C and a relative humidity of 40 %.

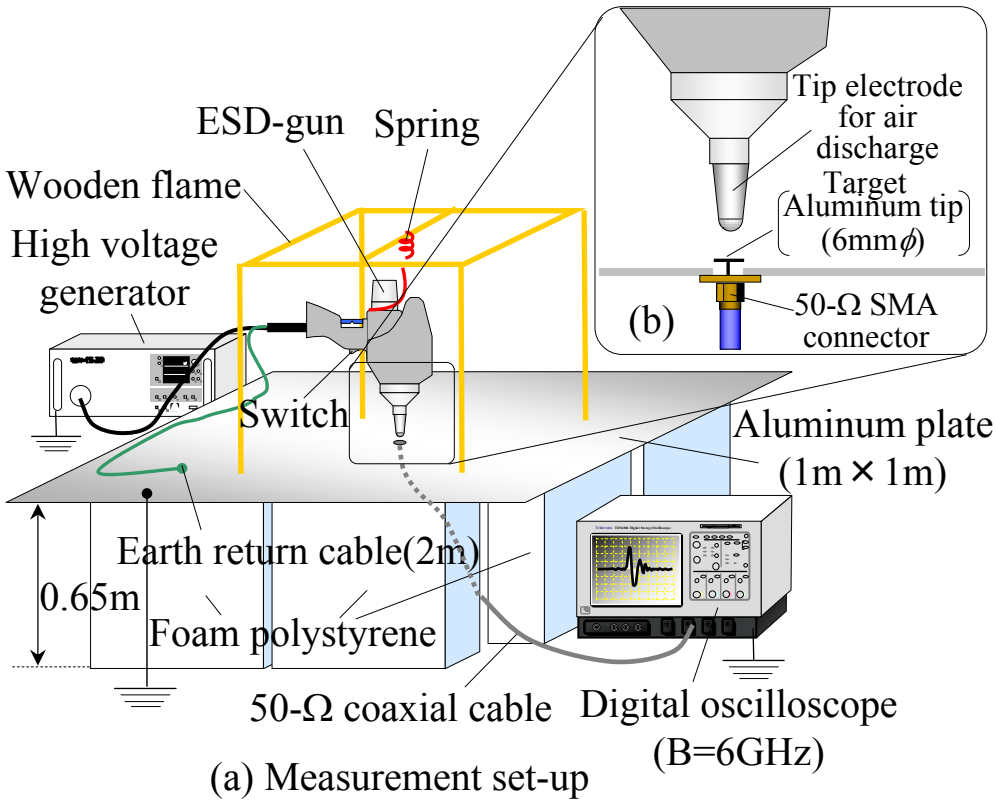

Figure 4.1: Measurement set-up for air discharge of the ESD-gun onto an inner conductor of a 50-Ω SMA connector (a), and enlargement around the tip electrode and the inner conductor (b)(B=6GHz).

4.1.3 Results and discussion

Figure 4.2 shows examples of measured current waveforms for charge voltages V_C of 0.5 and 2.5 kV. The horizontal axis indicates time in ns and the vertical axis indicates discharge current in A. They are shown from the beginning of the discharges to 5 ns, and the waveforms for V_C=0.5 kV are shifted the horizontal axis for viewability. Thick solid black lines indicate the measured waveforms for fast approach, the thin gray line indicate those for slow approach, and the dotted lines indicate those for contact discharge. From this figure, in V_C=0.5 kV, we found that the waveforms for air discharge is not affected by the approaching speed of the gun, and the rising slopes and current peaks for them are almost in good agreement. It is also found that compared with contact discharge, air discharge produces the higher current peaks and the steeper rising slopes. In V_C=2.5 kV, it is found that the fast approach gives the higher current peak than the slow approach, while contact discharge produces the same current peaks but the more gentle rise time than air discharge.

Figures 4.3 (a) and (b) indicate the dependence of peak current and that of rise time on charge voltages, respectively. The horizontal axes indicate charge voltage in both figures, and the vertical axes indicate current peak in Figure 4.3 (a) and rise time in Figure 4.3 (b).

In the figures, the open and closed circles, and crosses show the average values for fast and slow approaches, and contact discharge, respectively. The Error bars denote the standard deviation. For air discharge, they were average of 10 times measurement, and for contact discharge, they were that of 5 times.

In Figure 4.3 (b), the shaded regions indicate the IEC specification of rise time for contact discharge (t_r=0.7-1.0 ns) and the measurement limit due to the limitation of a bandwidth of the 6-GHz oscilloscope (rise time of the oscilloscope=70 ps) based on the flat response of the oscilloscope (rise time=0.40/3dB bandwidth) [5].

In Figure 4.3 (a), comparing the current peaks for contact and air discharges at charge voltages of below 2 kV, we found that the current peaks of air discharge are higher than those of contact discharge. We also found that below 2 kV the approaching

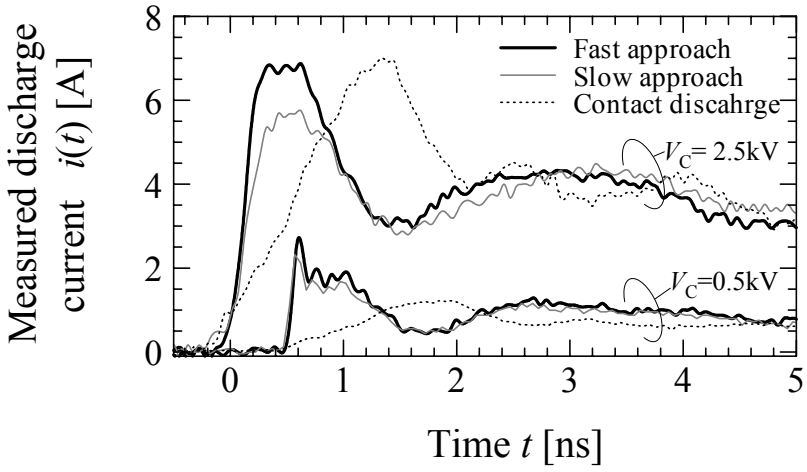

Figure 4.2: Measured waveforms for air discharge of the ESD-gun onto the inner conductor of the 50-Ω SMA connector (V_C=0.5, 2.5 kV)(B=6GHz).

speeds of the gun do not almost have influence on current peaks. Figure 4.3 (b) shows that measured rise time for contact discharge is almost constant and satisfies the IEC specification, while current rise time due to air discharge is shorter by far than the specification and it becomes shorter as charge voltage decreases. We also found that below 1 kV rise time is not almost affected by the approaching speed of the gun, and above 1 kV fast approach gives the shorter rise time.

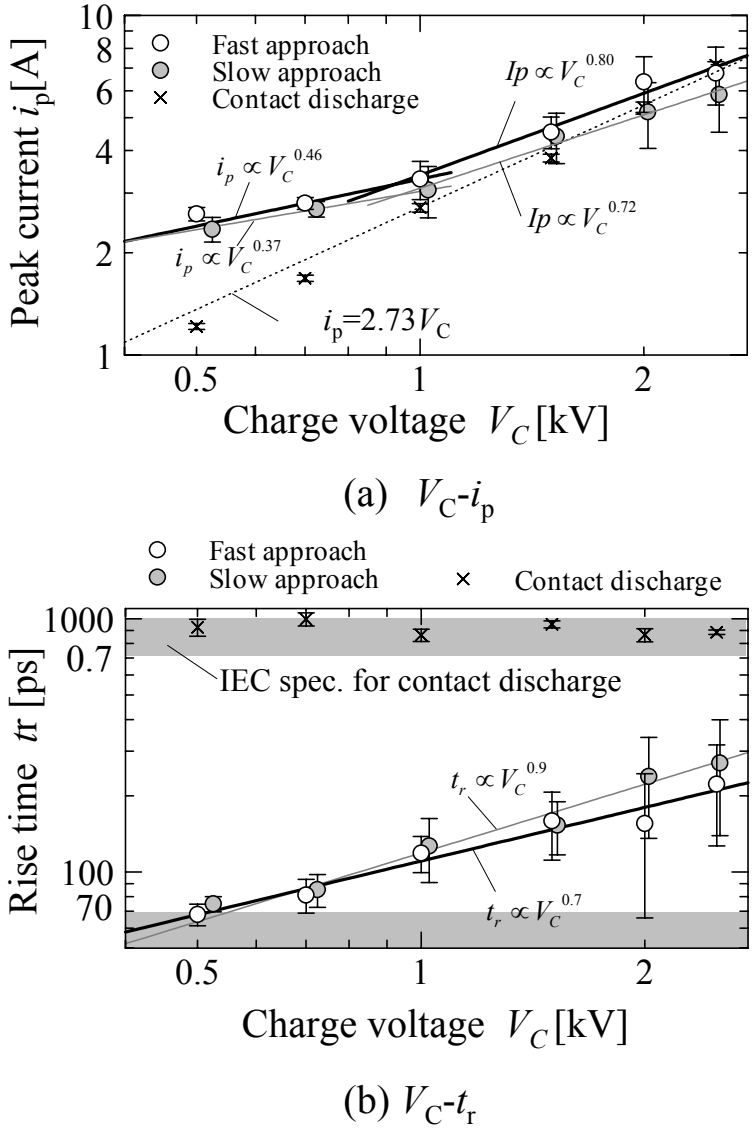

Figure 4.3: Dependence of peak current (a) and rise time (b) on charge voltages.

4.1.4 Conclusion

In this section, to understand the behavior of current waveforms for contact and air discharges of an ESD-gun with low charge voltages, we measured the discharge current waveforms onto a 50-Ω SMA connector and investigated the dependence of rise time and current peaks on charge voltages. As a result, we found that regardless of the approaching speeds, air discharge at charge voltages of below 1 kV gives the higher current peak and the shorter rise time than those of contact discharge.

This indicates that if the test levels of the ESD-gun are set 1 kV and below, air discharge can provide a severer immunity test method than contact discharge.

The rise time was also found to reach a measurement limit due to the limitation of a bandwidth of the oscilloscope (70 ps). Thus in the next section more wideband measurement for air discharge is described.

4.2 12-GHz measurement

4.2.1 Introduction

In the preceding section, in order to understand the behavior of discharge currents for an ESD-gun with low charge voltages , we measured with a 6-GHz digital oscilloscope discharge currents for air discharge for charge voltages below 2.5 kV. From the viewpoint that the rise time and current peaks of discharge currents are the dominant factors of the severity for immunity testing, we investigated them. As a result, we found that for charge voltages below 500 V, the rise time reaches a measuring limit due to a bandwidth of the digital oscilloscope [6].

In this section, at first, with a 12-GHz digital oscilloscope, we measured discharge currents for air discharge at charge voltages below 1 kV, and investigated the characteristics of discharge currents for contact and air discharges focusing on their rise time and current peaks.

4.2.2 Measurement method of discharge currents

Figure 4.4 (a) shows an experimental set-up for measuring discharge current waveforms for air discharge of an ESD-gun. Also shown in Figure 4.4(b) is an enlargement around the tip electrode of the ESD-gun and a 50-Ω SMA connector. An aluminum square plate with a size of 1 m was placed as a ground horizontally on a wooden desk at a height of 0.65 m from the floor. As can be seen in Figure 4.4 (b), a 50-Ω SMA connector was fixed at the center of the aluminum plate, which was connected through two 20-dB attenuators in series and a 50-Ω coaxial cable to a digital oscilloscope with a frequency band of 12 GHz and a sampling frequency of 40 GHz. The ESD-gun was hung vertically above the SMA connector through a spring from a wooden flame, and was connected to the ground plate through an earth return cable with 2 m long.
While pressing the switch for charging, we approached the gun from a distance of about 6 cm the inner conductor of the 50-Ω SMA connector until a spark happened. The charge voltages were set from 200 V to 1000 V (every 100 V) and 7-times measurements were conducted for each charge voltage. The approaching speeds were about 20 cm/s. Since we have already shown that below 1 kV the approaching speed of the gun does not affect the discharge current waveforms, in this section, we used one kind of the approaching speed (the same speed as the fast approach in the previous section).

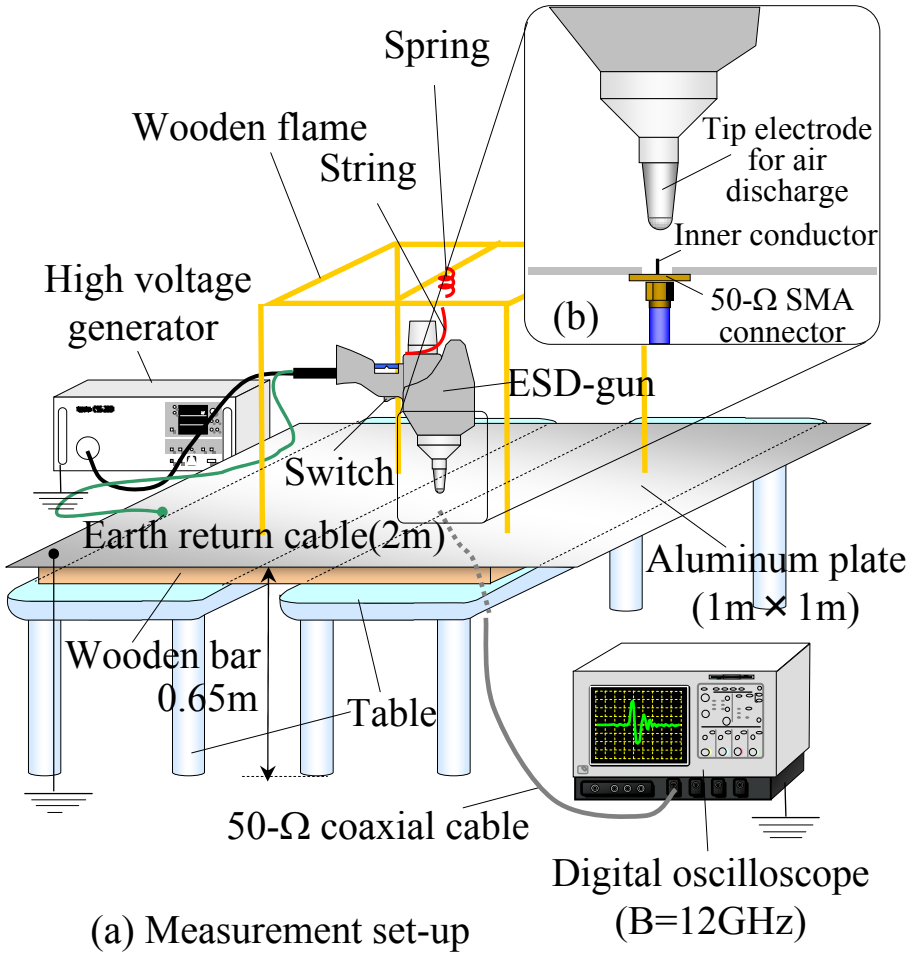

Figure 4.4: Measurement set-up for air discharge of the ESD-gun onto an inner conductor of a 50-Ω SMA connector (a), and enlargement around the tip electrode and the inner conductor (b) (B=12GHz).

4.2.3 Measurement result

Figure 4.5 shows observed current waveforms at charge voltages of 300, 600, and 900 V. The abscissa and ordinate indicate time t in ns and current $i(t)$ in A, respectively. The upper figure shows an enlargement of the waveforms in the lower figure during the period of -0.5 to 1.5 ns. Each dot indicates measured points at 25 ps interval. The time origin of $t = 0$ was taken at the intersection time point of the tangent line to the rising slope of each current waveform. This figure demonstrates that as charge voltages increase, the peak currents increase, while rise time does not almost change.

Figure 4.6 shows the dependence of measured rise time t_r on charge voltage V_C. In this figure, red and blue circles indicate measurement results and the results that we previously measured with a 6-GHz oscilloscope [6], respectively. Here, the above-mentioned rise time is defined as the time interval of the leading edge between the instants at which the instantaneous value first reaches specified lower and upper limits of 10 % and 90 % of current amplitude, respectively. Figure 4.6 demonstrates that for charge voltages below 600 V, the rise time is close to 35 ps corresponding to the measuring limit specified for the 12-GHz digital oscilloscope we used, which is shown with solid line. The measuring limit (70 ps) specified for the 6-GHz oscilloscope was also shown in the same figure with dotted line.

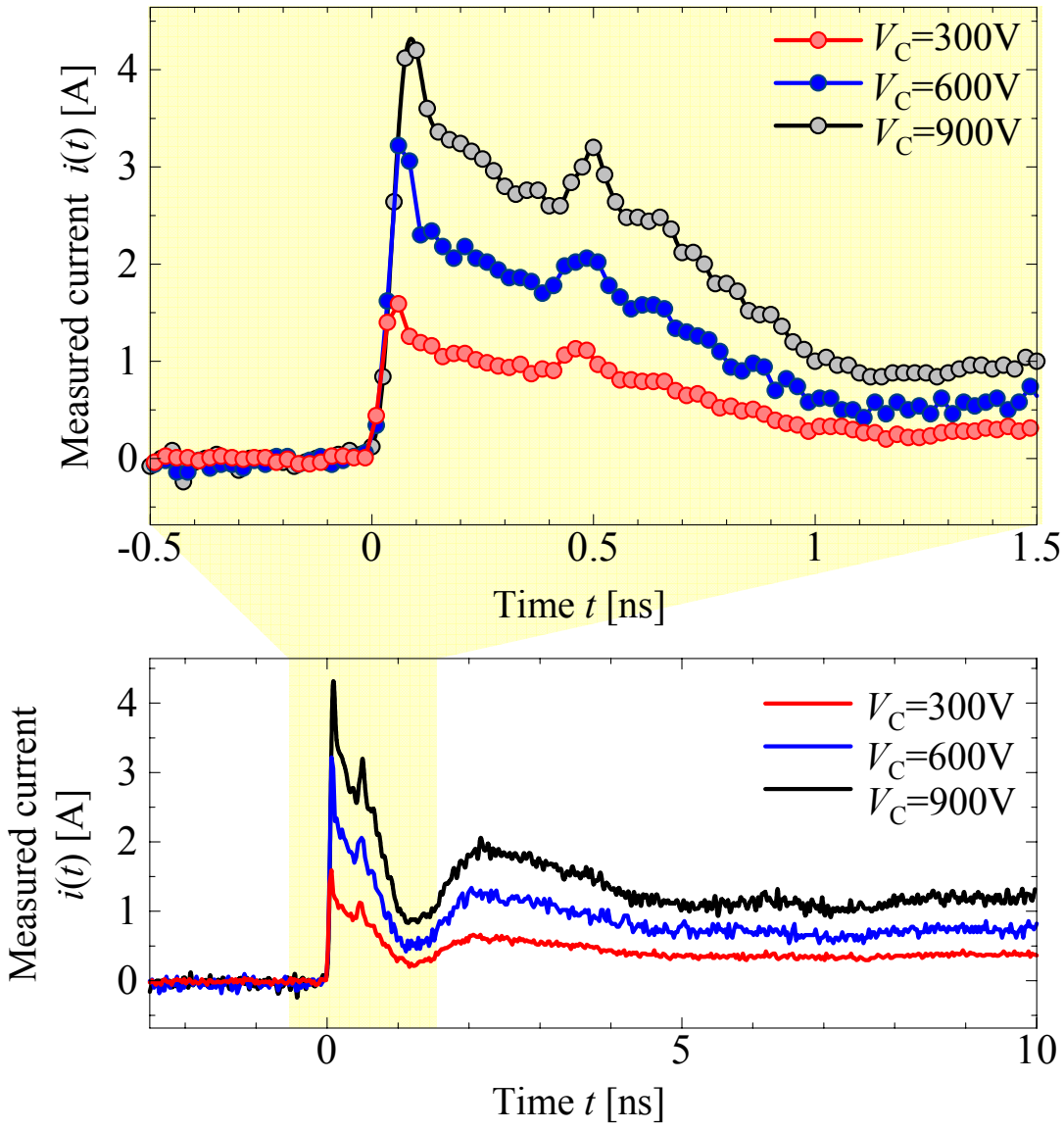

Figure 4.5: Observed current waveforms for air discharge of an ESD-gun onto the inner conductor of the 50-Ω SMA connector (V_C=300, 600, 900V) (B=12GHz).

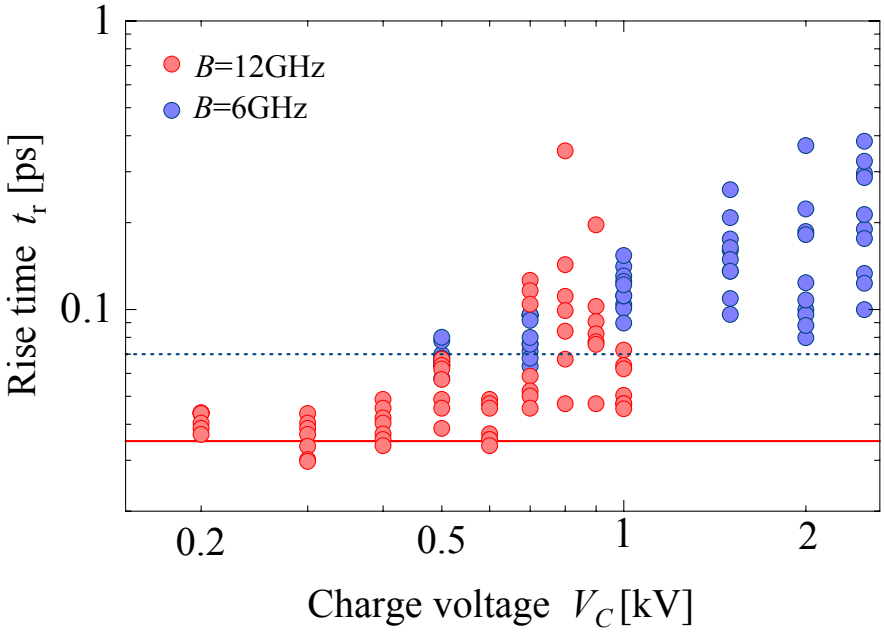

Figure 4.6: Dependence of rise time on charge voltage (B=12GHz).

4.2.4 Conclusion

With a 12-GHz digital oscilloscope, we measured discharge currents for air discharge with low charge voltages below 1000 V. We found that the rise time for charge voltages below 500 V reached a measurement limit of 35 ps due to the limitation of a bandwidth of the oscilloscope.

In the previous section, we have already shown with a 6-GHz measurement that below a charge voltage of 1 kV the current peak of air discharge is higher than that of contact discharge and the rise time for air discharge is shorter than that of contact discharge. The results obtained by 12-GHz measurement support those by 6-GHz measurement. Moreover, these results imply that air discharge can provide a severer immunity-test than contact discharge.

Future tasks are estimation of the rise time limit for air discharge at low charge voltages, comparison of these results with the real ESD phenomena, and proposal for the test condition for low charge voltages.

References

[1] M. Honda,"EMI aspects of the metal-metal ESD to the electronic equipment", J.IEICE, Vol.78, No.9, pp. 849–850, Sept.,1995 (in Japanese).

[2] Japanese Industrial Standards Committee: "Electromagnetic Compatibility (EMC) -Part 4: Testing and measurement techniques - Section 2. Electrostatic discharge immunity test", JIS C 1000-4-2: 1999 (IEC 61000-4-2: 1995/Amd. 1), 1999 (in Japanese).

[3] For example, M.Masuigi, "Analysis of transient responses of electric fields accompanied by a movement of a discharge electrode", Trans. IEICE, Vol.J76-B-II, No.11, pp. 916—917, Nov., 1993 (in Japanese).

[4] T. Gotoh, O. Fujiwara, S. Ishigami, Y. Yamanaka, "Characteristic measurement of transfer impedance of Pellegrini target in contact discharge with ESD-gun", IEICE Technical Report, EMCJ2003-68, pp. 9–13,Oct., 2003 (in Japanese).

[5] Agilent Technologies, "Understanding oscilloscope frequency response and its effect on rise–time", Agilent Note NO, 1420, pp. 1–8, Jan., 2003 (in Japanese).

[6] I. Mori, Y. Taka, O. Fujiwara and S. Ishigami, "Characteristic comparison of discharge current caused by electrostatic discharge gun for the IEC immunity testing," IEICE Trans. COMMUN. (Japanese Edition), Vol. J88-B, no.12, pp. 2401–2403, Dec. 2005.

Chapter 5

Conclusion

This thesis is a summary of a study on characteristic measurement of discharge currents from an ESD-gun.

In chapter-2, to grasp the levels of magnetic near-fields generated by contact discharge of an ESD-gun, we calculated the resultant magnetic near-field generated by contact discharge with an equivalent circuit model aimed at calculating the discharge current for contact discharge. Firstly, the feasibility of the circuit model was validated by simultaneous measurement of the discharge current and induced voltage at the magnetic field probe for contact discharge on a 50-Ω SMA connector. The measured and calculated waveforms from the rising slope to the first peak of induced voltage at the probe were in good agreement. Next, we investigated the dependence on charge voltages of the magnetic fields generated by contact discharge.

As a result, we found that the peak levels of the measured magnetic near-fields increased in proportion to charge voltages and its tendency approximately agreed with calculated results from the equivalent circuit model.

Future tasks, for example, are estimation of discharge currents for air discharge and elucidation of the dependence on charge voltages of peak levels of the magnetic near field for the air discharge.

In chapter-3, for the purpose of grasping the behavior of discharge currents injected by air discharge, firstly we observed with a 6-GHz digital oscilloscope the discharge current waveforms through the IEC-recommended target, with intentionally fast and slow approaches of the gun to it. As a result, we found that the approaching speed of

the gun greatly affects the waveforms of discharge currents with respect to rise time and current peaks. In comparison with waveforms of contact discharge, the waveforms of fast approach have the higher current peak and the shorter rise time, while those of slow approach have the lower current peak but the shorter rise time. A specific relationship between the rise time and current peaks for air discharge was also found regardless of the approaching speed of the gun.

Secondly, air discharge onto the ground assumed the chassis was conducted, and the relationship mentioned above was confirmed. In that case, because the discharge current for air discharge onto the ground can not be directly observed, and the discrepancy of the tip electrode of the gun from the discharge targeted point exists, we proposed an estimation method for discharge current for air discharge onto the ground using two magnetic field probes, which enable us to estimate discharge currents independent of the distance between the electrode and the probes. The estimated method was validated by simultaneous measurement of the discharge current and magnetic near-field induced at the probes for contact discharge on a 50-Ω SMA connector. As a result, we showed that the above-mentioned relationship also holds for air discharge onto the ground.

The future tasks are to elucidate the mechanism of the specific relationship between current peaks and rise time for air discharge, and to apply the relationship to ESD-immunity tests.

In chapter-4, grasping the characteristics of discharge currents for contact and air discharges of an ESD-gun with low charge voltages of 2.5 kV and below, we measured with wideband digital oscilloscopes discharge currents with respect to the charge voltages. As a result, we found that air discharge at charge voltage of 1 kV and below gives the higher current peaks and shorter rise time, and that the approaching speeds of the gun do not almost affect these characteristics. The finding above suggests that if the test levels of the ESD-gun are set 1 kV and below, air discharge can provide a severer immunity test method than contact discharge. The rise time was also found to reach a measurement limit due to the limitation of a bandwidth of the 12-GHz band oscilloscope (35 ps).

Future tasks are estimation of the rise time limit for air discharge at low charge voltages*, comparison of these results with the real ESD phenomena, and application of this result to the test condition for low charge voltages. In addition, because the waveforms for air discharge have very steep rising slopes, to measure them more accurately, to build more wideband measurement system should be considerd.

Finally, we would be grateful if this study will be of help to the investigation of ESD phenomena as well as ESD-immunity test methods.

∗The rise time limit of air discharge for low charge voltages are discussed in the appendix.

Acknowledgements

This thesis is a summary of my three-year-study conducted in the Graduate School of Engineering, Nagoya Institute of Technology. First of all, I would like to thank all of the people concerned directly or indirectly with my work.

Especially, I am deeply grateful to Doctor Professor Osamu Fujiwara, my supervisor, for his incredibly patient guidance, continuous support and valuable technical advice. It has been a great honour and the greatest experience in my life to be a member of his laboratory and to study under his instructions. I would like to thank Doctor Professor Nobuyoshi Kikuma for his helpful suggestion. I also thank Doctor Professor Wang Jianqing for his significant comments and advice, which always inspired me to greater efforts.

I would like to thank Dr. Akimasa Hirata and Dr. Yoshinori Taka for their practical advice and suggestions.

I would like to express my gratitude to Dr. Shinobu Ishigami and Mr. Yukio Yamanaka, National Institute of Information and Communications Technology, for useful comments and suggestions.

I would like to express my sincere thanks to Dr. Ken Kawamata, Hachinohe Institute of Technology, for useful discussion, comments and suggestions.

I must say thank you to all present and past members of Fujiwara Laboratory, Nagoya Institute of Technology. Their continuing support and encouragement have been helpful in the progress I have made in my work. In particular, I would like to thank Dr. Toshihiko Terado, Gifu University, for his practical advice for measurement techniques. I would also like to thank Mr. Hideyuki Tanaka and Mr. Eiichiro Tsuji, who were my senior when I was in undergraduate and master courses and now work for Toy-

ota Motor Corporation and Aisin Seiki Co., Ltd., respectively, for their kind supports and suggestions.

I also appreciate Ms. Satoko Fukukoka and Ms. Hiromi Saeki for their continuous encouragements.

Appendix A

Rise time limit of discharge currents for air discharge

A.1 Introduction

In Chapter-4, with a 12-GHz digital oscilloscope, we measured discharge currents for air discharge with low charge voltages below 1000 V. As a result, we found that the rise time for charge voltages below 500 V reached a measurement limit of 35 ps due to the limitation of a bandwidth of the oscilloscope.

In this chapter, based on the frequency responses of the oscilloscope, we estimated rise time of the input waveforms from observed waveforms. Firstly, the estimation based on the Gaussian response is done. Secondly, the estimation based on the first and second order low pass filter is conducted.

A.2 Estimation based on Gaussian response

Based on the Gaussian response of the oscilloscope, we simulated the rise time t_{ri} of an exponential input waveform from its rise time t_{rm} to be observed, which is shown in Figure A.1.

The measured results on rise time t_{rm} for a charge voltage of 300 V (shown in Chapter-4) are plotted again with red circles on the abscissa in Figure A.1. Thick black solid line indicates simulated results of the Gaussian response with a bandwidth of 12-GHz. Red dotted line indicates approximate rise time t_{ri} obtained from the Gaussian response,

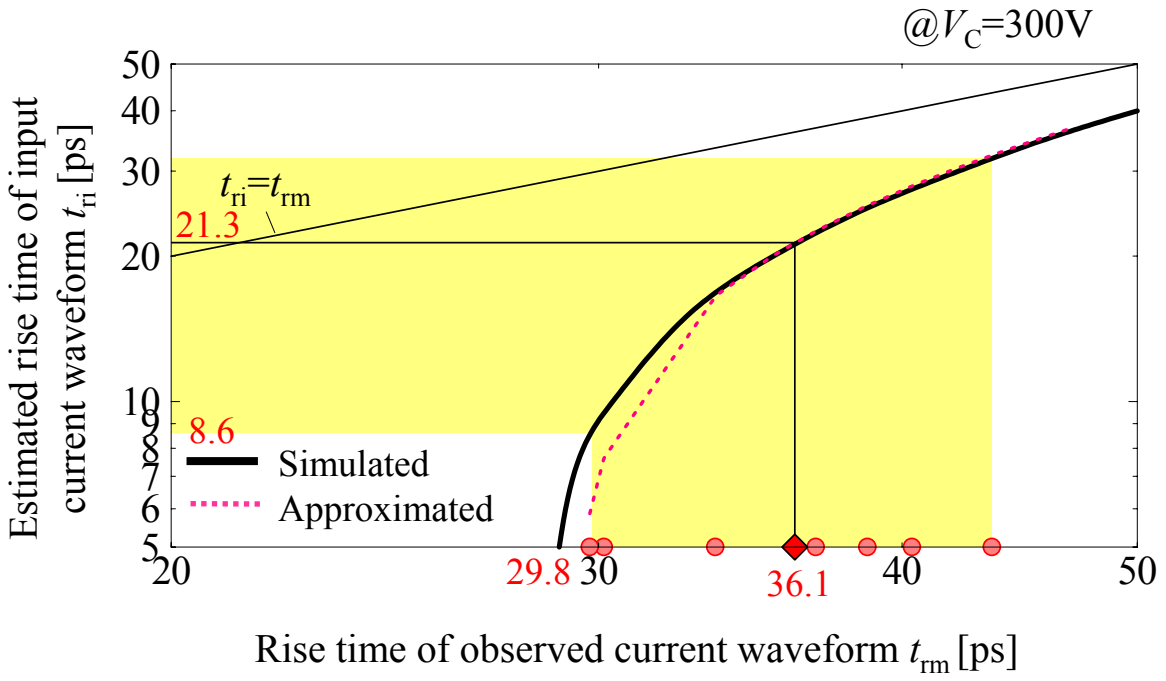

Figure A.1: Estimated rise time of input waveform versus observed rise time (V_C=300V).

which is given by

$$t_{ri} = \sqrt{t_{rm}^2 - t_{ro}^2} = \sqrt{t_{rm}^2 - (0.35/\mathrm{B})^2} \tag{A.1}$$

where $t_{ro} = (0.35/B)^2$ is the rise time determined by a bandwidth B of the oscilloscope. Figure A.1 shows that the approximate values agree with the simulated result. We found also from the figure that the measured average rise time t_{ri} (36 ps), which is shown with a red diamond, is 21 ps, while the minimum rise time simulated for the measured one (29.8 ps) is 8.6 ps.

The first result may be supported by Ref. [1] that gives a rise time limit of 20 ps for the fastest discharges from a theoretical consideration on a 50-Ω TEM transmission line discharge model. For the latter result, however, it is too short to measure even though the fastest commercially available oscilloscope could be used.

The finding validity was investigated in the following way.

Even to the situation as shown in Figure 4.4 (b), we can apply a discharge circuit approach [2] for a charged stray capacitance between the tip electrode and the ground plate. Based on a spark resistance formula, the approach can provide a discharge

current $i(t)$ in a closed form, which is expressed as

$$i(t) = \frac{CV_C}{2} \times \frac{\left(\frac{\alpha}{p}\right)\left(\frac{V_C}{\delta}\right)^2 \exp\left\{\left(\frac{\alpha}{p}\right)\left(\frac{V_C}{\delta}\right)^2 (t-t_0)\right\}}{\left[1+\exp\left\{\left(\frac{\alpha}{p}\right)\left(\frac{V_C}{\delta}\right)^2 (t-t_0)\right\}\right]^{1.5}}. \tag{A.2}$$

Current peak i_p and maximum rising slope $di/dt|_{\max}$ are also given by

$$i_p = \frac{CV_C\left(\frac{\alpha}{p}\right)\left(\frac{V_C}{\delta}\right)^2}{3\sqrt{3}} \tag{A.3}$$

$$\left.\frac{di}{dt}\right|_{\max} = \frac{2\sqrt{21}-3}{75\sqrt{6-\sqrt{21}}} CV_C \left(\frac{\alpha}{p}\right)^2 \left(\frac{V_C}{\delta}\right)^4. \tag{A.4}$$

Then the rise time t_{ri} of discharge current $i(t)$ is expressed as

$$t_{ri} = \frac{0.8 \times i_p}{\left.\frac{di}{dt}\right|_{\max}} = \frac{0.8}{3\sqrt{3}} \cdot \frac{75\sqrt{6-\sqrt{21}}}{2\sqrt{21}-3} \cdot \left(\frac{\alpha}{p}\right)^{-1} \cdot \left(\frac{V_C}{\delta}\right)^{-2} \tag{A.5}$$

where i_p is the peak current, α is the spark coefficient decided by the atmosphere, p is the pressure in atm and δ is the gap length in m. The above equation should give the minimum rise time of a discharge current to be measured through a 50-Ω coaxial cable as shown in Figure 4.4 (b). As regards the gap breakdown field V_C/d, Ref. [3] estimates 2×10^7 V/m for charge voltages below 1000V, which gives t_{ri} =51 ps from Eq. (A.5). According to Ref. [1], on the other hand, a theoretical consideration of field emission shows that the gap breakdown field never surpasses 3×10^7 V/m for polished surfaces of electrodes in very dry air, which yields $t_{ri} = 23$ ps. However, Ref. [4] experimentally gives 7×10^7 V/m for a charge voltage of 400 V, which leads to very short rise time of t_{ri} =4 ps.

The above-mentioned discussion implies that the rise time of discharge currents through air discharges of ESD-guns is likely to be below 10 ps despite a claim in Ref. [1] that the rise time limit is 20 ps. Note that Ref. [3] gives estimated gap breakdown length using the measured discharge currents through a hand-held metal piece from a charged human body, while Ref. [4] gives measured gap length with a micrometer when a discharge happened between a needle electrode with a curvature of 0.5 mm and flat-plate electrode.

A.3 Estimation based on first and second order low-pass filters

Though the Gaussian response is well known as one of the frequency responses of oscilloscopes and has been widely used, today a frequency response called "flat response" is adopted for the latest digital oscilloscope [5]. The characteristics of the flat response are not easy to be numerically expressed. Thus we actually measured the frequency response of the oscilloscope we used, and compared it with those of first and second order low pass filters, and as a reference, the Gaussian response.

Generally, frequency responses of oscilloscopes (bandwidth: B) $G(j\omega)$ are given as follows. Let $G_1(j\omega)$, $G_2(j\omega)$, and $G_g(j\omega)$ be the frequency responses of the first, second orders and the Gaussian response, respectively. According to Ref. [6], they can be expressed as

$$G_1(j\omega) = \left(1 + \frac{j\omega}{2\pi B}\right)^{-1} \tag{A.6}$$

$$G_2(j\omega) = \left\{1 + \mathrm{P}\left(\frac{j\omega}{2\pi B}\right)^2 + \frac{\sqrt{P}}{Q}\left(\frac{j\omega}{2\pi B}\right)\right\}^{-1} \tag{A.7}$$

$$P = 1 - \frac{1}{2Q} + \sqrt{\left(1 - \frac{1}{2Q}\right)^2 + 1}$$

$$G_g(j\omega) = \exp\left\{\left(\frac{1}{2}\ln 2\right) \cdot \left(\frac{j\omega}{2\pi B}\right)^2\right\} \cdot \exp(-j\omega\tau). \tag{A.8}$$

Figure A.2 shows the measured frequency response of an oscilloscope (bandwidth: B=12 GHz, sampling frequenccy: 40 GHz). In the figure, red circles indicate masured data, th gray solid line indicates calculation result for the first ofder, and the dotted line shows calculated results for the Gaussian response.

The thin blue line, thick red line, and thin pink line indicate the calculated results for the second order of Q=0.6, 0.7, and 0.8, respectively. From Figure A.2, measured data at frequencies below 14GHz agree well with the frequency response of the second order (Q=0.7) as Ref. [6].

Table A.1: Examples of estimation results of rise time of input waveforms (300 V).

Measured [ps]	Estimated [ps]		
	2nd	1st	Gauss
29.8	26.6	30.9	5.9
33.5	33.0	34.7	16.5
36.9	27.0	30.4	22.5
43.6	39.9	39.9	32.0

Let $v_i(t)$ and $v_m(t)$ be the input waveform of the oscilloscope and observed (measured) waveform, respectively. By directly changing Eq. (A.6) and Eq. (A.7) into time domain expression, the input waveforms can be given by

$$v_i(t) = v_m(t) + \frac{1}{2\pi B}\frac{dv_m(t)}{dt} \tag{A.9}$$

$$v_i(t) = v_m(t) + \frac{\mathrm{P}}{(2\pi \mathrm{B})^2}\frac{d^2v_m(t)}{dt^2} + \frac{\sqrt{\mathrm{P}}}{Q}\frac{1}{2\pi \mathrm{B}}\frac{dv_m(t)}{dt}. \tag{A.10}$$

From measured waveforms for air discharge of an ESD-gun (300V), input waveforms are estimated by Eq. (A.9) and Eq. (A.10). They are shown in Figure A.3. In the figure, the black line with circles is measured data, and blue and red lines indicate calculated results for first and second order, respectively. Rise time is read by the same way as the previous chapters. Examples of the results for some of the fastest measured data are shown in Table A.1. From this table, we found that the rise time given by the Gaussian response is fastest, followed by that of the first order and that of the second order. Since the second order characteristics can well explain measured frequency response of the oscilloscope, the results from Eq. (A.10) are appropriate. Thus the fastest rise time obtained from measurement is estimated to be 27 ps at 300V.

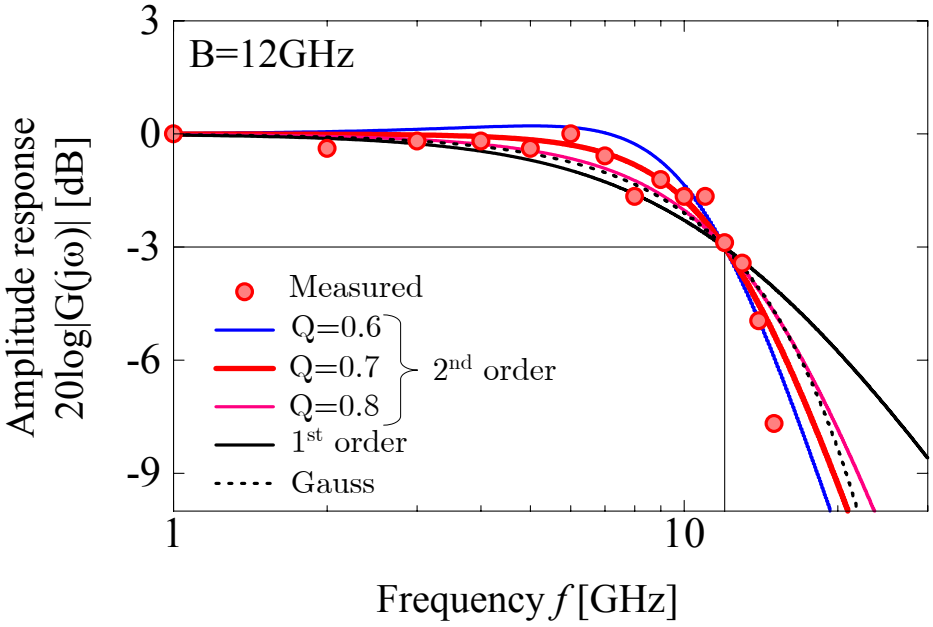

Figure A.2: Frequency response of the digital oscilloscope (B=12 GHz).

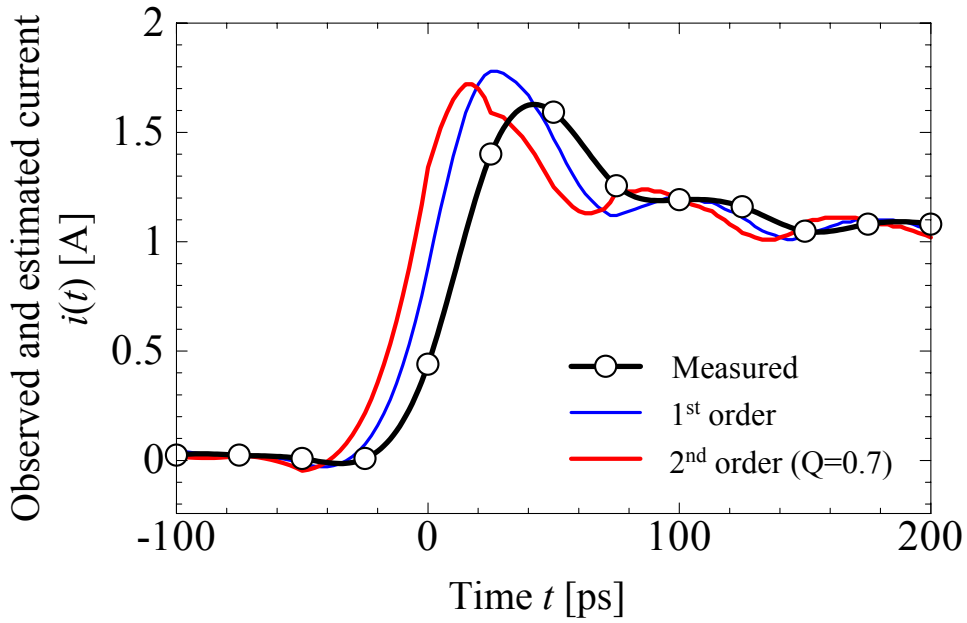

Figure A.3: Examples of estimated and observed current waveforms (V_C=300V).

A.4 Conclusion

We found that the rise time for charge voltages below 500 V reached a measurement limit of 35 ps due to the limitation of a bandwidth of the oscilloscope we used. Based on the Gaussian response of the oscilloscope, we estimated that the rise time limit may be below 10 ps. Based on the second order low-pass filter that well explains the flat responses of actual digital oscilloscopes, however, we estimated that the fastest rise time obtained from our measurement is 27 ps a charge voltage of 300 V.

Our future task is to elucidate the factors that determine rise-time limit of the discharge current waveform for air discharge of an ESD-gun with a few hundreds of charge voltages.

References

[1] D. Pommerenke, "ESD:transient fields, arc simulation and rise time limit", Journal of Electrostatics, Vol.36, pp. 31–54, 2005.

[2] O. Fujiwara: "An analytical approach to model indirect effect caused by electrostatic discharge", IEICE Trans. COMMUN., Vol. E79-B, No.4, pp. 483–489 (1996-4).

[3] I.Mori, Y.Taka, O.Fujiwara,"Wideband measurement of discharge current caused by air discharge through hand-held metal piece from charged human-body", IEEJ Trans. FM, Vol.126, No.9, pp. 902–908, Sep., 2006 (in Japanese).

[4] K. Kawamata, S. Minegishi and A. Haga, "Measurement of frequency spectra of transient voltage due to micro gap discharge", IEICE Technical report, EMCJ2004-109, pp. 41–45, Dec., 2004 (in Japanese).

[5] Agilent Technologies, "Understanding oscilloscope frequency response and its effect on rise–time", Agilent Note NO, 1420, pp. 1–8, Jan., 2003 (in Japanese).

[6] C. Mittermayer, A. Steininger, "On the determination of dynamic errors for rise time measurement with an oscilloscope", IEEE Trans. Inst. and meas., Vol.48, No.6, Dec., 1999.

Appendix B

Wideband measurement of discharge current caused by air discharge through hand-held metal piece from charged human-body

B.1 Introduction

As described in the main chapters, in conjunction with high speed and low voltage operation of ICs, the electromagnetic (EM) immunity of electronic devices has been degrading. Especially it is well known that the transient EM fields due to electrostatic discharge (ESD) events have broadband frequency spectra, which cause a serious failure to high-tech information equipment [1−2]. From this perspective, an ESD-immunity test is being prescribed in the IEC 61000-4-2 [3], which is normally conducted by contact discharge of an ESD-gun. The ESD-gun is a device that simulates the ESD event from a charged human body, while it consists of a lumped resistor and a lumped capacitor corresponding to a skin resistance and a human-body capacitance, respectively. In actual ESD events, however, charges distributed on the body surface are discharged through a spark and thus its situation should be quite different from that of the ESD-gun. To achieve a better method of immunity testing, we need grasping the characteristics of discharges from a charged human body.

In addition, a strange phenomenon observed in low voltage ESD events is well known in the related industries. The ESD of this kind causes more serious failure to electronic equipment, while the mechanism has not yet been elucidated [2].

In order to understand the behavior of discharge currents from a human body charged below 1 kV, we previously measured the discharge current through a metal piece from a charged human body with a 6GHz band digital oscilloscope, and proposed an equivalent circuit model to explain it from a time invariant spark-resistance and human-body impedance [4].

In this study, with respect to its approaching speed of the hand-held metal piece, we measured discharge currents through a metal piece from a human-body with a charge voltage ranging from 200 V to 1000 V, and estimated the resultant voltage waveforms from the above-mentioned equivalent circuit model. Through the results, in conjunction with the metal piece speed, we demonstrated the dependence on the charge voltage of current rise time, time-varying spark resistance, spark length and breakdown field.

B.2 Measurement and calculation methods

B.2.1 Measurement method and an equivalent circuit model

Figure B.1 (a) shows an experimental set-up for measuring the discharge currents from a charged human body. Also shown in Figure B.1 (b) is an equivalent circuit model to calculate the discharge currents, which was proposed in [4]. An aluminum plate (1m×2m) was placed as a ground vertically on a square aluminum plate with a side of 1m. As can be seen in Figure B.1 (a), a 50-Ω SMA connector was fixed at the center of the vertical aluminum plate, which was connected through a 50-Ω coaxial cable to a digital oscilloscope with a frequency band of 6 GHz and a sampling frequency of 20-GHz. For easy contact, a small circular metal plate (hereafter called target) with a diameter of 6mm was attached to the inner conductor of the SMA connector. The tip electrode for air discharge of the ESD-gun was used as a metal piece. In the Figure B.1 (a), $Z_B(j\omega)$ is the human body impedance including the tip electrode seen from the point of contact between the target and the edge of the electrode.

After a subject with a metal piece, standing on form polystyrenes, is charged through a resistor of 100 MΩ from a DC power supply, the hand-held metal piece is approached the target from a distance of about 5.5 cm. When a spark occurs between the metal

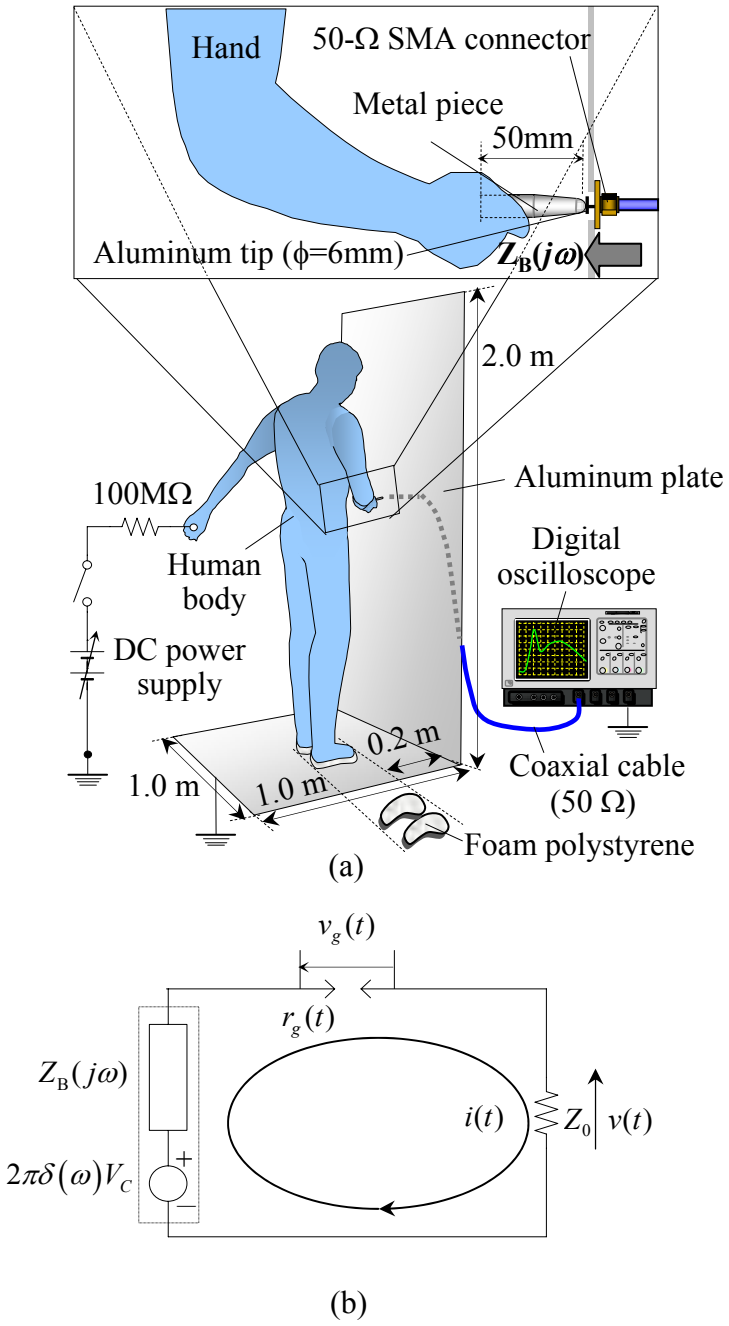

Figure B.1: Measurement set-up for observing current waveforms through a hand-held metal piece from a charged human body (a) and an equivalent circuit model to calculate discharge current (b).

piece and the target, a charge accumulated in the human-body is discharged and a discharge current flows through the SMA connector into the coaxial cable.
The charge voltage is set from 200 to 1000 V, in increments of 200 V, and the approaching speeds of the metal piece are the fast approach (approaching speed: about 20 cm/s) and the slow approach (approaching speed: about 2 cm/s). Five times measurements were made for discharges at each of the two approaching speeds of a charge voltage. Measurement were performed in a room temperature at 23 ^{o}C and a relative humidity of 40 %.

In the equivalent circuit model to calculate the discharge current, shown in Figure B.1 (b), V_C and $2\pi\delta(\omega)V_C$ indicate a charge voltage of the human-body and its Fourier transformed expression, respectively. Note that $\delta(\omega)$ indicates the Dirac delta function. $Z_B(j\omega)$ is a human-body impedance, and $Z_0(=50\Omega)$ is a characteristic impedance of the coaxial cable. $v_s(t)$, $r_s(t)$ and $i(t)$ are the discharge voltage appearing between the metal piece and the target just before the contact (hereafter called discharge voltage), the time-varying spark resistance, and the discharge current, respectively.
The discharge voltage $v_s(t)$, which can not be directly observed by this measurement se-tup, can be given from Figure B.1 (b) as

$$\begin{aligned} v_s(t) &= r_s(t)\, i(t) \\ &= V_C - \frac{1}{2\pi}\int_{-\infty}^{+\infty}\int_{-\infty}^{+\infty}\{Z_0 + Z_B(j\omega)\}\cdot i(\tau)\cdot e^{j\omega(t-\tau)}d\tau d\omega \\ &= V_C - Z_0\cdot i(t) - \frac{1}{2\pi}\int_{-\infty}^{+\infty}\int_{-\infty}^{+\infty} Z_B(j\omega)\cdot i(\tau)\cdot e^{j\omega(t-\tau)}d\tau d\omega \\ &= V_C - Z_0\cdot i(t) - \int_0^t z_B(t-\tau)\cdot i(\tau)\, d\tau. \end{aligned} \tag{B.1}$$

The above equation enables us to calculate the discharge voltage $v_s(t)$ from measured human body impedance $Z_B(j\omega)$ and discharge current $i(t)$.
Here, in Eq. (B.1), $z_B(t)$ is the inverse Fourier transformation of $Z_B(j\omega)$. Dividing $v_s(t)$ by measured current $i(t)$, we derive the time variation of the spark resistance $r_s(t)$. We also estimate the spark length, which will be described later.
Under the assumption that Ohm's law locally holds between current densities and electric fields, the spark resistance can be defined as $v_s(t)/i(t)$. In addition, the calculation

of Eq. (B.1) was conducted by using subroutines in Ref. [5].

Figure B.2 shows the frequency characteristics of the human-body impedance seen from the metal piece, which was measured with a network analyzer in the set-up shown in Figure B.1 (a). The subject is a 35-year male, whose height and weight are 168 cm and 60kg, respectively. In this figure, the abscissa and ordinate indicate frequency in MHz and impedance in ohm, respectively.

The measurement condition of the discharge current $i(t)$ and human-body impedance $Z_B(j\omega)$ and the calculation condition of them in Eq. (B.1) are shown in Table B.1.

In the next section, the calculation method will be validated.

Table B.1: Measurement and calculation conditions.

		Range	Sampling interval	Total number	
$i(t)$	Measured	0–50ns	50ps	1000	
	Data used	0–50ns	5ps	9991	$*1$
Z_B	Measured	300k–6GHz	3.75MHz	1601	
	Data used	300k–7.68GHz	3.75MHz	2049	$*2$
z_B	Calculated	0-266.6ns	65.1ps	4096	$*3$
	Data used	0-133.3ns	5ps	53323	$*4$
Convolution of $i(t)$ and $z_B(t)$	Calculated	0-50ns	5ps	9991	$*5$

$*1$: Used cubic Spline subroutine (DG1SPC).

$*2$: Added zero data from 6 GHz to 7.68 GHz.

$*3$: Used complex Fourier transformation subroutine (DFC1FB).

$*4$: Used cubic Spline subroutine (DG1SPC).

$*5$: Used fisrt-order convolution subroutine (DFCN1D).

B.2.2 Validation of the calculation method

It is quite difficult to examine the numerical errors of Eq. (B.1) from actual discharge currents and measured human-body impedance under the conditions shown in Table B.1. Thus we assume the human body with a metal piece as a capacitance C, and also

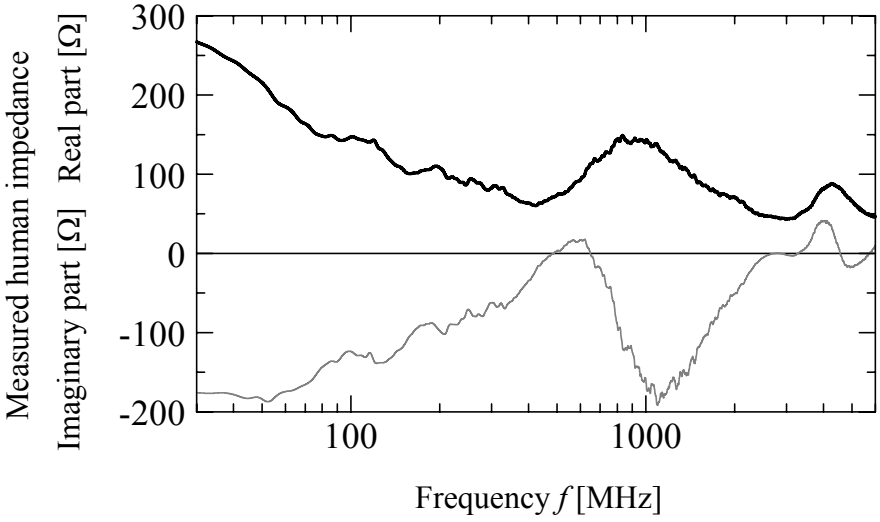

Figure B.2: Measured human-body impedance seen from a metal piece.

assume that the discharge voltage $v_s(t)$ between the metal piece and the target rapidly changes at the time t=0 from the charge voltage V_C to 0. Then we can theoretically derive the discharge current $i(t)$ and the inverse Fourier transformation $z_B(t)$ of the human-body impedance $Z_B(j\omega)$. In case of the discharge voltage $v_s(t)$, by comparing the theoretical results from Eq. (B.1) with calculation results based on the condition shown in Table B.1, the numerical errors are examined.

From $Z_B(j\omega)$=$1/j\omega C$, $i(t)$ and $z_B(t)$ can theoretically be expressed as

$$i(t) = \begin{cases} \frac{V_C}{Z_0} \cdot e^{-\frac{t}{CZ_0}} & (t > 0) \\ 0 & (t < 0), \end{cases} \tag{B.2}$$

$$\begin{aligned} z_B(t) &= \frac{1}{2\pi} \int_{-\infty}^{+\infty} Z_B(j\omega) e^{j\omega t} d\omega \\ &= \frac{1}{2\pi} \int_{-\infty}^{+\infty} \frac{1}{j\omega C} \cdot e^{j\omega t} d\omega \\ &= \begin{cases} +\frac{1}{2C} & (t > 0) \\ -\frac{1}{2C} & (t < 0). \end{cases} \end{aligned} \tag{B.3}$$

Then the theoretical value of $v_s(t)$ is given from Eq. (B.1) as

$$v_s(t) = \begin{cases} \frac{V_C}{2} \cdot \left(1 - e^{-\frac{t}{CZ_0}}\right) & (t > 0) \\ V_C & (t < 0). \end{cases} \tag{B.4}$$

The results calculated under the condition indicated in Table 1 are shown in Figure B.3. In Figure B.3 (a), the solid line indicates the theoretical value of the discharge current

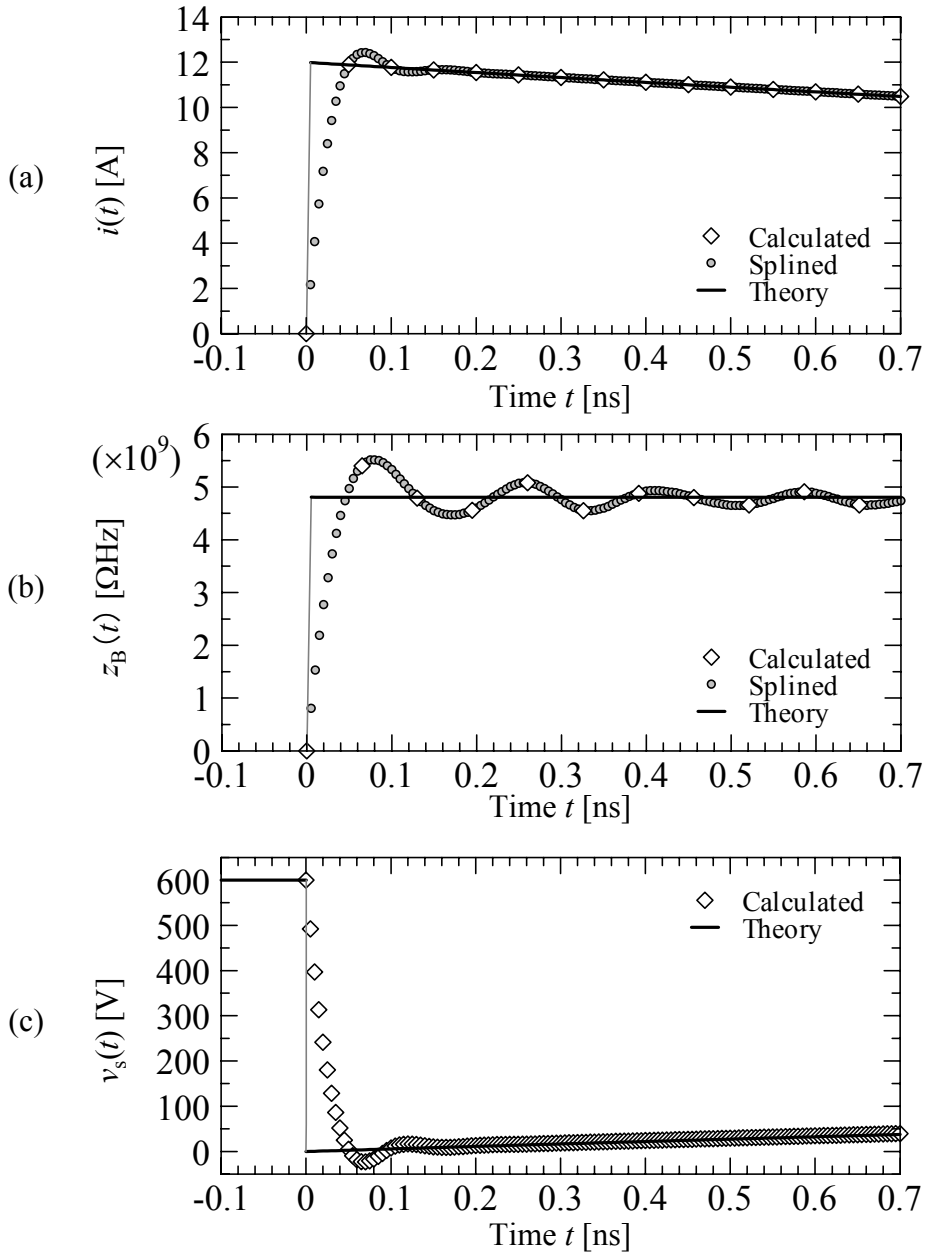

Figure B.3: Comparison of calculated and theoretical results of $i(t)$, $z_B(t)$ and $v_s(t)$ for $Z_B = 1/j\omega C$ when $v_s(t)$ changes stepwise.

$i(t)$ given by Eq. (B.2), the diamonds indicate the measured data of 50 ps interval, and the gray circles indicate the splined data. From Figure B.3 (a), it is found that the rising slope of the discharge current based on the discrete data becomes gentler than that of the theoretical waveform due to the spline interpolation.

In Figure B.3 (b), the solid line indicates the theoretical waveform of the inverse Fourier transformation of $Z_B(j\omega)$ or $z_B(t)$ given by Eq. (B.3), the diamonds indicate the numerical calculation results of 65 ps interval, and the gray circles indicate the results of the spline interpolation. The rising slope of the numerical calculation is also gentler and the waveform oscillates. The reason of the oscillation is due to the bandwidth-limited discrete data of $Z_B(j\omega)$=$1/j\omega C$.

In Figure B.3 (c), the solid line indicates the theoretical waveform of the discharge voltage by Eq. (B.4), the diamonds indicate the result of the convolution of splined data in Figures B.3 (a) and (b). Figure B.3 (c) demonstrates that, though the falling slope of the calculation result of $v_s(t)$ is gentler than that of the theoretical waveform, the discharge voltage waveform can be calculated from the discharge current and the human-body impedance. Based on the fact that the estimated falling slope 40 ps of $v_s(t)$ is below the sampling interval 50 ps of the digital oscilloscope, which is used to obtain the discharge current waveform, the calculation results based on Table B.1 are validated.

B.3 Result and discussion

Figure B.4 (a) shows examples of measured discharge current waveforms. Figure B.4 (b) shows those of discharge voltage waveforms estimated by Eq. (B.1). Figure B.4 (c) shows those of time-varying spark resistance, which was derived from dividing the discharge voltage waveform by discharge current waveform. The thick amd thin solid lines indicate the results for the fast and slow approaches, respectively, of the metal piece. The left figures show waveforms of charge voltages ranging from 200 V to 600V, and the right figures show those of charge voltages of 800 V and 1000 V. In Figre B.4 (c), the results for only 200 V and 1000 V are shown. From Figure B.4 (c), it is

found, except 800 V, that the approaching speeds of the metal piece do not affect the waveforms.

The gap length (hereafter called spark length) was estimated as follows. Figure B.5 shows examples of discharge current waveforms (a) and of time-variation of spark resistance (b) at charge voltages of 200 V and 800 V. According to the Rompe-Weizel's spark resistance formula, a spark resistance is calculated as

$$r_s(t) = \frac{\delta}{\sqrt{\frac{2\alpha}{p}\int_{-\infty}^{t} i^2(t)dt}} \tag{B.5}$$

where p atm is the air pressure, α the spark constant, and δ the spark length.

Eq. B.5, the spark length δ can be calculated from the measured current waveform and estimated spark resistance waveform, and the value which gives the minimal value of the gap length δ was adopted. They are shown in the figures. From the adopted spark length, the time-variation of the spark resistance are shown in Figure B.5 (b) with thin solid lines (the spark length δ was 10μm at V_C=200 V, and 45μm at V_C=800 V. The figure shows good agreement between the estimated spark resistance and calculated one.

In this case, the breakdown fields (V_C/δ) range from 1.8×10^7 V/m (δ=45μm) to 2.0×10^7 V/m (δ=10μm). Ref. [7] gives a breakdown field of 1.75×10^7 V/m for the unpolished surfaces of the sphere versus sphere electrodes at atmospheric pressure. Ref. [8] also estimated the maximum breakdown field as 3×10^7 V/m for moving charged metal object whose surface is polished. These findings validate our calculated spark length δ.

From Ref. [5], assuming a time invariant spark resistance yields the discharge current waveform given as

$$i(t) = \frac{1}{2\pi}\int_{-\infty}^{+\infty} \frac{1}{r + Z_0 + Z_B(j\omega)} \cdot \frac{V_c}{j\omega} \cdot e^{j\omega t} d\omega \tag{B.6}$$

where r is the time-invariant discharge resistance corresponding to the minimal value of the spark resistance (hereafter called spark resistance) in Figure B.5. This figure indicates good agreement between the calculated and measured waveforms.

This implies that the spark resistance, which is basically time-variant, at the time when the current reaches the peak determines the behavior of the current waveform.

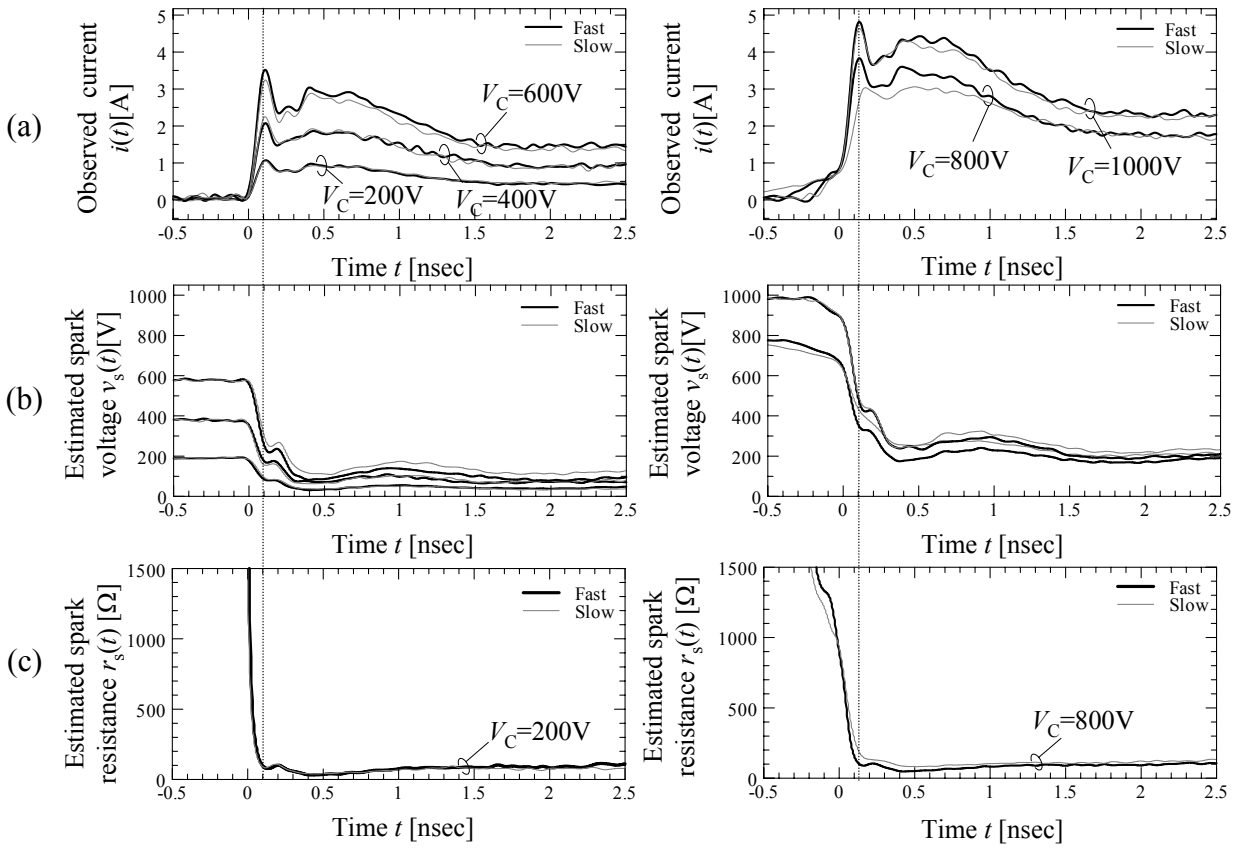

Figure B.4: Examples of observed discharge current waveforms (a), of estimated discharge voltage waveforms (b), and of estimated time-variation of spark resistance (c).

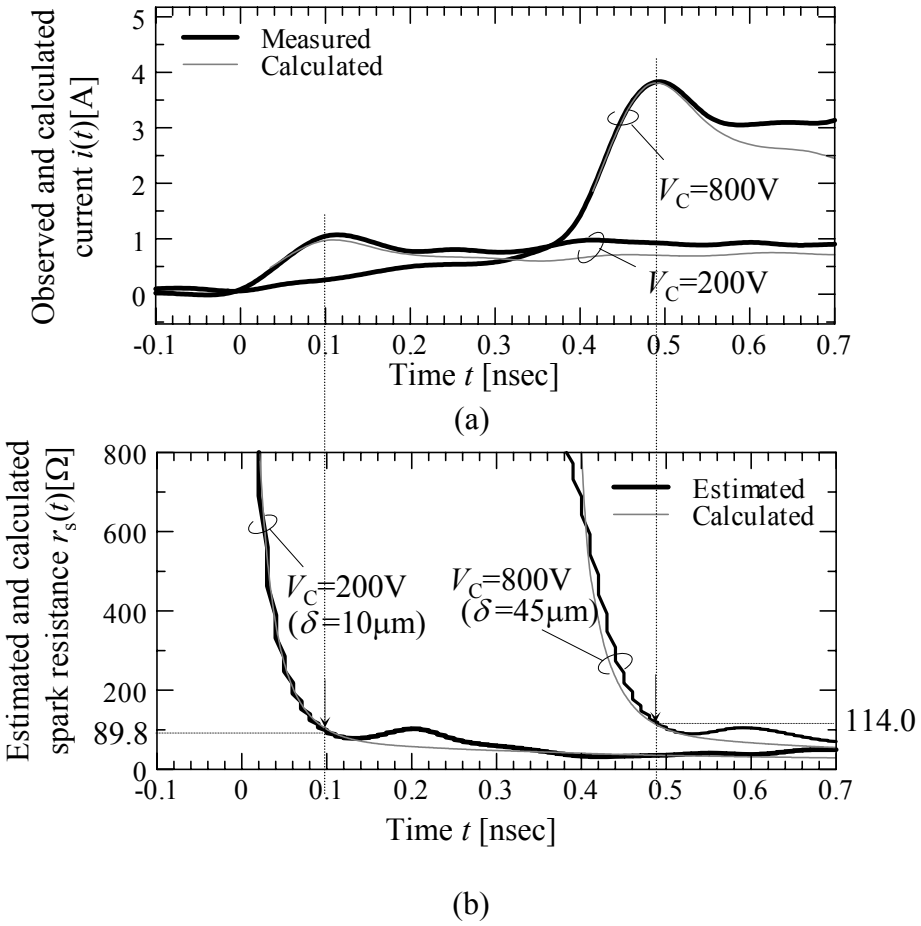

Figure B.5: Examples of discharge current waveforms (a) and of time-variation of spark resistance (b) (V_C=200, 800V).

Table B.2: Characteristics of air discharge through a hand-held metal piece from a charged human body.

charge voltage V_C[V]	Current peak I_p[A]	Rise time t_r[ps]	Spark length $\delta[\mu$m]	Breakdown voltage $V_C/\delta[10^7$V/m]
200	1.04 ± 0.06	71.7 ± 6.2	10.2 ± 0.8	1.97 ± 0.17
	1.02 ± 0.03	73.1 ± 8.7	10.2 ± 0.4	1.96 ± 0.08
400	2.06 ± 0.06	70.0 ± 4.4	19.4 ± 0.5	2.06 ± 0.06
	2.24 ± 0.11	71.6 ± 8.0	19.0 ± 0.7	2.11 ± 0.08
600	3.29 ± 0.09	67.0 ± 6.3	28.0 ± 0.0	2.14 ± 0.0
	3.21 ± 0.09	75.6 ± 5.2	29.4 ± 0.9	2.04 ± 0.06
800	3.80 ± 0.11	89.5 ± 15.0	45.8 ± 1.1	1.75 ± 0.04
	2.96 ± 0.18	147.3 ± 35.5	64.4 ± 4.4	1.25 ± 0.08
1000	4.69 ± 0.16	91.4 ± 14.1	59.0 ± 1.4	1.70 ± 0.04
	4.54 ± 0.18	93.9 ± 12.5	58.6 ± 1.3	1.71 ± 0.04

Table B.2 summarizes the characteristics of air discharge through a hand-held metal piece from a charged human-body, which are the current peak, rise time, spark length and breakdown field. The upper and lower rows show the results for fast and slow approaches, respectively. They are also presented in Figure B.6 with the mean value ± standard deviation. We found that for charge voltages below V_C=600 V, the spark length increases with V_C, which results in a constant breakdown field of 2×10^7V/m, and the discharge current waveform has a peak proportional to V_C and a constant rise time around 70 ps, while these properties are not almost affected by the approaching speed of the metal-piece. For a charge voltage of V_C=800 V, however, the properties are greatly affected by the approaching speed. The cause remains unknown at present.

B.4 Conclusion

In this study, with respect to the approaching speed of a hand-held metal piece, we measured discharge currents through the metal piece from a human-body with a charge voltages ranging from 200 V to 1000 V, and estimated the resultant voltage waveforms from the equivalent circuit model. Through these results, in conjunction with the metal piece speed we demonstrated the dependence on the charge voltage of current peak,

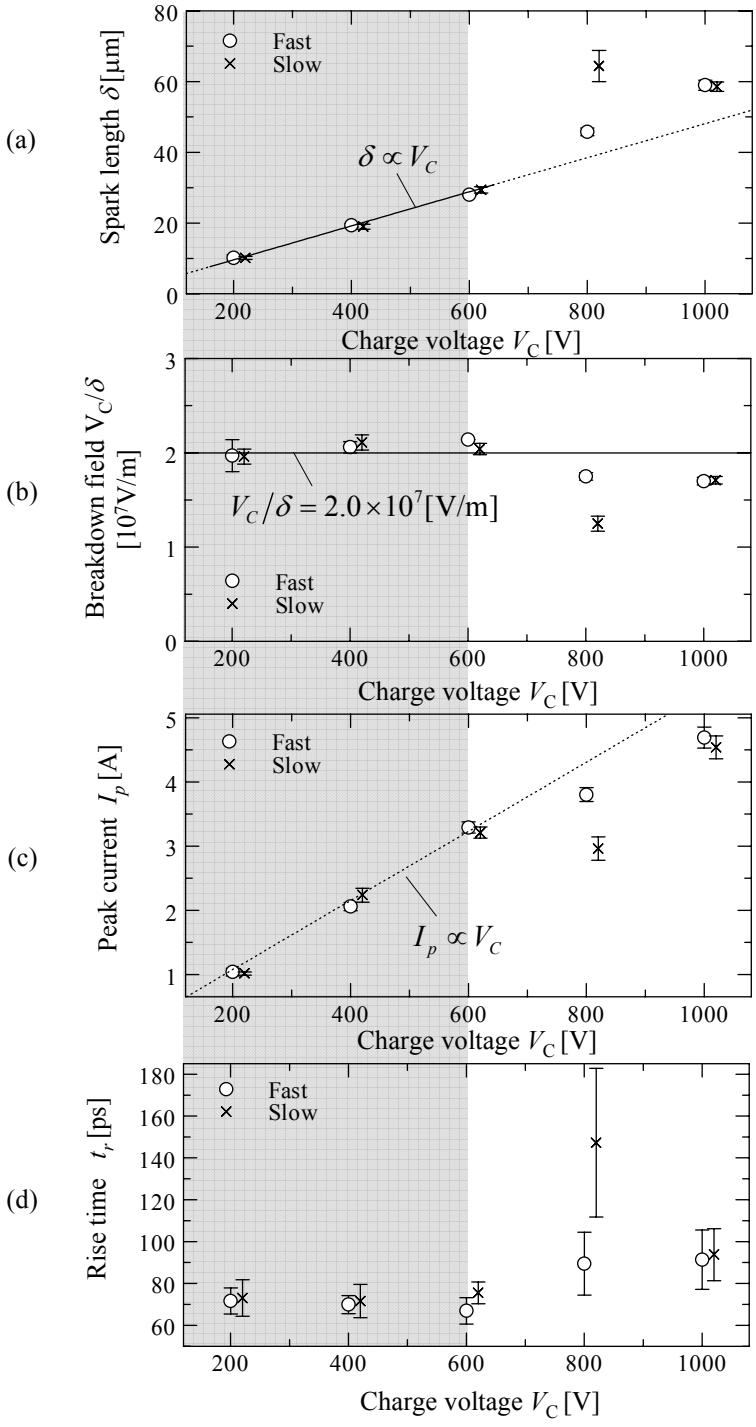

Figure B.6: Dependence on charge voltage V_C of spark length (a), breakdown field V_C/d (b), current peak I_p (c), and rise time t_r (d) of air discharge through a hand-held metal piece from a charged human body.

rise time, time-varying spark resistance, spark length and breakdown field.

We found that for charge voltages below V_C=600 V, the spark length increases with V_C, which results in a constant breakdown filed of 2×10^7 V/m, and the discharge current waveform has a constant rise time around 70 ps and a peak proportional to V_C, while these properties are not affected by the approaching speed of the metal piece. Note that the rise time is affected by the bandwidth limit of the oscilloscope used to observe the discharge current waveforms. We also confirmed that discharge current waveforms can be calculated from the spark resistance value at the time when the current has its peak.

Future tasks are checking whether or not this circuit model can be applied to the discharges for charge voltages over 1000 V, and elucidating a strange discharge phenomenon observed for charge voltages around 800 V.

References

[1] For example, T. Takagi, "Research and development on EMC/EMI measurements and technologies in Japan", Trans. IEICE, Vol. J79-B-II, No.11, pp. 718–726, Nov.1996(in Japanese).

[2] M. Honda,"EMI aspects of the metal-metal ESD to the electronic equipment", J.IEICE, Vol.78, No.9, pp. 849–850, Sept.,1995 (in Japanese).

[3] Japanese Industrial Standards Committee: "Electromagnetic Compatibility (EMC) -Part 4: Testing and measurement techniques - Section 2. Electrostatic discharge immunity test", JIS C 1000-4-2: 1999 (IEC 61000-4-2: 1995/Amd. 1), 1999 (in Japanese).

[4] Y.Taka,I.Mori, O.Fujiwara, "Measurement of discharge current through hand-held metal piece from charged human body", IEEJ Trans. FM, Vol.125, No.7, pp. 600-6001, Jul., 2005.

[5] NEC Corporation," Super-UX scientific and engineering calculations library, manual of ASL/SX (basic functions Vol.2)", G1AY22-2, p. 296, 430, 1996 (in Japanese).

[6] O. Fujiwara: "An analytical approach to model indirect effect caused by electrostatic discharge", IEICE Trans. COMMUN., Vol. E79-B, No.4, pp. 483–489, April, 1996..

[7] N.Masui, H.Fujihara, Y.Ebinuma, T.Shinjo, "Effects of surface roughness of electrode on electrostatic discharge in short air gap", J. Inst. Electrostat. Jpn., Vol.27, No.2, pp. 85-91, 2003 (in Japanese).

[8] D. Pommerenke, "ESD:transient fields, arc simulation and rise time limit", Journal of Electrostatics, Vol.36, pp. 31–54, 2005.

Appendix C

Publication List

C.1 Papers

Included in this thesis

[1] Osamu Fujiwara, **Ikuko Mori**, Shinobu Ishigami, and Yukio Yamanaka, "Calculation of Magnetic Near-Field Generated by the Contact Discharge of an ESD-gun", IEEJ Transactions on Fundamental and Materials, Vol.124, No.9, pp.763-768, Sep. 2004 (in Japanese).

藤原修，**森育子**，石上忍，山中幸雄，"ESDガンの接触放電に対する近傍空間の磁界計算"，電気学会論文誌 A，Vol.124, No.9, pp.763-768, Sep. 2004.

[2] **Ikuko Mori**, Osamu Fujiwara, Shinobu Ishigami, and Yukio Yamanaka, "Characteristic Measurement of Discharge Current Injected by the Air Discharge of an ESD-gun onto a Ground", IEEJ Transactions on Electronics, Information and Systems, Vol.125, No.12, pp.1798-1804, Dec. 2005 (in Japanese).

森育子，藤原修，石上忍，山中幸雄，"ESDガンのグラウンドへの気中放電に対する放電電流の特性測定"，電気学会論文誌 C，Vol.125, No.12, pp. 1798-1804, Dec. 2005.

[3] **Ikuko Mori**, Yoshinori Taka, Osamu Fujiwara, "Wideband Measurement of Discharge Current Caused by Air Discharge through Hand-Held Metal Piece from Charged Human-Body", IEEJ Transactions on Fundamental and Materials, Vol.126, No.9, pp.902-908, Sep. 2006 (in Japanese).

森育子，高義礼，藤原修，”帯電人体からの金属棒を介した気中放電による放電電流の広帯域測定”，電気学会論文誌 A，Vol.126, No.9, pp.902-908, Sep. 2006.

C.2 Letters

Included in this thesis

[1] **Ikuko Mori**, Osamu Fujiwara, Shinobu Ishigami, and Yukio Yamanaka, ”A Study on Rise-time and Peak of the Transient Current Injected through Air Discharge of an ESD-gun”, IEEJ Transactions on Fundamental and Materials, Vol.125, No.7, pp.598-599, July 2005.

[2] **Ikuko Mori**, Yoshinori Taka, Osamu Fujiwara, and Shinobu Ishigami, ”Characteristic Comparison of Discharge Currents Caused by Electrostatic Discharge Gun for IEC Immunity Testing”, IEICE Transactions on Communications, Vol. J-88-B, No.12, pp.2401-2403, Dec. 2005 (in Japanese).

森育子，高義礼，藤原修，石上忍，”ESDガンの ESD イミュニティ試験法に対する放電電流の特性比較”，電子情報通信学会論文誌 B，Vol. J-88-B, No.12, pp.2401-2403, Dec. 2005.

Other

[1] Yoshinori Taka, **Ikuko Mori**, and Osamu Fujiwara, ”Measurement of Discharge Current through Hand-Held Metal Piece from Charged Human Body”, IEEJ Transactions on Fundamental and Materials, Vol.125, No.7, pp.600-601, July 2005.

C.3 International Conferences

Included in this thesis

[1] **Ikuko Mori**, Osamu Fujiwara, Sinobu Ishigami, and Yukio Yamanaka, "Characteristic Measurement of Transient Current Injected by Air Discharge of an ESD-gun", Proceedings of 2004 International Symposium on Electromagnetic Compatibility, EMC'04 Sendai, 2D-1-1, pp.417-420, Sendai, Japan, June 2004.

[2] **Ikuko Mori**, Shinobu Ishigami, and Osamu Fujiwara, "Wideband Measurement of Discharge Current Waveform due to Air Discharge of an ESD-gun with Low Charge Voltages", Proceedings of The 23rd International Conference on Electrical Contacts,

ICEC2006/Sendai, pp.426-429, Sendai, Japan, June 2006.

[3] **Ikuko Mori**, Osamu Fujiwara, and Sinobu Ishigami, "Rise Time Limit of Discharge Current for Air Discharge of an ESD-gun", Proceedings of The Fourth Asia-Pacific Conference on Environmental Electromagnetics, CEEM'2006,Vol.1, pp.34-37, Dalian, China, Aug. 2006.

Others

[1] **Ikuko Mori**, Yoshinori Taka and Osamu, Fujiwara, "A Circuit Approach to Calculate Discharge Current through Hand-Held Metal Piece from Charged Human-Body", Proceedings of 2005 International Conference on Electromagnetic Compatibility, ICEMC 2005/Phuket,4A-4, Phuket, Thailand, July 2005.

[2] Yoshinori Taka, **Ikuko Mori**, and Osamu Fujiwara, "Estimation of Gap Breakdown Field in Contact with Hand-Held Metal Piece from Charged Human Body", Proceedings of The 23rd International Conference on Electrical Contacts, ICEC2006/Sendai, pp.411-414, Sendai, Japan, June 2006.

C.4 Technical Reports

[1] **Ikuko Mori**, Yoshinori Taka, and Osamu Fujiwara, "An Equivalent Circuit Model for Calculating Discharge Current thorough Hand-held Metal Piece from Charged Human Body", Technical Report of IEICE, EMCJ2004-108, pp.35-40, Dec. 2004 (in Japanese).

森育子，高義礼，藤原修，"帯電人体の接触放電による電流計算モデル"，電子情報通信学会技術報告，EMCJ2004-108, pp.35-40, Dec. 2004.

[2] **Ikuko Mori**, Osamu Fujiwara, Sinobu Ishigami, and Yukio Yanamaka, "An Analytical Model for Current Injected Through Air Discharge of an ESD-Gun", IEICE Technical Report", EMCJ2004-142, pp.67-72, Dec. 2005 (in Japanese).

森育子，藤原修，石上忍，山中幸雄，"ESDガンの気中放電を介する放電電流の解析モデル"，電子情報通信学会技術報告，EMCJ2004-142, pp.67-72, Dec. 2005.

[3] Yoshinori Taka, **Ikuko Mori**, and Osamu Fujiwara, "Characteristic Measurement for Air Discharge through Hand-Held Metal Piece from Charged Human-Body", IEICE Technical Report, EMCJ2005-40, pp.109-114, June. 2005 (in Japanese).

高義礼，**森育子**，藤原修，"帯電人体のもつ金属棒を介した気中放電の特性測定"，電子情報通信学会技術報告，EMCJ2005-40, pp.109-114, June. 2005.

C.5 Domestic Conferences

[1] **Ikuko Mori**, Osamu Fujiwara, Shinobu Ishigami, and Yukio Yamanaka, "Specific Characteristics of the Current Injected through Air Discharge of an ESD-gun", 2004 Annual Conference of Fundamentals and Materials Society IEE Japan, Aug. 2004 (in Japanese).

森育子，藤原修，石上忍，山中幸雄，"ESDガンの気中放電を介する放電電流の特異特性"，2004年電気学会基礎・材料・共通部門大会，Aug. 2004.

[2] Yoshinori Taka, **Ikuko Mori**, and Osamu Fujiwara, "Characteristic Measurement of Discharge Current through Finger Touch of Charged Human Body", 2004 Annual Conference of Fundamentals and Materials Society IEE Japan, Aug. 2004.

高義礼，**森育子**，藤原修，"帯電人体の指先接触による放電電流の特性測定"，2004年電気学会基礎・材料・共通部門大会, Aug. 2004.

[3] **Ikuko Mori**, Yoshinori Taka, Osamu Fujiwara, and Shinobu Ishigami, "Estimation of Discharge Voltage Waveform for Air Discharge of an ESD-gun", 2005 Annual Conference of Fundamentals and Materials Society IEE Japan, IV-1,p.168,Aug. 2005.

森育子，高義礼，藤原修，石上忍，"ESDガンの気中放電に対する放電電圧波形の推定"，2005年電気学会基礎・材料・共通部門大会，IV-1,p.168, Aug. 2005.

[4] Yohinori Taka, **Ikuko Mori**, and Osamu Fujiwara, "Calculation of Discharge Current from Charged Human Body", 2005 Annual Conference of Fundamentals and Materials Society IEE Japan, IV-2,p.169, Aug. 2005.

高義礼，**森育子**，藤原修，"帯電人体の接触の際に生ずる気中放電の特性測定"，2005年電気学会基礎・材料・共通部門大会，IV-2,p.169 Aug. 2005.

[5] **Ikuko Mori**, Osamu Fujiwara, and Shinobu Ishigami, "Maximum Rising Slope of Discharge Current for Air Discharge of an ESD-Gun with Low Charge Voltages",

2006 Annual Conference of Fundamentals and Materials Society IEE Japan, V-5,p.238, Aug. 2006.

森育子，藤原修，石上忍，”低充電 ESD ガンの気中放電に対する放電電流の最大勾配” 2006 年電気学会基礎・材料・共通部門大会，V-5,p.238, Aug. 2006.

[6] **Ikuko Mori**, Osamu Fujiwara, and Shinobu Ishigami, ”Characteristic Measurement of Discharge Current Caused by Air Discharge of an ESD-gun with a Low Charge Voltage”, Proceedings of the 2006 IEICE General Conference, B-4-3,p.298, Mar. 2006.

森育子，藤原修，石上忍，”低充電電圧 ESD ガンの気中放電に対する放電電流の特性測定”，電子情報通信学会 2006 年総合大会，B-4-3, p.298,Mar. 2006.

[7] Yoshinori Taka, **Ikuko Mori**, and Osamu Fujiwara, ”Estimation and Validation of Breakdown Field due to Air Discharge from Charged Human-Body”, Proceedings of the 2006 IEICE General Conference, B-4-5,p.300, Mar. 2006.

高義礼，**森育子**，藤原修，”帯電人体からの気中放電による絶縁破壊電界の推定と検証”，電子情報通信学会 2006 年総合大会，B-4-5, p.300,Mar. 2006.

[8] **Ikuko Mori**, Yoshinori Taka, Osamu Fujiwara, and Shinobu Ishigmi, ”Calculation of Discharge Current due to Air Discharge of an ESD-gun with a Low Charge Voltage”, Proceedings of the 2005 IEICE Society Conference, B-4-24, Sep. 2005.

森育子，高義礼，藤原修，石上忍”低充電電圧 ESD ガンの気中放電で生ずる放電電流の計算”，電子情報通信学会 2005 年ソサイエティ大会，B-4-24, Sep. 2005.

[9] **Ikuko Mori**, Osamu Fujiwara, and Shinobu Ishigami, ”Estimation of Rise Time of Discharge Current for Air Discharge of an ESD-gun with a Low Charge Voltage”, Proceedings of the 2006 IEICE Society Conference, B-4-47, Sep. 2006.

森育子，藤原修，石上忍，”低充電電圧 ESD ガンの気中放電のライズタイム推定”，電子情報通信学会 2006 年ソサイエティ大会，B-4-47, Sep. 2006.

[10] **Ikuko Mori**, Osamu Fujiwara, Shinobu Ishigami, and Yukio Yamanaka, ”Frequency Spectra of Current Injected onto Pellegrini Target with Air Discharge

of an ESD-gun", 2004 Tokai-Section Joint Convention of Institute of Electrical Engineers, O-254, Sep. 2004.

森育子，藤原修，石上忍，山中幸雄，"ESDガンの気中放電で生ずる放電電流の周波数スペクトル"，平成16年度電気関係学会東海支部連合大会，O-254, Sep. 2004.

[11] Yoshinori Taka, **Ikuko Mori**, and Osamu Fujiwara, "Characteristic Measurement of Discharge Current due to Human-Metal ESD", 2004 Tokai-Section Joint Convention of Institute of Electrical Engineers, O-253, Sep. 2004.

高義礼，**森育子**，藤原修，"金属人体ESDによる放電電流の特性測定"，平成16年度電気関係学会東海支部連合大会，O-253, Sep. 2004.

[12] **Ikuko Mori**, Yoshinori Taka, and Osamu Fujiwara, "Characteristic Measurement of Air Discharge Caused by contact of Charged Human-Body", 2005 Tokai-Section Joint Convention of Institute of Electrical Engineers, O-385, Sep. 2005.

森育子, 高義礼, 藤原修，"帯電人体の接触の際に生ずる放電電流の計算"，平成17年度電気関係学会東海支部連合大会，O-385, Sep. 2005.

[13] **Ikuko Mori**, Yoshinori Taka, Osamu Fujiwara, and Shinobu Ishigami, "Characteristics and Comparison of Currents for Contact/Air Discharge of an ESD-gun with Low Charge Voltages", 2005 Tokai-Section Joint Convention of Institute of Electrical Engineers, O-391, Sep. 2005.

森育子，高義礼，藤原修，石上忍，"低充電電圧ESDガンの接触／気中放電に対する放電電流特性の比較"，平成17年度電気関係学会東海支部連合大会，O-391, Sep. 2005.

[14] Yoshinori Taka, **Ikuko Mori**, and Osamu Fujiwara, "Characteristics of Discharge Current due to Air Discharge through Hand-Held Metal Piece from Charged Human-Body", 2005 Tokai-Section Joint Convention of Institute of Electrical Engineers, O-388, Sep. 2005.

高義礼，**森育子**，藤原修，”帯電人体からの金属棒を介した気中放電に対する放電電流特性”，平成１７年度電気関係学会東海支部連合大会，O-388, Sep. 2005.

[15] **Ikuko Mori**, Osamu Fujiwara, and Shinobu Ishigami, ”Specific Characteristics of Discharge Current for Air Discharge of an ESD-Gun”, 2006 Tokai-Section Joint Convention of Institute of Electrical Engineers, O-241, Sep. 2006.

森育子，藤原修，石上忍，”ESDガンの気中放電で生ずる放電電流の特異特性”，平成18年度電気関係学会東海支部連合大会，O-241, Sep. 2006.

[16] Yoshinori Taka, **Ikuko Mori**, and Osamu Fujiwara, ”Calculation of Gap Voltage Waveform Using Discharge Current from Charged Human-Body”, 2006 Tokai-Section Joint Convention of Institute of Electrical Engineers, O-244, Sep. 2006.

高義礼，**森育子**，藤原修，”帯電人体からの放電電流を用いたギャップ電圧波形の計算”，平成18年度電気関係学会東海支部連合大会，O-244, Sep. 2006.

Biography

IIkuko Mori was born in Mie, Japan on January 5, 1973. She received her B.A. degree in Japanese Literature from Aichi Prefectural University, Japan in 1995. She received her B.E. and M.E. degrees in electrical and computer engineering from Nagoya Institute of Technology, Japan in 2002 and 2004, respectively, and was a Ph.D. student there. Her research interests include electromagnetic compatibility, especially electrostatic discharge.